Electropermutation Assisted by Ion-Exchange Textile - Removal of Nitrate from Drinking Water

by

Carl-Ola Danielsson Department of Mechanics

May 2006 Technical Reports from Royal Institute of Technology Department of Mechanics FaxénLaboratoriet S-100 44 Stockholm, Sweden Typsatt i $\mathcal{A}_{\mathcal{M}}\mathcal{S}\text{-}\mathbb{P}_{\mathbf{E}}\mathbf{X}.$

Akademisk avhandling som med tillstånd av Kungliga Tekniska Högskolan i Stockholm framlägges till offentlig granskning för avläggande av teknologie doktorsexamen torsdagen den 8:de juni 2006 kl 10.00 i sal D3, Kungliga Tekniska Högskolan, Lindstedsvägen 5, Stockholm.

©Carl-Ola Danielsson 2006

Tryck: Universitetsservice US AB, Stockholm 2006



Electropermutation Assisted by Ion-Exchange Textile Removal of Nitrate from Drinking Water

Carl-Ola Danielsson

FaxénLaboratoriet, Department of Mechanics, Royal Institute of Technology SE-100 44 Stockholm, Sweden.

Abstract

Increased levels of nitrate in ground water have made many wells unsuitable as sources for drinking water. In this thesis an ion-exchange assisted electromembrane process, suitable for nitrate removal, is investigated both theoretically and experimentally. An ion-exchange textile material is introduced as a conducting spacer in the feed compartment of an electropermutation cell. The sheet shaped structure of the textile makes it easy to incorporate into the cell. High permeability and fast ion-exchange kinetics, compared to ion-exchange resins, are other attractive features of the ion-exchange textile.

A steady-state model based on the conservation of the ionic species is developed. The governing equations on the microscopic level are volume averaged to give macro-homogeneous equations. The model equations are analyzed and relevant simplifications are motivated and introduced. Dimensionless parameters governing the continuous electropermutation process are identified and their influence on the process are discussed. The mathematical model can be used as a tool when optimising the process parameters and designing equipment.

An experimental study that aimed to show the positive influence of using the ion-exchange textile in the feed compartment of an continuous electropermutation process is presented. The incorporation of the ion-exchange textile significantly improves the nitrate removal rate at the same time as the power consumption is decreased. A superficial solution of sodium nitrate with a initial nitrate concentration of 105 ppm was treated. A product stream with less than 20 ppm nitrate could be obtained, in a single pass mode of operation. Its concluded from these experiments that continuous electropermutation using ion-exchange textile provides an interesting alternative for nitrate removal, in drinking water production. The predictions of the mathematical model are compared with experimental results and a good agreement is obtained.

Enhanced water dissociation is known to take place at the surface of ion-exchange membranes in electromembrane processes operated above the limiting current density. A model for this enhanced water dissociation in presented in the thesis. The model makes it possible to incorporate the effect of water dissociation as a heterogeneous surface reaction. Results from simulations of electropermutation with and without ion-exchange textile incorporated are presented. The influence of the water dissociation is investigated with the developed model.

Descriptors: Ion-exchange textile, Ion-exchange membrane, Electropermutation, Electroextraction, Electrodialysis, Electrodeionisation, Modeling, Conducting spacer, Nitrate removal, Water treatment, Water dissociation.

Preface

This thesis treats ion-exchange assisted electropermutation both theoretically and experimentally. The research was conducted within the framework of FaxénLaboratoriet, a center of excellence in industrial fluid mechanics located at the Royal Institute of Technology in Stockholm, Sweden. Vattenfall AB has been the main industrial partner and parts of the work has been performed at Vattenfall Utveckling AB's electrochemistry laboratory. The thesis is divided into two parts. In the first of these, an introduction to the process and a summary of the research conducted is given in order to clarify its context. The second part consists of 4 appended scientific papers.

Stockholm, May 2006

Carl-Ola Danielsson

Appended articles:

Paper 1. Carl-Ola Danielsson, Anders Dahlkild, Anna Velin & Mårten Behm Nitrate Removal by Continuous Electropermutation Using Ion-Exchange Textile Part I: Modeling *Published in Journal of The Electrochemical Society* 153(4) D51-D61, 2006

Paper 2. Carl-Ola Danielsson, Anna Velin, Mårten Behm & Anders Dahlkild Nitrate Removal by Continuous Electropermutation Using Ion-Exchange Textile Part II: Experiments *Published in Journal of The Electrochemical Society* **153**(4) D62-D67, 2006

Paper 3. Carl-Ola Danielsson, Anders Dahlkild Mårten Behm & Anna Velin A Model for the Enhanced Water Dissociation On Monopolar Membranes. *To be Submitted*

Paper 4. Carl-Ola Danielsson, Anders Dahlkild, Anna Velin & Mårten Behm Modeling Continuous Electropermutation with Effects of Water Dissociation Included $To\ be\ Submitted$

Division of work between authors

The work presented in this thesis has been done in collaboration with other researchers. The respondent has performed the major part of the work. Docent Anders Dahlkild, Department of Mechanics KTH, Dr. Anna Velin, Vattenfall Utveckling AB and Dr. Mårten Behm, Department of Chemical Engineering and Technology, Applied Electrochemistry KTH, have acted as supervisors. They have all contributed with comments and discussions of the the work and the manuscripts.

Parts of the modeling activities have been presented in a poster at, The 53rd Annual Meeting of the International Society of Electrochemistry, Düsseldorf, Germany, in September 2002, and in a talk given at, The 205th meeting of the electrochemical society in San Antonio, Texas, U.S.,

The 205th meeting of the electrochemical society in San Antonio, Texas, U.S. in May 2004.

Contents

Preface		
Chapter 1. Introduction	1	
Removal of Nitrate from drinking water		
Background	3	
Outline of thesis	4	
Chapter 2. Ion-Exchange and Electromembrane Processes	5	
Ion-exchange (IX)	5	
Ion-exchange membrane processes	6	
Electrodialysis (ED)	6	
Electropermutation (EP)	8	
Ion-Exchange assisted electromembrane processes	9	
Ion-exchange textiles	13	
Chapter 3. Modelling	14	
Volume averaging	15	
Conservation of mass	16	
3.1. Enhanced Water Dissociation	20	
Chapter 4. Experimental Investigations	22	
Nitrate removal	22	
Characterization of textile		
Permeability		
Conductivity of fiber bed	25	
Chapter 5. Summary of Papers	30	
Paper I	30	
Paper II	33	
Paper III	35	
Paper IV	37	

x CONTENTS

Chapter 6. Concluding Discussion and Outlook Concluding Discussion	42 42			
Acknowledgment				
Bibliography	46			
Nitrate Removal by Continuous Electropermutation Using Ion- Exchange Textile Part I: Modeling				
Nitrate Removal by Continuous Electropermutationusing Ion- Exchange Textile as Conducting Spacer Part II: Experiments				
A Model for the Enhanced Water Dissociation On Monopolar Membranes				
Modeling Continuous Electropermutation with Effects of Water Dissociation Included				

CHAPTER 1

Introduction

To obtain freshwater of high quality directly from the kitchen tap is something that many of us take for granted. We use it every day to prepare our food, to wash our clothes and for many other things. In Sweden the consumption of water is about 200 l of water per person per day [1]. Increasing environmental pollution has made many wells unsuitable as freshwater sources. Use of water treatment techniques is needed in order to meet society's need of high quality water. The regulations on the water quality is continuously getting more and more strict as new and better analytical instruments are developed making it possible to detect lower and lower levels of impurities.

What is regarded as good water quality depends on the application. Potable water should be free from toxic and harmful substances. Ultrapure water on the other hand, is not considered as high quality drinking water, where some minerals are desirable. The taste, smell and visual appearance of the water are other important aspects of drinking water quality. Furthermore, there are some technical aspects of a suitable drinking water that are considered. For example there are regulations on the pH and conductivity of the water in order to reduce corrosion problems in the pipes.

The definition of clean water in many industrial applications is completely different compared to the potable water. The microelectronic and pharmaceutical industries require extremely pure water in their processes. In powerplants ultrapure water is used to reduce problems with corrosion that could be a serious problem at the temperatures and pressures present in the boilers. The production of this ultrapure water requires sophisticated water treatment systems.

For many industrial processes a zero waste target is on the agenda. Water treatment systems are used to reduce discharge of e.g. heavy metals for environmental reasons. There might also be an economical advantage if chemicals used in the process can be recycled.

Removal of Nitrate from drinking water

The primary health concern regarding nitrate, NO_3^- , is that it is reduced to nitrite, NO_2^- , in the body. Nitrite in turn reacts with the red blood cells to form methemoglobin, which affects the blood's capability to transport oxygen. Infants are especially sensitive due to their low gastric acidity, which is favorable

2 1. INTRODUCTION

for the reduction of nitrate. High intake of nitrate by infants e.g. when bottle-fed, can cause a condition known as "blue-baby" syndrome that can be fatal. It is also claimed by some researchers that there exist a correlation between exposure to nitrate and the risk of developing cancer. This is however still not established.

According to European Union regulations, drinking water must not contain more than 50 ppm of nitrate, although the recommended value is a concentration of less than 25 ppm [2]. German health authorities demands that the nitrate level in water used in the preparation of baby food should be less than 10 ppm [3]. In the guidelines for drinking water quality published by [4] in 2004 the maximum level of nitrate is given as 50 mg/litre. In drinking water derived from surface water the nitrate level rarely exceeds 10 ppm; however increased nitrate concentrations in ground water have made many wells unsuitable as drinking water sources.

The accumulation of nitrate in the environment results mainly from the use of nitrogenous fertilizers and from poorly or untreated sewage. In addition, many industrial processes produces waste streams containing nitrate. Since agricultural activities are involved in the nitrate pollution problem, farmers and rural communities are the most threatened populations.

The removal of nitrates from water can be accomplished in a number of different ways e.g. ion-exchange, biological processes or with membrane techniques. The ideal process for nitrate removal would be able to treat large volumes of water at a low cost. Furthermore it is desirable that the process adapts well to different feed loads and works without the addition of any chemicals. A review of different alternatives for nitrate removal is presented by [5].

Biological denitrification is commonly used for treatment of municipal and industrial wastewater. A concern for bacterial contamination of the treated water has made the transfer to production of drinking water slow. The main advantage of using biological nitrate reduction is that the nitrate is turned into nitrogen gas reducing problems with waste solutions. Biological denitrification is however quite slow and thus large installations are required. Furthermore the bacteria responsible for the transformation of nitrate into nitrogen are sensitive to changes in their working conditions. Temperature and pH has to be kept within a narrow range, this together with the need for relatively large installations makes the biological methods expensive.

Using conventional ion-exchange for nitrate removal involves the passing of the water through a bed of nitrate selective anion-exchange resin beads. The nitrate ions present in the water are usually exchanged for chloride or bicarbonate ions until the bed is exhausted. The exhausted resin then has to be regenerated using concentrated solutions of e.g. sodium chloride. Problems with ion-exchange are related to the non-continuous mode of operation. This requires several IX columns to be installed in parallel in order to obtain a continuous production. The need for regeneration solution adds to the operational

cost as well as leads to a problem of waste disposal. There are some installations where the spent regeneration solution is treated with biological denitrification. The advantages with IX are that very low nitrate concentrations can be reached. The technique is very flexible and relatively insensitive to changes in temperature. The time needed for start up is very short and the capital cost is much less than for biological denitrification plants. Furthermore operating costs are slightly lower for IX compared to biological denitrification [5].

There are several options for nitrate removal, which makes use of ion-exchange membranes to accomplish a nitrate separation. Salem [6] claims that these processes are the most suitable when large volumes of water are to be treated. The main advantage compared to conventional ion-exchange is that a continuous mode of operation can be obtained. The same problem with disposal of the generated waste streams as for ion-exchange are experienced with the ion-exchange membrane processes.

This thesis deals with an electromembrane process called electropermutation. This technique is capable of removing ionic impurities from water with low conductivity. A product stream free from the undesired ions and a concentrated waste stream are generated. The concentrated waste stream can be treated with other techniques or, depending on the application, the concentrate might be recycled. The specific application studied in this thesis is nitrate removal from ground water to produce drinking water. It is possible to improve the performance of the process by incorporation of an ion exchange material and in the work presented here a newly developed ion-exchange textile material is considered. The influence of using this anion-exchange textile as conducting spacer in the feed compartment is investigated both theoretically and experimentally.

Background

The research presented in this thesis has been performed within FaxénLaboratoriet, a competence center for fluid mechanics of industrial processes. The work has been done in close collaboration with the main industrial partner in this project, Vattenfall Utveckling AB (VUAB). The electrochemistry group at VUAB had been engaged to develop an efficient system for nitrate removal from ground and industrial waters. The system was based on the integration of conventional ion-exchange technique for nitrate removal with selective electrochemical nitrate reduction. Part of this nitrate program was the participation in the EU funded research project Iontex [7]. The purpose of Iontex was to develop new functionalized textile materials made from cellulosic fibers. VUAB's task was to develop an electrodialysis module, which utilized a textile with ion-exchange properties. As part of this task both theoretical and experimental studies were conducted and the results are presented in this thesis.

4 1. INTRODUCTION

Outline of thesis

The main part of the work is presented in the four appended scientific articles. Before the articles are presented a summary the work is presented. Conventional ion exchange and electromembrane processes are presented in the second chapter. In the third chapter the basis of the theoretical investigation is presented and in chapter four the experimental work is described. A summary of the appended articles is given in the fifth chapter. Finally a concluding discussion and a presentation of some ideas for future work is given in chapter six.

CHAPTER 2

Ion-Exchange and Electromembrane Processes

In this chapter, the principles behind conventional ion-exchange and different electromembrane processes are presented.

Ion-exchange (IX)

The use of ion-exchange technology on a large scale is described already in The $\mathrm{Holy}\ \mathrm{Bible}^1$

23: And when they came to Marah, they could not drink of the waters of Marah, for they were bitter: therefore the name of it was called Marah. 24: And the people murmured against Moses, saying, What shall we drink? 25: And he cried unto the LORD; and the LORD shewed him a tree, which when he had cast into the waters, the waters were made sweet: there he made for them a statute and an ordinance, and there he proved them, Exodus 15:23-25

This is an example of were ion-exchange have been used to prepare drinking water from brackish water.

Ion-exchangers consist of a framework carrying a positive (anion-exchangers) or negative (cation-exchangers) surplus charge, which is compensated by mobile counter ions of opposite sign. A simple model for the ion-exchanger is a sponge carrying an electric charge that must be compensated by charged particles in its pores. The counter ions can be exchanged for other ions of the same polarity. Ion-exchangers which can exchange cations are called *cation-exchangers* and, analogously *anion-exchangers* holds exchangable anions. An *amphoteric ion-exchanger* is capable of exchanging both cations and anions. The exchange is stoichiometric and in general reversible. Ion-exchange is essentially a diffusion process and has little, if any, relation to chemical reaction kinetics in the usual sense. Usually the ion-exchanger is selective, i.e., it takes up certain counter ions in preference to others.

Ion-exchange is widely used for softening water, i.e., calcium and magnesium ions present in the water are exchanged for sodium ions by passing the water through a bed of cation-exchange material. After some time of operation all the sodium ions that initially were present in the cation-exchange material have been exchanged for magnesium or calcium ions, that is, the ion-exchange material has become exhausted. As was mentioned in chapter 1, one then has

 $^{^1{}m King}$ James version.

to stop the process and regenerate the ion-exchanger. This highlights the draw-backs of the ion-exchange technique. First and foremost it is not a continuous process, the production has to be stopped while the bed is regenerated, and in order to obtain a continuous production several IX columns has to be installed in parallel. To accomplish the regeneration a strong salt solution has to be prepared, which requires the handling and storage of chemicals. The regeneration step also generates a waste stream, which might be a problem. There are some installations where the spent regeneration solution is treated with biological denitrification.

A good introduction to ion-exchange technology in general is given by Helfferich in his book *Ion Exchange* [8].

Ion-exchange membrane processes

Ion-exchange membranes are sheet shaped ion-exchangers with a typical thickness of about $100\mu m$. There are several different separation processes that make use of ion-exchange membranes. Examples of such are Donnan dialysis, electrodialysis, and ion-exchange assisted electromembrane processes.

Electrodialysis (ED)

Electrodialysis is an electrochemical separation process which combines ion-exchange membranes and an electric field to separate ionic species from aqueous solutions. In an electrodialysis stack cation(CEM) and anion(AEM) exchange membranes are alternated between an anode, i.e. a negatively charged electrode, and a cathode, i.e. a positively charged electrode, to form individual cells or compartments. An actual electrodialysis stack can consist of a few hundred membranes [9]. A five compartment ED stack consisting of only four membranes and only one repeating unit of one cation permeable and one anion permeable membrane is shown in figure 2.1.

If an ionic solution such as a salt solution is passed through the cells of an ED stack and an electric potential is applied between the anode and the cathode, the positively charged cations in the liquid solution migrates towards the cathode and the negatively charged anions migrates towards the anode. The cations can pass through the cation-exchange membranes but are retained by the anion-exchange membranes. Likewise the anions can pass through the anion-exchange membranes but not the cation-exchange membranes. As a result of this the concentration of the salt solution will go down in every other compartment, known as dilute compartments (D.C), while the remaining compartments, called concentrate compartments (C.C) will experience an increase in the salt concentration. The dilute compartment, i.e. the central compartment, in figure 2.1, is characterized by having an anion permeable membrane located closest to the anode and a cation permeable membrane facing the cathode. In the concentrate compartments the situation is the opposite.

The main application for electrodialysis is desalination of brackish water to produce potable water. In this application it is the water leaving the dilute

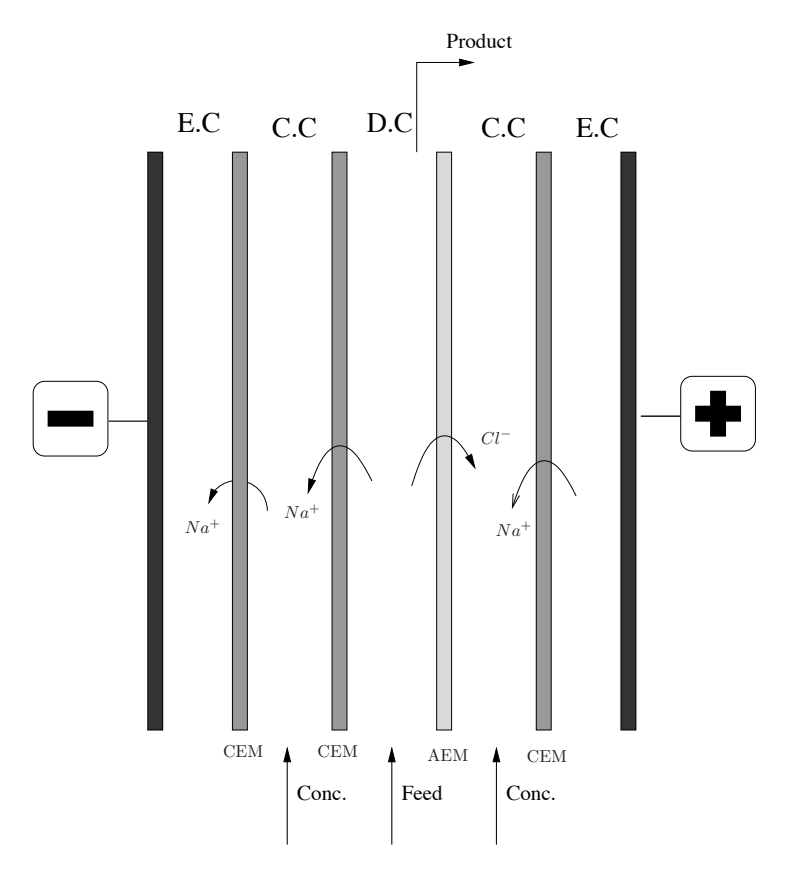


FIGURE 2.1. The principles of electrodialysis for desalination of brackish water.

compartments that is the product of the process. Electrodialysis is also used for increasing the salt concentration e.g. before evaporation to produce table salt or for direct use in the chlor-alkali process, in these cases it is instead the water leaving the concentrate compartments that is the product stream.

Advantages of ED compared to conventional ion-exchange are that no chemicals need to be added and the process can be operated continuously. Pretreatment of the feed might be necessary in order to reduce fouling problems. Short periods of reversed polarity can also be applied to reduce fouling problems and to improve the lifetime of the membranes. A low conductivity of the water to be treated makes the power consumption for driving the electric current through the ED stack relatively high. Furthermore, concentration polarisation limits the intensity of the current density that can be applied. This makes the electrodialysis process unsuitable for treatment of solutions of low conductivity.

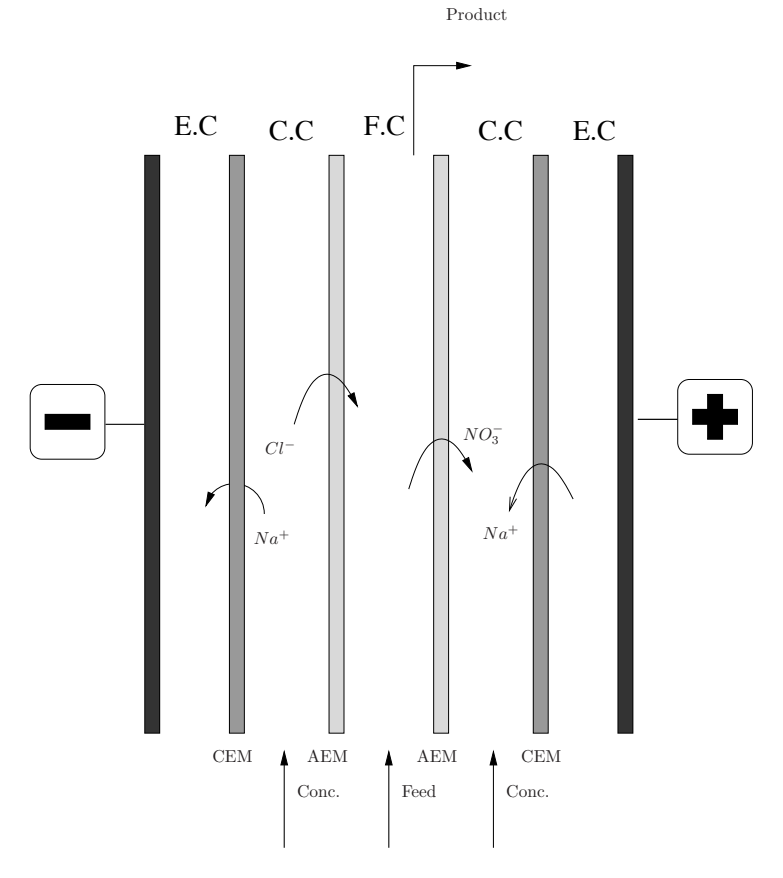


FIGURE 2.2. The principles of continuous electropermutation for nitrate removal.

Electropermutation (EP)

The idea of electropermutation [10, 11, 12, 13] is to replace the unwanted anions or cations for more desirable once. So instead to removing all ions from the feed, which might be an unwanted feature in drinking water production, the anions in the feed are replaced by other anions initially present in a concentrate solution. In figure 2.2 the principles of nitrate removal by electropermutation are illustrated. The water to be treated is fed through a feed compartment (F.C). On each side of the F.C are concentrate compartments (C.C) in which a solution with high concentration of e.g. chloride Cl^- is circulated. The feed and concentrate compartments are separated by anion permeable membranes. Under the influence of an applied electric field the anions initially present in the feed water are replaced by those in the concentrate solution. Hence, a product in which the nitrate has been replaced for chloride is obtained from the process is shown in figure 2.2. By keeping the concentration of the concentrate solution

sufficiently high a repeating unit of two compartments can be used. The nitrate concentration in the concentrate stream becomes relatively large compared to the feed water. This makes it possible to use electrochemical reduction to transfer the nitrate to nitrogen [14] in a subsequent process step, as a solution to the waste disposal problem.

The main drawback with using electroper mutation for nitrate removal compared to electrodialysis is that salt need to be added to maintain the desired composition of the concentrate solution. This drawback can, however, be utilized as an advantage of the process. The composition of the concentrate solution can be tailored as to obtain a product water with desired properties, e.g. by adjusting the pH of the concentrate solution it might be possible to adjust the pH of the product. It is often desired to have a drinking water with a pH of about 8 in order to reduce problems associated with corrosion in the distribution systems.

Donnan dialysis (DD)

Donnan dialysis is in principle very similar to electropermutation. The driving force in Donnan dialysis is the difference in electrochemical potential over, the ion-exchange membranes, due to the difference in chemical composition of the solutions, rather than by an applied electric field. Using the example of nitrate separation as illustrated in figure 2.2; the concentration gradient of chloride through the membrane gives rise to an electric field in the membrane that will transport nitrate from the F.C into the two C.C's and chloride is transported in the opposite direction. Although Donnan dialysis has been discussed rather extensively in the literature it has not had any major industrial break through [15]. Examples of applications where Donnan dialysis has been studied includes removal of fluoride from dilute solutions [16, 17, 18, 19], softening of water [15] and enrichment of nobel metals such as gold [20].

Ion-Exchange assisted electromembrane processes

Hybrid ion-exchange/electromembrane processes, capable of treating solutions of low conductivity, have been investigated since the mid 1950's. The first publication is generally ascribed to Walter et.al [21] in 1956. They studied the regeneration of an ion-exchange bed, exhausted by radioactive wastewater, by an applied electric field. The idea was to regenerate the ion-exchange bed without the need of strong acids and bases as regeneration solution. Thus, the process investigated by Walters et.al [21] was a batch electrodeionization process.

Later Glueckauf was the first to investigate the theory of these hybrid processes in the late 1950s [22]. He proposed a theoretical model of continuous electrodeionization where the process was divided into two stages. First the mass transfer to the surface of the ion-exchange resins followed by the transfer of ions in a chain of ion-exchange resin beads. The actual ion-exchange reaction was considered to be in equilibrium, which is still a generally accepted

assumption. A one-dimensional model along the flow direction, averaged over the width of the inter-membrane spacing, was formulated and compared with experiments.

In continuous electrodeionization, CEDI, the strengths of conventional ionexchange and electrodialysis are combined in one process. Thus, CEDI is capable of continuously treating solutions of low conductivity. The general idea behind CEDI, is to incorporate an ion-exchange bed between the membranes in the dilute compartment of an ED cell. In figure 2.3 a schematic of the CEDI process is given. One can think of the process as an ion-exchange process, which is continuously regenerated by the applied electric field. Dissociation of water in-situ provides the ions that regenerate the ion-exchange bed and thus no chemicals need to be added to run the CEDI process. Alternatively one may think of the process as an electrodialysis process, in which the added ionexchange material provides extra conductivity to the dilute compartment and reduces the problems associated with the limiting current. Ganzi [23, 24] talks about two distinct regimes of operation, each corresponding to the two ways of thinking of the process. In the enhanced transfer regime the ion-exchange bed, in the dilute compartment, is exhausted with salt ions. This is usually the situation close to the inlet of the dilute compartment where strongly ionized substances are removed. The role of the ion-exchange bed is as a conducting spacer, which reduces the power consumption as well as increases the limiting current density. In this regime the rate of water dissociation is low and the current efficiency is high. In the electroregeneration regime, on the other hand, the ion-exchange bed is continuously regenerated by H⁺ and OH⁻ ions produced in-situ by dissociation of water. This dissociation of water is crucial for the removal of weakly ionized species like silica, carbon dioxide and boron. These species are weak acids and are not ionized until the pH of the water is rather high. Due to the dissociation of water in the dilute compartment the local pH in the dilute compartment might become sufficiently high for the weak acids to dissociate and be captured by the ion-exchange bed. The main application is the production of ultrapure water, used for example as feed water to boilers in power plants or as rinse water in the micro electronics industry [15, 23, 25, 26]. Ionpure introduced the first commercially available CEDI equipment on the market in 1987. This equipment was based on a plate and frame device with a dilute compartment filled with a mixed bed of both anion- and cation-exchange resins. This design of the equipment is more effective if the dilute compartments are made thin, 2-3 mm. A thin dilute compartment increases the chance of finding an unbroken path of ion-exchange resins of the same polarity from one membrane to the other. Consequently this CEDI design is known as thin-cell EDI. Intense water dissociation providing hydrogen and hydroxide ions that regenerates the ion-exchanger can occur at contact points between ion-exchange resins of opposite polarity in the dilute compartment [27].

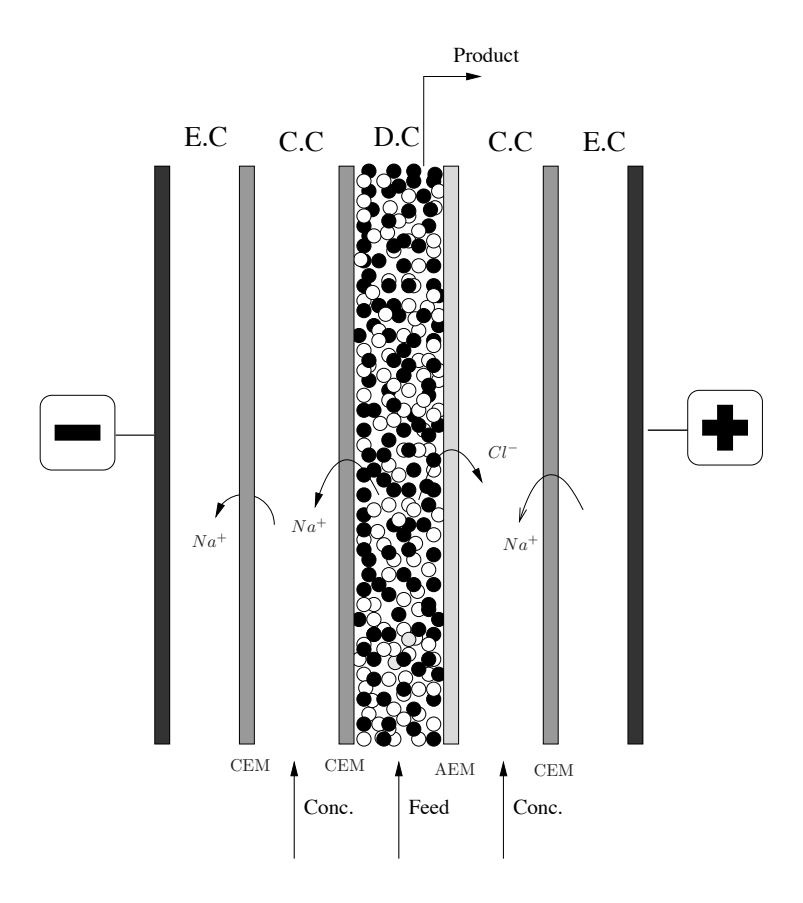
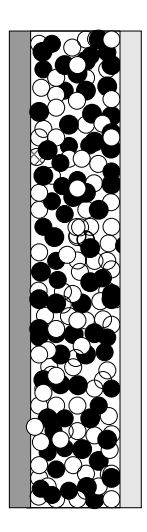


FIGURE 2.3. A schematic of CEDI for production of ultrapure water.

Later thick cell CEDI, with dilute compartment thicknesses of 8-10 mm, was developed. In these designs the dilute compartment is filled with separate layers or zones of ion-exchange material of the same polarity in order to guarantee that a continuous path exists from one side to the other of the compartment. A schematic of a mixed and a layered bed is shown in figure 2.4. In thick cell EDI, dissociation of water is critical for the removal of both weak and strong ions. In the layers filled with anion-exchange resins water is dissociated at the interface between the resins and the cation-exchange membrane. The pH in a layered bed device alternates from basic in the anion layers to acidic in the cation layers. In figure 2.4 the difference between a mixed thin cell CEDI and a layered thick cell CEDI dilute compartment is illustrated.

Thate et.al [28] investigated the how the configuration of the layers influenced the separation of weak acids. They used an equipment with two layers one with cation-exchange resins and one with anion-exchange resins. It was found that a more effective separation of weak acids could be obtained if the



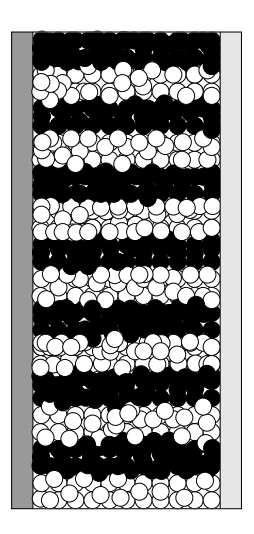


FIGURE 2.4. Mixed and layered bed CEDI. To the left an example of a mixed bed thin cell CEDI dilute compartment. To the right a thick cell layered bed dilute compartment.

layered bed was operated with the cation-exchange bed in front of the anion-exchange bed. This is somewhat surprising since it is expected that the pH in the cation-exchange bed should be acidic and then as the liquid passes through the anion-exchange bed the pH should return to a more or less neutral pH. A high pH as is required to dissociate the weak acid is not expected anywhere in the dilute compartment using this configuration. Thus, the mechanisms behind the separation of weak acids by CEDI are not fully understood.

Also the performance of electropermutation can be improved by filling the feed compartment with ion-exchange material [12, 10]. In this case the anion-exchange material should be used if anions are to be replaced as is the case in the nitrate removal example discussed above, and cation-exchange material if cations are to be replaced. Thus, there are no contact points between ion-exchange material of opposite polarity and water dissociation is not expected to take place. Water dissociation is an unwanted phenomenon in the ion-exchange assisted electropermutation process since it reduces the current efficiency as well as changes the pH of the product. The advantages of using an ion conducting spacer in the feed compartment of an electropermutation process is that it reduces the power consumption for driving the current density through the feed compartment as well as improves the mass transfer. The limiting current density is moved from the surface of the membrane to the much larger surface area of the ion-exchange bed.

Ion-exchange textiles

The use of ion-exchange textiles as conductive spacers in the ion-exchange assisted electromembrane processes have some advantages compared to ordinary ion-exchange resins [10, 11, 12, 29, 30, 31, 32]. First of all the textile material is much easier to incorporate into an electro-membrane cell. The sheet shape nature of the textile makes it convenient to cut a sheet of the desired shape and place it in the compartment. Using ion-exchange resins one has to be very careful when filling the compartments with the resin beads, in order to minimize the risk of creating preferential flow channels. The diameter of the fibers in the textile is generally one order of magnitude lower than typical diameters of resin beads. This gives the fibers a large surface to volume ratio and ensures fast ion-exchange kinetics. Small fiber diameters should also give an improved contact with the membranes compared to a resin bed. The ion-exchange textiles gives a lower pressure drop and hence less energy is required to force the flow through the cell. The hydrophilic nature of the fibers and the high porosity of the textiles compared to a resin bed explain the high permeability of the textile filled compartments.

The capacity of the ion-exchange textile available at present day is low compared to available ion-exchange resins, about 1 $\mathrm{meq/g}$ [7] for an anion-exchange textile compared to above 2 $\mathrm{meq/g}$ for resins. Taking the high porosity of the ion-exchange textile into account one finds that the capacity per volume in the dilute compartment is significantly lower for the ion-exchange textile bed. However, it is not the capacity of the ion-exchange spacer alone that determines the effective conductivity. Also the ionic mobility in the ion-exchanger as well as contact resistances at the membrane surface and in between different resin beads/fibers influences the effective conductivity of the spacer filled compartment.

CHAPTER 3

Modelling

In this chapter the basic concepts of the theoretical investigations of the electropermutation process is described. The main motivation for developing a mathematical model is to better understand the different mechanisms of the process, their interaction and how the process is affected by different parameters. Simulations based on the model are a valuable tool that can be used to optimize equipment design as well as operating conditions.

The basis of the model of the are mass-balances for each ionic specie i is given by,

$$\frac{\partial c_i}{\partial t} = -\nabla \cdot \mathbf{N}_i + R_i. \tag{3.1}$$

In the above expression c_i is the concentration, \mathbf{N}_i is the flux vector and \mathbf{R}_i is the sink/source term of specie i.

Only steady state models are considered, thus the left hand side of equation 3.1 is zero. The next problem is how the fluxes of the ionic species are to be described. It is assumed that the Nernst-Planck equations [33] gives a sufficiently accurate description of the fluxes of all ions. Thus, the flux of specie i relative a stationary frame of reference is given by,

$$\mathbf{N}_{i} = -D\nabla c_{i} - zu_{i}c_{i}\nabla\Phi + \mathbf{u}c_{i}$$
Diffusion Migration Convection (3.2)

In the expression above \mathbf{u} is the velocity of the electrolyte, D_i is the diffusion coefficient, u_i is the mobility and ϕ is the electrical potential. The flow of electrolyte is assumed to be a forced flow, i.e. the flow is not influenced by concentration gradients or the applied electric field. This means that the flow field can be solved independently of the mass-balance equations. Momentum balance equations are solved in order to obtain the velocity field. The electrical potential is obtained by solving a Poisson equation,

$$\nabla^2 \phi = -\frac{F}{\epsilon} \sum_i z_i c_i, \tag{3.3}$$

where F is Faradays constant and ϵ is the dielectric constant. As ϵ , relatively speaking is a small quantity the balance of eq. 3.3 requires that

$$\sum_{i} z_i c_i = 0, \tag{3.4}$$

i.e. the electroneutrality condition. This assumption holds everywhere except in a thin layer close to the surface of ion-exchange materials. These thin layer, of order $\sqrt{\frac{\epsilon\phi_0}{Fc_0}}$, called electric double layers are not resolved in the models presented in this thesis.

The unknowns that are solved for in the model are the concentrations of the ionic species included in the model together with the electrical potential. Thus, for a system with four ionic species there are five unknowns. For this system the mass balances gives four differential equations, which together with the algebraic electroneutrality constraint can be solved provided that boundary conditions are specified. This is the basis of the model in all subdomains included in the model.

In the ion-exchange membranes all convective transport is neglected. Hence, the fluxes through the membranes are due to diffusion and migration. The membranes are treated as solid electrolytes with a homogeneous distribution of fixed charges. Due to the Donnan exclusion effect, which makes the coion concentration in the membranes low, the membranes are treated as ideally selective. This means that all co-ion concentrations are taken to be zero.

The complexity of the model increases when the feed compartment is filled with an ion conducting spacer. In the models presented in paper 1 and 4 an ion-exchange textile is used in the feed compartment. The textile is treated as a porous bed consisting of a network of solid fibers and the interstitial liquid. Ionic transport can take place in both phases, and the exchange of mass between the phases takes place via ion-exchange, which is assumed to be rate-controlled by the mass transfer on the liquid side. Equations for conservation of mass are solved in each phase together with the electroneutrality constraint. What makes this situation complicated is that the exact location of the interface between the liquid and textile phases is unknown. Even if this information were available it would not be realistic to solve the problem by resolving every fiber in the dilute compartment. Instead macro-homogeneous equations are formulated through a volume averaging procedure.

Volume averaging

To overcome the difficulties associated with the heterogeneous structure of the porous medium, the concept of volumetrical averaging is applied. The details are given by Whitaker [34].

The superficial averaged concentration of component i in the liquid phase is defined as,

$$\langle c_i \rangle = \frac{\int_{V_{\alpha}} c_i \, dV}{\int_{V_T} dV} = \frac{1}{V_T} \int_{V_{\alpha}} c_i \, dV,$$
 (3.5)

 V_{α} =Volume of liquid phase,

 V_T =Total volume.

; ξ is used to denote a superficial average. The subscript α relates to the liquid phase. If the average is taken over the volume of the liquid phase instead

of the total volume the interstitial or intrinsic average of the concentration is obtained.

$$\langle c_i \rangle_{\alpha} = \frac{\int_{V_{\alpha}} c_i \, dV}{\int_{V_{\alpha}} dV}$$
 (3.6)

 $<>_{\alpha}$ is used to denote a intrinsic average of the liquid phase.

The interstitial and superficial averages are related through the porosity, ϵ_{α} ,

$$\epsilon_{\alpha} = \frac{\int_{V_{\alpha}} dV}{\int_{V_{T}} dV} \tag{3.7}$$

$$\langle c_i \rangle = \epsilon_{\alpha} \langle c_i \rangle_{\alpha} .$$
 (3.8)

Similar averages are also formed in the textile phase.

Conservation of mass

Conservation of mass at steady state on the microscopic scale was given in equations 3.1 above. The macro-homogeneous versions of the mass conservation equations are obtained by taking the superficial volume average of the balance equations. The steady state version of conservation of mass is written as,

$$\langle \nabla \cdot \mathbf{N}_i \rangle = \langle R_i \rangle.$$
 (3.9)

Applying the spatial averaging theorem [34] allows us to express the average of the divergence of the flux as,

$$\langle \nabla \cdot \mathbf{N}_i \rangle = \nabla \cdot \langle \mathbf{N}_i \rangle + \frac{1}{V} \int_{A_{\alpha}} \mathbf{N}_i \cdot \mathbf{n}_{\alpha} \, d\mathbf{A}$$
 (3.10)

Where the integral term in equation 3.10 represents the rate of exchange between the solid and liquid phase, i.e. the ion-exchange kinetics. The ion-exchange rate may be seen as a sink/source term in the macro-homogeneous mass balance equation.

$$S_i = \frac{1}{V} \int_{A_\alpha} \mathbf{N}_i \cdot \mathbf{n}_\alpha \, \mathrm{dA} \tag{3.11}$$

Thus, the macro-homogeneous version of the equations for conservation of mass is given by,

$$\nabla \cdot \langle \mathbf{N}_i \rangle + S_i = \langle R_i \rangle. \tag{3.12}$$

A model for ion-exchange rate is introduced later.

The volume averaged flux need to be expressed in terms of the volume averaged potential, fluid phase velocity and concentrations. The volume average of the flux expression is given by,

$$\langle \mathbf{N}_i \rangle = -\langle D_i \nabla c_i \rangle - \langle z_i u_i c_i \nabla \phi \rangle + \langle \mathbf{u} c_i \rangle.$$
 (3.13)

Expressing the concentration as

$$c_{i} = \langle c_{i} \rangle_{\alpha} + c_{i}', \tag{3.14a}$$

the potential as

$$\phi = <\phi>_{\alpha} + \phi^{'}, \tag{3.14b}$$

the velocity as

$$\mathbf{u} = \langle \mathbf{u} \rangle + \mathbf{u}', \tag{3.14c}$$

and introducing this into equation 3.13 gives,

$$\langle \mathbf{N_{i}} \rangle = -D_{i} \epsilon_{\alpha} \nabla \langle c_{i} \rangle_{\alpha} - z u_{i} \epsilon_{\alpha} \langle c_{i} \rangle_{\alpha} \nabla \langle \phi \rangle_{\alpha} + \mathbf{j} \langle c_{i} \rangle_{\alpha}$$
$$- z u_{i} \langle c_{i}^{'} \nabla \phi^{'} \rangle + \langle \mathbf{u}^{'} c_{i}^{'} \rangle - z u_{i} \langle c_{i} \rangle_{\alpha} \frac{1}{V} \int_{A_{\alpha}} \phi \mathbf{n}_{\alpha} \, dA$$
$$- D_{i} \frac{1}{V} \int_{A_{\alpha}} c_{i} \mathbf{n}_{\alpha} \, dA. \tag{3.15}$$

j is the superficial average of the fluid velocity vector, i.e.

$$\mathbf{j} = \epsilon_{\alpha} < \mathbf{u} > . \tag{3.16}$$

In the expression above the instrinsic averages of the concentration and potential are used together with the superficial average of the fluid velocity vector.

The first three terms in the equation above are the obvious candidates for the volume averaged fluxes in a porous material. The rest of the terms describe effects of the inherent structure of the material. To obtain a closed set of equations these terms need to be modeled. This closure problem is recognized from other branches of engineering where averaged equations are used, e.g. the Reynolds stressed in turbulent flows, for which numerous models can be found in the literature. In the present work focus has not been on finding closure relations that are suitable for the textile material. The closure relations used are presented below.

Mechanical Dispersion

The term $< \mathbf{u'}c' >$ in eq. 3.15, describes a mixing process known as the mechanical dispersion, its value will depend on both flow field and the geometry. To deal with this term in the model it need to expressed in terms of the averaged quantities. The following model is used to incorporate the effects of dispersion [34],

$$\langle \mathbf{u}'c' \rangle = -\mathcal{D}\nabla \langle c \rangle_{\alpha}$$
 (3.17)

where \mathcal{D} is a tensor which in the case of uniaxial flow along one of the coordinate axes is a diagonal tensor. Note that \mathcal{D} is not an isotropic tensor. Usually the effect of mechanical dispersion is more pronounced in the flow direction. For a uniaxial flow along the y-axis through a isotropic porous material the dispersion tensor would look like,

$$\mathcal{D} = \begin{pmatrix} \mathcal{D}_T & 0 & 0\\ 0 & \mathcal{D}_L & 0\\ 0 & 0 & \mathcal{D}_T \end{pmatrix}$$

$$(3.18)$$

where \mathcal{D}_L is known as the longitudinal coefficient of dispersion and \mathcal{D}_T as the transverse coefficient of dispersion. In the model empirical correlations found in the literature will be used to obtain the values of \mathcal{D}_L and \mathcal{D}_T .

Effective Diffusivity

The following terms remaining from the flux expression (eq. 3.15) above need to be modeled,

$$zu_{i} < c_{i}^{'} \nabla \phi^{'} >$$
, $zu_{i} < c_{i} >_{\alpha} \frac{1}{V} \int_{A_{\alpha}} \phi \mathbf{n}_{\alpha} \, dA$ and $D_{i} \frac{1}{V} \int_{A_{\alpha}} c_{i} \mathbf{n}_{\alpha} \, dA$. (3.19)

These terms are rather complicated and how they should best be modeled is a very interesting problem. The way the geometrical arrangement of the two phases influences the mass transfer through the porous bed enters through these terms. Volume averaged equations describing diffusion controlled mass transfer processes through a porous medium, where diffusion only takes place in one of the phases, can be found in the literature. In those cases only the last of the three terms above enters the equations. The heterogeneous structure of the porous medium makes the diffusion process slower due to the tortuosity. This is modeled by an effective diffusion coefficient, $D_{e,i}$ [35, 33]. Thus, the volume average of the diffusion flux is modeled by

$$-\langle D\nabla c \rangle = -D\epsilon_{\alpha}\nabla \langle c \rangle_{\alpha} - D\frac{1}{V} \int_{A_{\alpha}} c_{i} \mathbf{n}_{\alpha} \, d\mathbf{A} = \mathbf{D}_{e,i} \nabla \langle \mathbf{c} \rangle_{\alpha}, \quad (3.20)$$

were

$$D_{e,i} = D\epsilon_{\alpha}^{1+b}. (3.21)$$

The constant b is often taken as 0.5, which is known as the Bruggeman relation.

In the work presented in this thesis the mass transfer is allowed to take place in both the liquid and solid phase. This makes it harder to find the relations that close our equations. Two extreme situations of the mass transfer problem are obtained by assuming that the two phases are either in a parallel or a serial arrangement. In the parallel arrangement the fluxes through the two phases can be treated as independent of each other. A serial arrangement, on the other hand, requires that the fluxes have to be equal though both phases.

In the model presented in this thesis only a parallel phase arrangement have been considered. The concept of effective diffusion coefficients is applied in both phases. Furthermore, the Nernst-Einstein relation between ionic mobility and diffusivity is applied,

$$u_i = \frac{F}{RT}D_i \tag{3.22}$$

where the definition of the ionic mobility, u_i , given by Helfferich [8] is used. Hence, the effective diffusion coefficient is used also for the migration terms. Thus, effective diffusion coefficients are used in both the diffusion and migration term. This rather crude model has been used in the work presented in this thesis. The final expression for the volume average of the flux of specie i is given by,

$$<\mathbf{N_i}> = -(\mathcal{D} + D_{e,i})\nabla < c_i>_{\alpha} - z_i \frac{F}{RT} D_{e,i} < c_i>_{\alpha} \nabla < \phi>_{\alpha} + \mathbf{j} < c_i>_{\alpha}.$$
(3.23)

Ion-Exchange kinetics

The ion-exchange kinetics of fibrous ion-exchangers was studied by Petruzzelli $et.\ al\ [36]$ who suggested that the rate-determining step is the mass transfer in the liquid phase. A consequence of this is that ion-exchange equilibrium is always established at the surface of the ion-exchanger. Thus the electrochemical potential for all counter-ions are continuous over the phase interface. This can be expressed as

$$\bar{c}_i = k_i c_i^* \exp[-z_i F \Delta \phi / RT] \tag{3.24}$$

where $\Delta \phi = \bar{\phi} - \phi^*$ is the Donnan potential at the interface, k_i is the partition coefficient of species i which is assumed to be constant. In the expression above \bar{c}_i and $\bar{\phi}$ are the concentration and potential in the ion-exchanger respectively. The stars indicate an average value taken, on the liquid side, at the phase interface. Eliminating the Donnan potential from the above expression gives the separation factor,

$$\alpha_2^1 = \frac{\bar{c}_1 c_2^*}{\bar{c}_2 c_1^*} = \frac{k_1}{k_2}. (3.25)$$

This is a parameter that is often used to describe the affinity of an ion-exchanger. In the fourth paper where three different counter ions are included in the model it is assumed that the ion-exchange equilibrium can be described by two separation factors.

The ion-exchange kinetics is obtained by calculating the flux per unit volume from the bulk of the liquid phase to the surface of the ion-exchanger.

$$S_i = \langle N_i \rangle^* \mathfrak{S}_a \tag{3.26}$$

where \mathfrak{S}_a is the specific surface area of the ion-exchanger. $< N_i >^*$ is the average ionic flux density to the phase interface. For the fibrous ion-exchange material considered in this thesis the specific surface area is assumed to be given by

$$\mathfrak{S}_a = \frac{4}{d_f} (1 - \epsilon_\alpha). \tag{3.27}$$

The average flux to the phase interface is calculated by assuming a Nernstdiffusion layer around each fiber. This gives

$$< N_i >^* = \frac{D_i}{\delta} \left[(c_i^* - c_i) + z_i \frac{F c_i^*}{RT} (\phi^* - \phi) \right].$$
 (3.28)

In the first paper the model equations are analyzed and it is found that that the concentration difference over the Nernst-layer surrounding the fibers can be neglected under reasonable operating conditions. This greatly simplifies the model equations.

Source term

In the fourth paper the homogeneous dissociation/recombination of water is included in the model. On the microscopic scale the expression for the reaction

rate is given by

$$R_{OH^-/H^+} = k_f c_{H_2O} - k_b c_{OH^-} c_{H^+}$$
 (3.29)

where k_f and k_b are the rate constants of the forward and backward reaction rate respectively. This can be rearranged and written as

$$R_{OH^{-}/H^{+}} = K_{w}k_{b}(1 - \frac{c_{OH^{-}}c_{H^{+}}}{K_{w}})$$
(3.30)

where $K_w = k_f c_{H2O}/k_b$. In the macro-homogeneous form of the equations this reaction term becomes

$$< R_{OH^-/H^+} > = K_w k_b \epsilon_\alpha \left(1 - \frac{< c_{OH^-} >_\alpha < c_{H^+} >_\alpha}{K_w} - \frac{< c'_{OH^-} c'_{H^+} >}{K_w}\right).$$
 (3.31)

The problem with this formulation of the reaction term is that the last term includes the product of the unknown deviations from the averaged concentrations. In this thesis that last term is assumed to be zero. So the expression for the volume averaged reaction kinetics that is used in the model is given by

$$< R_{OH^-/H^+} > = K_w k_b \epsilon_\alpha (1 - \frac{< c_{OH^-} >_\alpha < c_{H^+} >_\alpha}{K_w}).$$
 (3.32)

In the first and fourth of the appended papers the model equations presented in the chapter are analyzed in more detail. Appropriate simplifications are introduced and results from simulations are presented.

3.1. Enhanced Water Dissociation

In the third article a model of the enhanced water dissociation at the membrane surface is presented. The general idea was to incorporate the enhanced water dissociation as a heterogeneous surface reaction. A literature survey gave that the actual mechanisms behind the enhanced water dissociation reaction are poorly understood. Thus, a semi empirical approach was chosen where the mechanism of the reaction is included in two model parameters, a rate constant and a symmetry factor. The over all reaction for the enhanced water



FIGURE 3.1. The reaction layer at the surface of the membrane. The ionic products are displaced to opposite sides of the reaction layer by the electric field.

dissociation is assumed to be described by,

$$H_2O \underset{k'_h}{\overset{k'_f}{\rightleftharpoons}} H^+ + OH^{m-}, \tag{3.33}$$

In figure 3.1 a schematic of the over all reaction is given. A water molecule enters the reaction layer at the membrane surface. In the reaction layer it dissociates into ${\rm H^+}$ and ${\rm OH^-}$ ions which are transported out of the reaction layer on opposite sides. The driving force for the water dissociation reaction is the difference in electrochemical potential between the reactants and the products. A consequence of the space separation of the ionic products of the water dissociation reaction is that the potential jump over the reaction layer enters the rate constants,

$$k_f^{'} = k_f^{'0} \exp\left(\frac{\alpha F}{RT} \Delta \phi_r\right) \tag{3.34}$$

$$k_b^{'} = k_b^{'0} \exp\left(-\frac{(1-\alpha)F}{RT}\Delta\phi_r\right)$$
 (3.35)

where α is a symmetry factor. $k_f^{'0}$ and $k_b^{'0}$ are the surface reaction rate constants at zero potential difference of the reaction layer. Using these rate constants for the overall reaction rate of the water dissociation gives

$$R_{s} = k_{f}^{'0} c_{H_{2}O} \exp\left(\frac{\alpha F \Delta \phi_{r}}{RT}\right) - k_{b}^{'0} c_{OH^{-}}^{m} c_{H^{+}} \exp\left(-(1-\alpha)\frac{F \Delta \phi_{r}}{RT}\right). \quad (3.36)$$

 R_s expresses the reaction rate per area and $\Delta\phi_r$ is the potential jump over the reaction layer. It is further assumed that that the reaction layer is so thin that Donnan equilibrium holds over it. Electroneutrality is also assumed to hold on both sides of the reaction layer. In the third paper this model is incorporated in a small model problem to study the influence of the model parameters on polarization curves. Finally the model is also incorporated in a model of electropermutation in the fourth article.

CHAPTER 4

Experimental Investigations

Nitrate removal

In the second of the appended articles an experimental investigation of nitrate removal by electropermutation is presented. All experiments were conducted with a five compartment cell similar to that shown in figure 2.2, except that the central compartment in some of the experimental cases presented was filled with an anion-exchange textile. Experiments were made with and without ion-exchange textile incorporated in order to test the influence of the textile as a conducting spacer.

The ion-exchange textile used was developed within the EU-funded research project Iontex [7]. It is a non-woven felt made of cellulosic fibers with ion-exchange groups introduced by electro beam grafting. Before the textile was introduced into the cell it was washed carefully with deionised water to remove any excess chemicals remaining from the grafting process, and it was turned into chloride form by treating the textile with a sodium chloride solution. The Neosepta standard grade ion-exchange membranes AMX and CMX from Tokuyama Soda were used to separate the compartments. The characteristics of the textile and membranes used are given in table 4.1.

	Textile	AMX	CMX
Type	Anion exchange	Anion permeable	Cation permeable
	Textile	membrane	membrane
Thickness [mm]	3.0-3.3	0.16-0.18	0.17-0.19
Capacity [meq/g]	0.5-0.7	1.4-1.7	1.5-1.8

Table 4.1. Properties of ion-exchange textile and membranes used.

A DSA[®] electrode, titanium coated with iridium-oxide, was used as anode and a nickel electrode as cathode. In figure 4.1 a photo of the experimental setup used for the experiments is presented and in figure 4.2 a photo of a textile filled compartment is shown. The frames used to incorporate the ion-exchange textile were developed as part of the Iontex project and are used together with electrode compartments taken from the ElectroSynCell [37, 38, 39]. The feed and concentrate compartments were 3 mm thick. In the compartments where

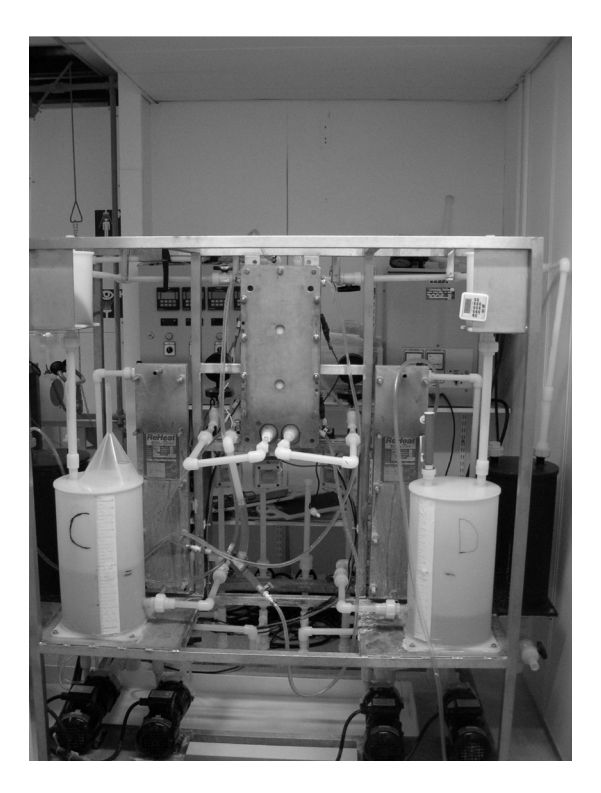


FIGURE 4.1. The experimental setup used to investigate the continuous electropermutation process.

the textile was not incorporated Net-type (PE) spacers were used to provide mechanical support to the membranes. Each compartment was 0.28 m in the streamwise direction and 0.15 m wide giving an active membrane area of 0.04 m².

A solutions containing a 1.7 mM sodium nitrate was prepared from deionized water and was used as feed solution. This corresponds to a nitrate level of 105 ppm, which is well above the regulated upper limit of 50 ppm nitrate in drinking water. In the electrode compartments a 0.3 M sodium sulphate solution was recirculated and the initial solution circulated through the concentrate compartment was a 0.2 sodium chloride solution. The experiments were performed in a single pass mode of operation. Samples were taken from the product stream, from the concentrate container and from the container with the electrode rinse solution at steady state. It was found that at least 30 min of operation was needed to reach steady state. The concentrations of nitrate, chloride and sulphate were determined by ion chromatography, using the Dionex Ag17 and As17 columns, and pH was measured with a pH-electrode from Radiometer. The total voltage applied and the current density passed between the electrodes was recorded.

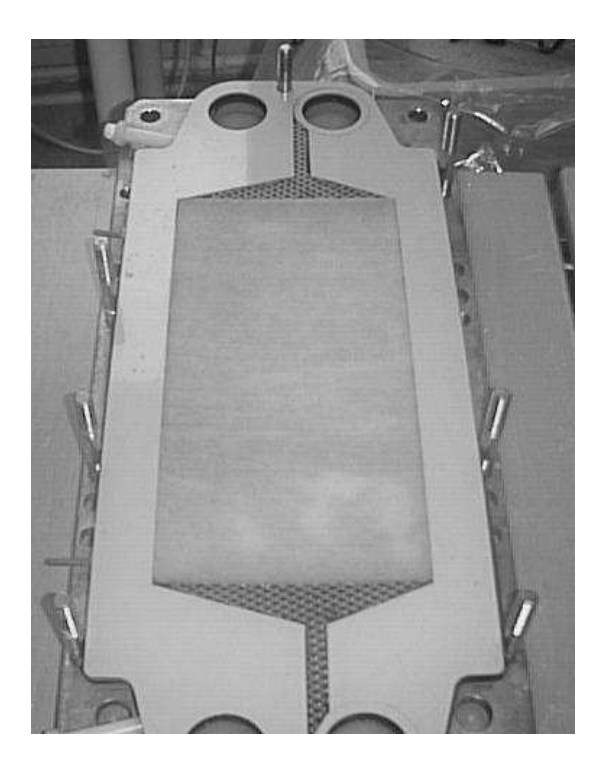


FIGURE 4.2. Photo of the developed frame. An ion-exchange textile is incorporated as spacer and net-type spacers are placed in the inlet and outlet sections.

The current was varied between 0 and 1 A corresponding to an average current density of 0 up to $25~\mathrm{A/m^2}$. The pressure drops over the feed and concentrate compartments were adjusted so that the same flow rate was obtained with and without textile. In order to ensure that sufficient contact was established between the textile and the membranes some experiments were conducted with an increased pressure in the concentrate compartment. The idea behind this was to press the membranes against the textile.

Characterization of textile

In the model there are a number of parameters that characterize the properties of the textile. The textile manufacturer gave information about some of these, such as the ion-exchange capacity. Values of other parameters were estimated. Here two experiments conducted as to get information about the characteristics of the textile material are described.

Permeability

The hydrodynamic resistance of a textile filled compartment was chosen as an important design parameter of the textile. High resistance for the flow

increases the power consumption for forcing a flow through the cell. A high pressure needs to be applied, which increases the risk for leakage problems.

The flow through the textile can be described as a flow through a fibrous porous media described by Darcy's law.

$$\mathbf{u} = -\frac{K}{\mu} \nabla P \tag{4.1}$$

where K is the permeability of the textile, μ is the dynamic viscosity of the fluid, \mathbf{u} is the superficial average of the fluid velocity vector and ∇P is the pressure gradient.

The permeability of the textile depends on characteristics of the fibers and on the structure of the fibrous network such as the orientation of the fibers. Empirical correlations found in the literature, for fibrous porous media with fibers of circular cross section, reveals that the permeability mainly depends upon two characteristic features of the textile, the porosity and the fiber diameter [40]. In the fourth appended article the following expression for the permeability is used [41],

$$K = \frac{3d_f^2}{20\epsilon} [-\ln(\epsilon) - 0.931]. \tag{4.2}$$

where d_f is the diameter of the fibers and ϵ is the porosity of the textile. This correlation has been compared to computer simulations of fluid flow through a small representative volume element of a fiber network and found to give a good prediction of the permeability for low porosities [42, 43].

The permeability of different textile samples was determined by measuring the flow rate through a textile bed as a function of the pressure drop. In figure 4.3 the flow rate versus pressure drop is plotted for three different textile samples. It was found that the permeability of the textile bed was closely related to the density of the textile. The lower the density the higher the permeability. Textiles with low density and very thin textile showed very poor mechanical stability properties. Hence it was decided that a textile with a density of about $150~{\rm kg/m^3}$ and a thickness of at least 3 mm should be used to ensure that high permeability, $K{=}O(10^{-10})~{\rm m^2}$, is combined with a sufficient mechanical stability.

Conductivity of fiber bed

The conductivity of the ion-exchange textile is influenced by the ionic mobilities in the fiber phase, the conductivity of the liquid phase and the structure of the fiber network. By measuring the conductivity of the ion-exchange textile as a function of the interstitial solution the assumption about the diffusion coefficient in the first and fourth article could be checked. These measurements also provided additional information about the arrangement of the phases in the textile, which could be useful for future improvements of the theoretical treatment of the mass transfer through the ion-exchange textile.

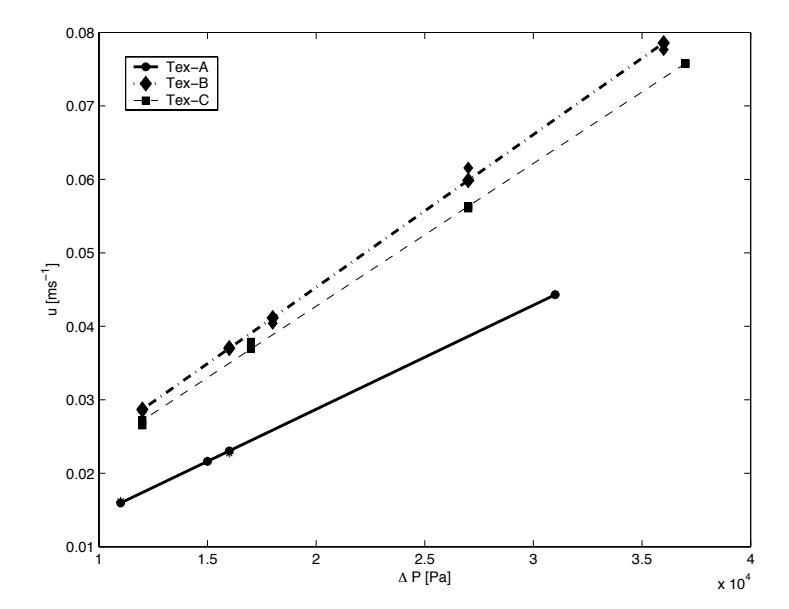


FIGURE 4.3. The flow rate as a function of pressure drop. The slope of the curves are given by $\frac{K}{\mu L}$, where K is the permeability of the textile, μ is the dynamic viscosity of water and L is the streamwise length of the textile sample. In the figure above $K_A = 2.1 \cdot 10^{-10} \, [\text{m}^2]$, $K_B = 3.1 \cdot 10^{-10} \, [\text{m}^2]$ and $K_C = 2.9 \cdot 10^{-10} \, [\text{m}^2]$

Since both phases are conductive the current density can pass from one phase to the other. The fluxes in the two phases of the porous media will in general not be independent of each other. Basically there are three different routes through the bed by which the ions can be transported:

- 1) Alternating through the liquid and the solid phase
- 2) Only through the solid phase
- 3) Only through the liquid phase

These are illustrated in the left of figure 4.4. The influence of the connectivity of the phases and how that influences the path of the ionic fluxes through a bed of ion-exchange material has been discussed several times in the literature [8, 44, 45, 46, 47, 48]. Spiegler *et.al* introduced the porous plug model. In this model five different parameters denoted A-E as shown to the right in figure 4.4 are used to describe the flux through the bed. To determine these parameters the conductivity of the bed as a function of the conductivity of the interstitial solution has to be measured.

In order to measure the conductivity of the textile bed a four electrode cell, as illustrated in figure 4.5, was constructed in plexiglas. A pice of anion-exchange textile was placed in the cell together with a solution with known

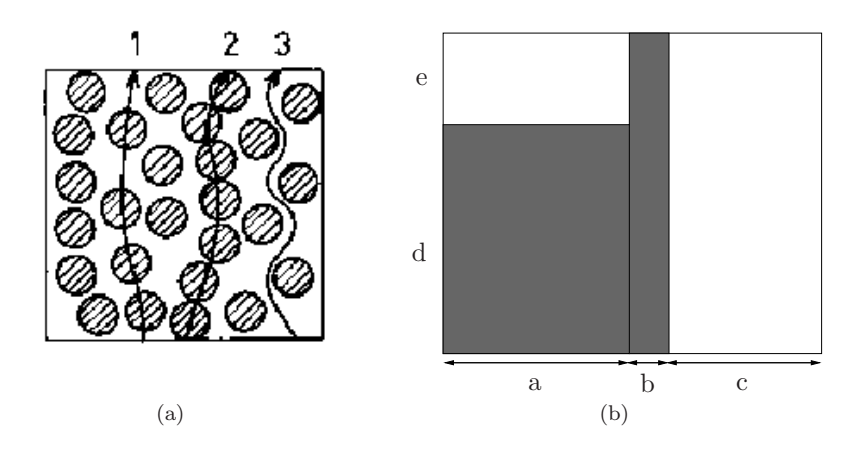


FIGURE 4.4. Schematic of the charge transport through a bed of solid ion-exchange material and liquid electrolyte [44].

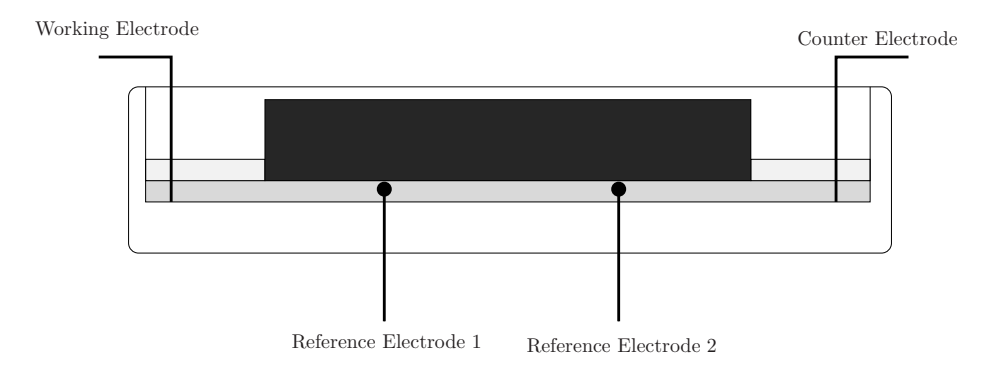


FIGURE 4.5. A drawing of the cell used to measure the conductivity of the textile bed as a function of the conductivity of the interstitial solution.

conductivity. The conductivity was measured by a four electrode impedance spectroscopy setup using a Gamry PCI4/750 potentiostat. To make sure that the current passed through the textile bed in between the two reference electrodes a light plexiglas block was placed on top of the central part textile, seen as the black box on top of the textile in figure 4.5. On the sides of this plexiglas block the electrolyte level was well above the textile, which ensured that the pores of the textile was completely filled. The distance between the reference electrodes was 50 mm, the textile piece was 30 mm wide and 3.5 mm thick.

In figure 4.6 the conductivity of an anion-exchange textile bed as a function of the conductivity of the interstitial sodium chloride solution is presented. If the capacity and volume fraction of the ion-exchange textile are known the result in figure 4.6 can be used to calculate the diffusion coefficient of chloride

in the fiber phase. The iso-conductance point, i.e. where the bed has the same

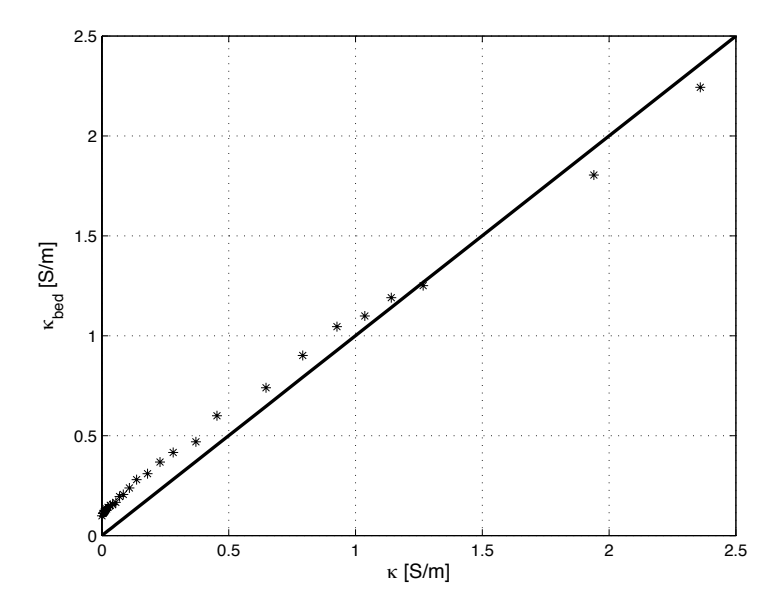


FIGURE 4.6. Bed conductivity as function of conductivity of the liquid phase. Textile in chloride form and liquid phase was a sodium chloride solution.

conductivity as the interstitial solution, is used to calculated the diffusivity in the ion-exchanger. In this point the interstitial conductivity is equal in both phases. Thus, the interstitial conductivity of the fiber phase, κ , in chloride form is obtained. From the expression for $\bar{\kappa}$ given by,

$$\bar{\kappa} = \frac{F^2}{RT} \bar{D}_{Cl} - \bar{c}_{Cl}, \qquad (4.3)$$

the diffusion coefficient for chloride in the fiber phase can be calculated. From the measurements presented in figure 4.6, assuming that the concentration in the textile phase was about 700 mM, the diffusion coefficient for chloride in the fiber phase was determined as $\bar{D}_{Cl^-}=4.8\cdot 10^{-10}m^2s^{-1}$. This is close to 25 % of the diffusivity in water. In the model presented in paper I and IV the diffusivity in the fiber phase was set to 15% of the value in the liquid phase.

The closure relations used in the model assumed that the liquid and fiber phases were in a parallel arrangement and that a Bruggeman relation gave the effective diffusion coefficients. This model predicts that the ratio between the conductivity of the textile bed at zero conductivity of the interstitial liquid phase and the conductivity at the iso-conductance point is given by,

$$\frac{\kappa_{bed}|_{\kappa=0}}{\kappa_{iso}} = \epsilon^{3/2}.\tag{4.4}$$

The volume fraction of fibers in the textile was estimated to be, $\epsilon=0.15$, and thus $\epsilon^{3/2}=0.06$. From the data presented in figure 4.6 it is found that $\frac{\kappa_{bed}|_{\kappa=0}}{\kappa_{iso}}=0.08$. Thus, the proposed model predicted this conductivity ratio rather accurately.

The values of the parameters in the porous plug model obtained when evaluating the data are presented in figure 4.6 are given in tabel 4.2. Further work

a	b	С	d	е
0.16	0.08	0.76	0.93	0.07

TABLE 4.2. Porous plug parameters determined from the experimental results presented in figure 4.6

is needed in order to investigate how the information about the connectivity of the textile material, given by the porous plug model, can be used to obtain better closure relations.

CHAPTER 5

Summary of Papers

In this chapter the appended articles are summarized.

Paper I

Nitrate Removal by Continuous Electropermutation using Ion Exchange Textile Part I: Modeling

Journal of The Electrochemical Society, 153(4) D51-D61, 2006

The aim of the work presented in the first paper was to gain some scientifically based theoretical knowledge about the electropermutation process, its possibilities and limitations. A feed compartment filled with an anion-exchange textile together with the adjacent anion permeable membranes are included in the model. The composition of the solution in the concentrate compartment was assumed to be known and constant through out the compartment. A schematic of the domain included in the model presented in the first paper is presented in figure 5.1. The textile is treated as a porous material. Mass balance equations are formulated for all ionic species included in the model in both the solid fiber phase and the liquid phase. Together with electroneutrality in both phases this forms the basis for the model. Since the exact geometry of the porous textile is unknown volume averaged macro homogeneous equations are formulated. This procedure was presented in chapter 3.

The model equations are analyzed and appropriate simplifications are motivated and introduced. One such simplification was the assumption of ion-exchange equilibrium between the two phases. This greatly reduced the number of differential equations that needed to be solved. A set of dimensionless parameters that need to be specified are identified. The influence of three of these dimensionless parameters on the electropermutation process is investigated through simulations.

 χ is found to be an important dimensionless parameter in the model,

$$\chi = \frac{\mathcal{V}}{\sigma^2 P e}.\tag{5.1}$$

Where $V = \frac{F\phi_0}{RT}$, $\sigma = \frac{h}{L}$ and $Pe = \frac{j_0L}{D_0}$. L is the length and h is the thickness of the feed compartment, ϕ_0 is the potential drop over the feed compartment and adjacent membranes, j_0 the linear velocity of the flow and D_0 is a typical diffusivity of the ions in water. The physical interpretation of χ is that it relates

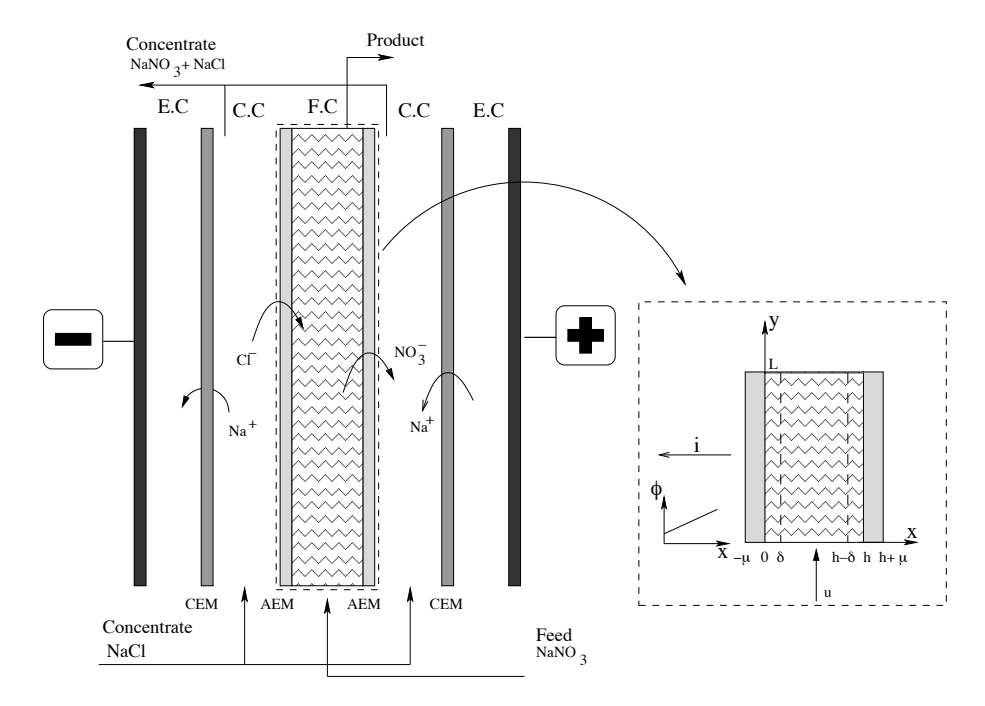


FIGURE 5.1. The domain included in the model presented in the first paper.

the ionic flux by migration, over the membranes, to the ionic flux by convection in the feed compartment. A parametric study of the influence of χ gives the optimal process conditions for a fixed equipment design.

Another dimensionless parameter whose influence on the process was investigated is

$$\Gamma = \frac{D_0^m c_0^m h}{D_0 c_{10} \mu \sigma^2 P e}. (5.2)$$

 D^m is a typical value for the diffusion coefficients in the membrane, c_0^m is the concentration of fixed charges in the membrane, μ is the thickness of the membranes and c_{10} is the nitrate concentration in the feed. The physical interpretation of Γ is that it relates the flux by diffusion through the membranes to the convective flux through the feed compartment. A high value of Γ indicates that no electric current need to be applied. The nitrate removal can then be achieved via Donnan dialysis; by a suitable choice of the composition of the concentrate solution. In figure 5.2 the concentration of nitrate in the product, scaled by the concentration at the inlet, is presented as a function of χ for three different values of Γ . It is clear that the nitrate level in the product decrease when χ is increased, approaching a lower limit asymptotically. Thus, the nitrate removal is improved by applying an external electric field. The results in figure 5.2 gives that the optimal χ value is approximately $\chi = 0.14$, where

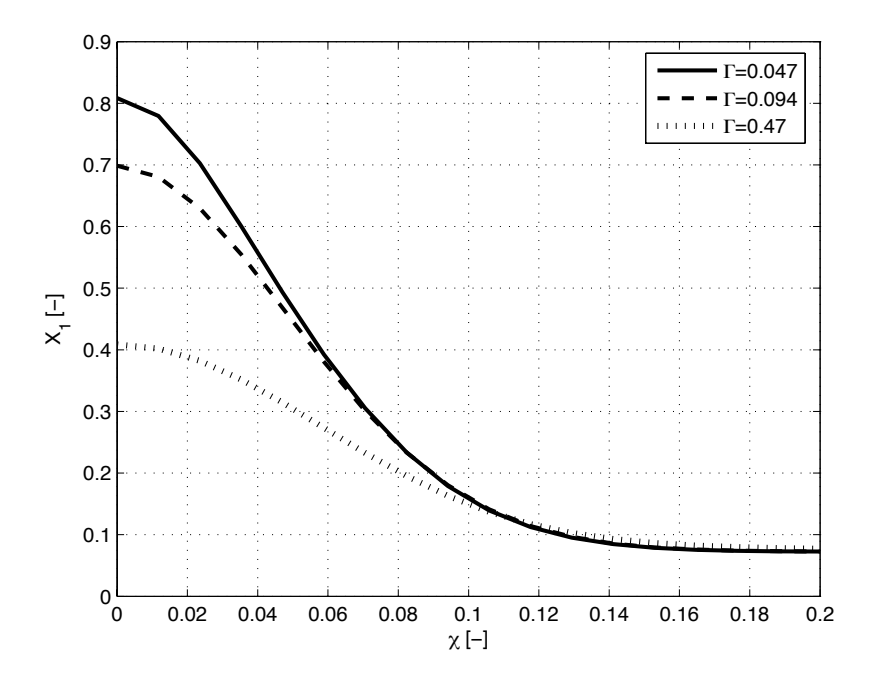


FIGURE 5.2. Nitrate concentration in the product as a function of χ obtained from simulations of continuous electropermutation. The different curves represent different values of the dimensionless number Γ as indicated in the figure. The value of Z in these simulations was 620.

the nitrate level is close to its limiting value, for all the three Γ values. The nitrate removal at low current densities differs for the different Γ values. A low Γ value corresponds to the case where the diffusion through the membrane is slow and hence the nitrate removal by Donnan dialysis decreases as the Γ value decreases. By applying an electric field the importance of diffusion is reduced and all the curves for different Γ values finally collapses on top of each other.

The third dimensionless number highlighted is,

$$Z = \frac{\omega}{c_{10}}. (5.3)$$

This is the ratio between the capacity of the textile, ω , and the nitrate concentration in the feed solution. In figure 5.3 the nitrate concentration in the product is presented as a function of χ for different values of Z. It is found that if the Z value is increased the optimal value of χ is reduced. If the dominating transport mechanism for nitrate through the feed compartment is through migration in the fiber phase one can conclude that the optimal operating conditions is given by a constant value of the product between χ and Z.

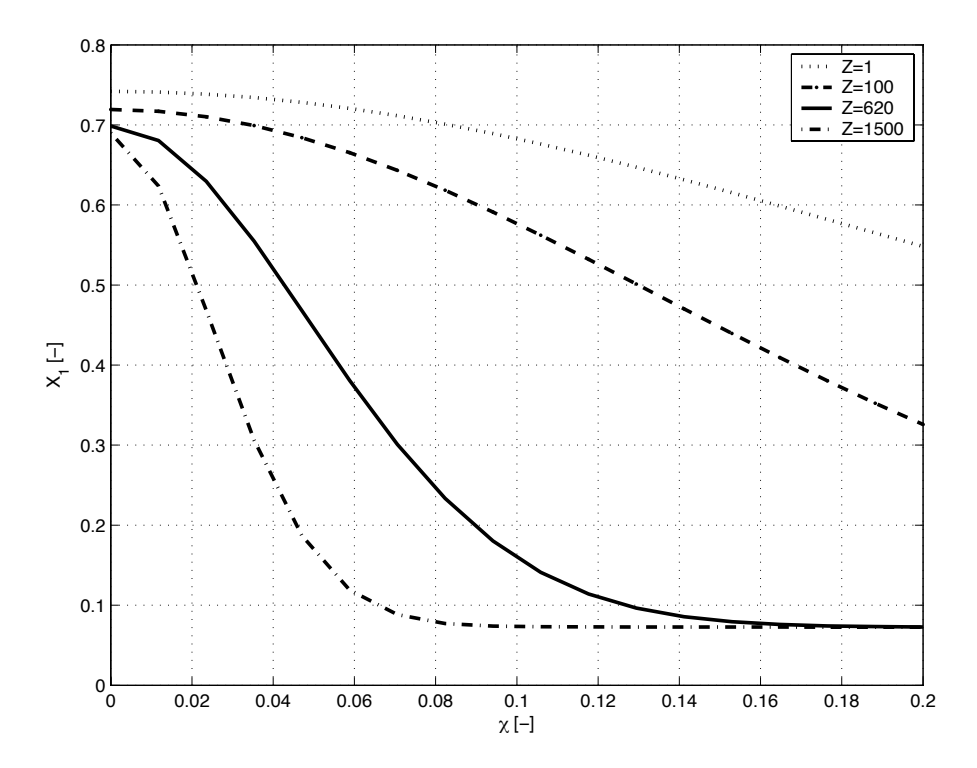


FIGURE 5.3. Concentration of nitrate in the product as a function of the dimensionless parameter χ , plotted for different values of the dimensionless parameter Z as indicated in the figure. The value of Γ in these simulations was 0.094.

Paper II

Nitrate Removal by Continuous Electropermutation using Ion Exchange Textile Part II: Experimental

Journal of The Electrochemical Society, 153(4) D62-D67, 2006

In the second paper an experimental investigation of nitrate removal by continuous electropermutation is presented. The influence of using an anion exchange textile as conducting spacer in the feed compartment was investigated by comparing experiments with and without the ion-exchange textile incorporated.

The experimental equipment and procedure was outlined in chapter 4. Five different experimental cases are discussed in paper II. Theses are denoted as cases A-E. The different cases and the separation obtained at zero current and at 25 $\rm A/m^2$ is presented in table 5.1 .The separation of nitrate was defined as the difference in nitrate concentration between product and feed normalized by

Cases	A	В	С	D	E
Spacer	Textile	Net-type	Textile	Textile	Net-type
ΔP F.C [bar]	0.17	0.13	0.15	0.30	0.10
ΔP E.C & C.C [bar]	0.17	0.13	0.25	0.40	0.20
Mean vel. in F.C [m/s]	0.017	0.017	0.004	0.012	0.012
$R_{NO_3^-}(0 \text{ A/m}^2)$	0.24	0.18	0.91	0.57	0.21
$R_{NO_3}^-(25 \text{ A/m}^2)$	0.35	0.29	0.97	0.86	0.40

TABLE 5.1. The experimental cases A-E presented in the second paper. F.C refers to feed compartment. E.C and C.C refer to electrode compartments and concentrate compartments respectively.

nitrate concentration of the feed,

$$R = \frac{C_{NO_3^-}(Feed) - C_{NO_3^-}(Product)}{C_{NO_3^-}(Feed)} \tag{5.4} \label{eq:5.4}$$

In the experiments without the ion exchange textile, cases B and E, a relatively poor nitrate removal could be obtained. Only a modest current density could be applied before the limiting current density was reached and water dissociation started to take place, which was indicated by a sudden drop in the pH of the product. Increasing the current density further only increased the dissociation of water and led to a very poor improvement of the nitrate removal.

In case A, a piece of textile was incorporated in the feed compartment. Despite this, it was not possible to reach very low nitrate levels in the product. It was believed that the reason for this was a poor contact between membrane and textile. This was supported by the similar results obtained with and without textile incorporated, i.e. cases A and B. One idea to reduce this contact problem was to increase the pressure in the concentrate compartments. This was tested in cases C and D. A much better nitrate removal was obtained in these experiments and it was concluded that it is essential to obtain good contact between the membranes and the ion exchange textile.

In figure 5.4 the pH of the product is presented as a function of the average current density for cases D and E. In case E, which is with a net-type spacer instead of a textile, the pH drops as the average current density is increased from 5 $\rm A/m^2$ to 10 $\rm A/m^2$. This indicates that the limiting current density in this case is located somewhere in this interval. In case D when an anion-exchange textile is incorporated the pH change is less even though the pH of the product at 25 $\rm A/m^2$ indicates that significant water dissociation is taking place in the feed compartment also in this case.

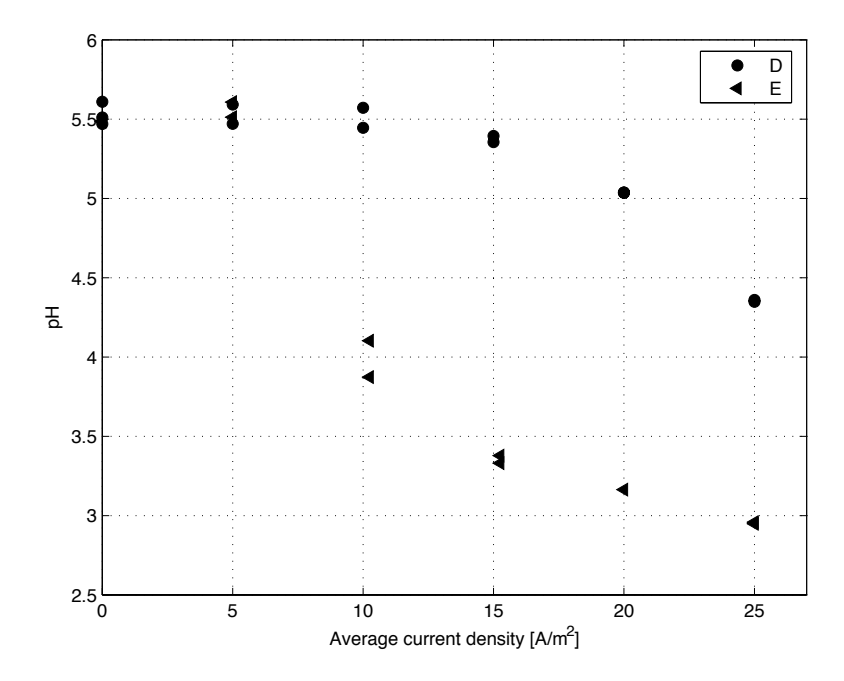


FIGURE 5.4. The pH of the product as a function of average current density for cases D and E.

Finally a comparison between the experimental results and the predictions obtained with the model presented in the first paper was made. In the model the potential drop over the membranes and the feed compartment was controlled in order to change the current density. In the experiments this potential drop could not be measured, instead the average current density passed through the cell was used to compare the model predictions with the experiments. As can be seen in figure 5.5 a good agreement between the model and the experiments was obtained.

Paper III

A Model for the Water Dissociation Taking Place at the Surface of a Monopolar Membrane.

To be submitted

The experiments presented in the second paper indicated that water dissociation became important in the electropermutation process also in the cases where an ion exchange textile was used as a conducting spacer. Water dissociation is an unwanted phenomenon in the electropermutation process and should be avoided if possible. Thus, it would be useful to be able to predict if,

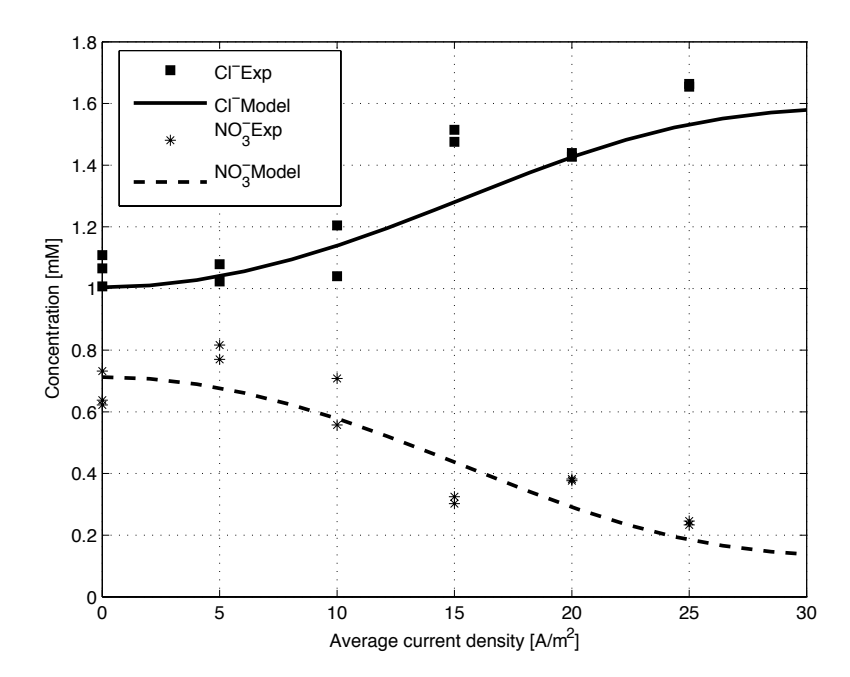


FIGURE 5.5. The model predictions for the outlet concentrations of chloride and nitrate plotted against the average current density together with the experimental results from case D.

when and where water dissociation could be expected to take place. The purpose of the third paper is to present a model of the enhanced water dissociation taking place at the surface of ion-exchange membranes. The model presented is not restricted to electropermutation but can also be implemented in models of other electromembrane processes.

An anion exchange membrane separating two infinitely large and perfectly mixed containers filled with a 1mM sodium chloride solution is considered. Next to the membrane on each side there are stagnant diffusion layer that are resolved in the model. This three layer model problem is reffered to as the Kharkat's problem [49] The potential difference over the membrane and the adjacent diffusion layers was varied in order to obtain polarization curves. A heterogeneous surface reaction is formulated to capture the enhanced water dissociation that can take place. The derivation of the expression for the surface reaction is presented in the article and a brief presentation was given in chapter 3.

Simulations were made to investigate the influence of the model parameters. In figure 5.6 examples of polarization curves are presented. The characteristic s-shape of the polarization reported from experiments in the literature [50, 51]

could be captured with the simple model. It was found that the rate of water dissociation increases with both increasing α and Υ values. If the reaction rate can be assumed to be sufficiently fast the rate of water dissociation is determined by the mass transfer of the produced ions away from the reaction layer. This is very convenient since the parameters Υ and α does not need to be determined as long as Υ is taken to be sufficiently large.

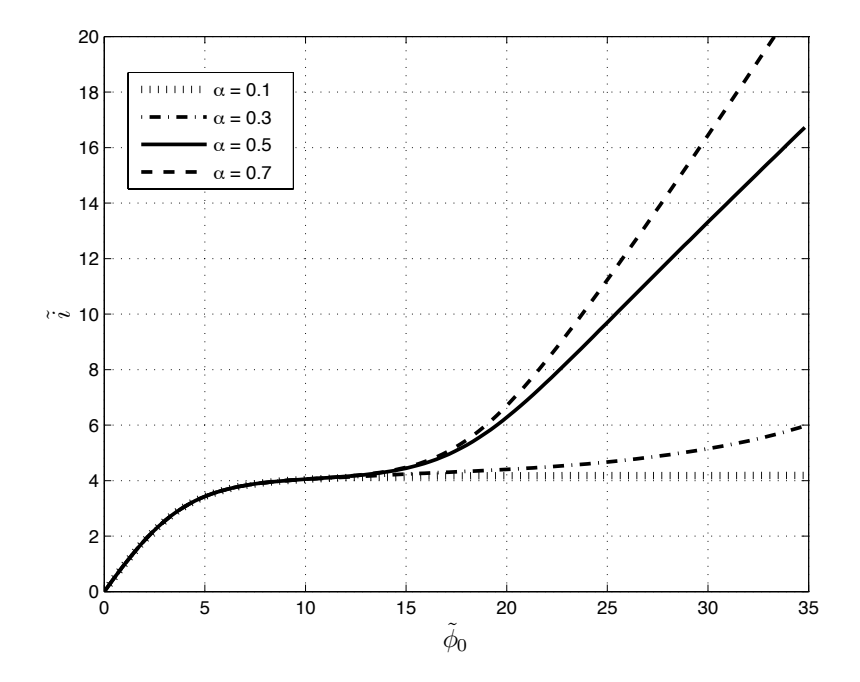


FIGURE 5.6. Current against voltage curves for different values of α . The Υ value in these simulations was 10^{-4} .

The enhanced water dissociation reaction, taking place at the membrane surface, makes the partial current carried by the ionic products of water, \tilde{i}_w , increase. The increased flux of H⁺ and OH⁻ also leads to an increased flux of the salt ions. This effect is known as the exaltation effect and was discovered by Kharkats [52]. In figure 5.7 the fraction of the current density carried by the salt ions and the products from the dissociation of the water molecules are presented. At very high current densities the fraction of the current carried by the salt ions asymptotically approaches 0.2 due to the exaltation effect [52].

Paper IV

A Model of Continuous Electropermutations with Water Dissociation Included.

To be submitted

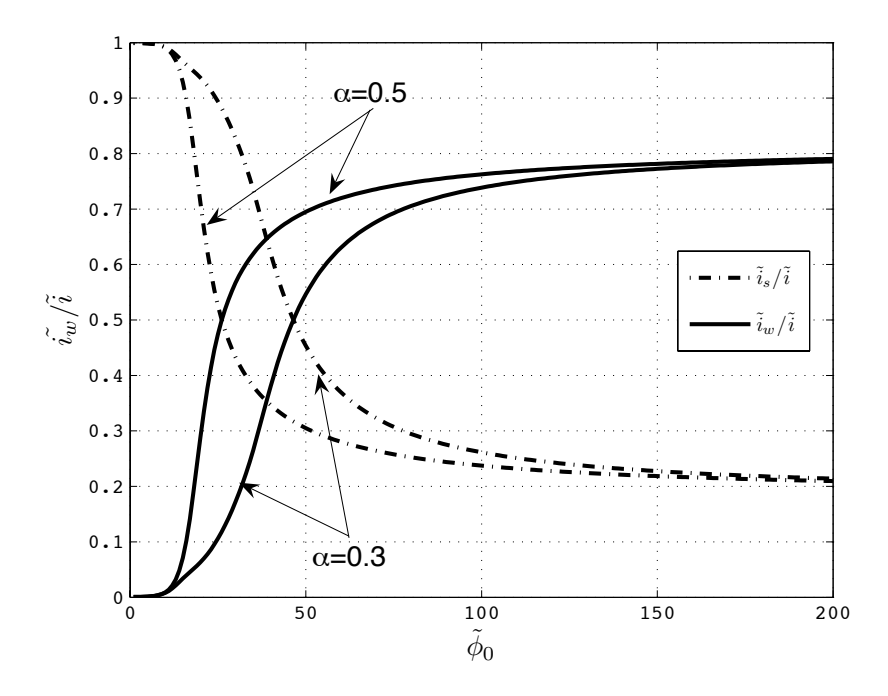


FIGURE 5.7. The fraction of the current carried by \tilde{i}_w and \tilde{i}_s as a function of $\tilde{\phi}_0$ for two different values of α . $\Upsilon=10^{-4}$ and $\gamma=10^{-4}$.

The aim of the fourth paper is to incorporate the model of the enhanced water dissociation, presented in the third article, into a model of continuous electropermutation. A whole repeating unit consisting of one concentrate and one feed compartment is included in the model domain. This makes the model of the continuous electropermutation more complete and a powerful tool that can be used to study the influence of water dissociation on the process efficiency and predict pH variations in the cell.

The model is first used to simulate the experimental results presented in paper two, both with and without ion exchange textile included in the feed compartment. This was done in order to test if the model was able to predict the change in pH of the product. In figure 5.8 the pH of the product as a function of the average current density passed through the cell is presented. The result obtained in the experimental cases D and E of the second paper are shown together with results obtained from simulations. Results from simulations of three different configurations corresponding to a conductive textile, a non-conductive textile and a non-conductive textile but with a reduced mechanical dispersion are presented in figure 5.8. It was found that the model could predict the drop in pH rather well, for the experimental cases where a

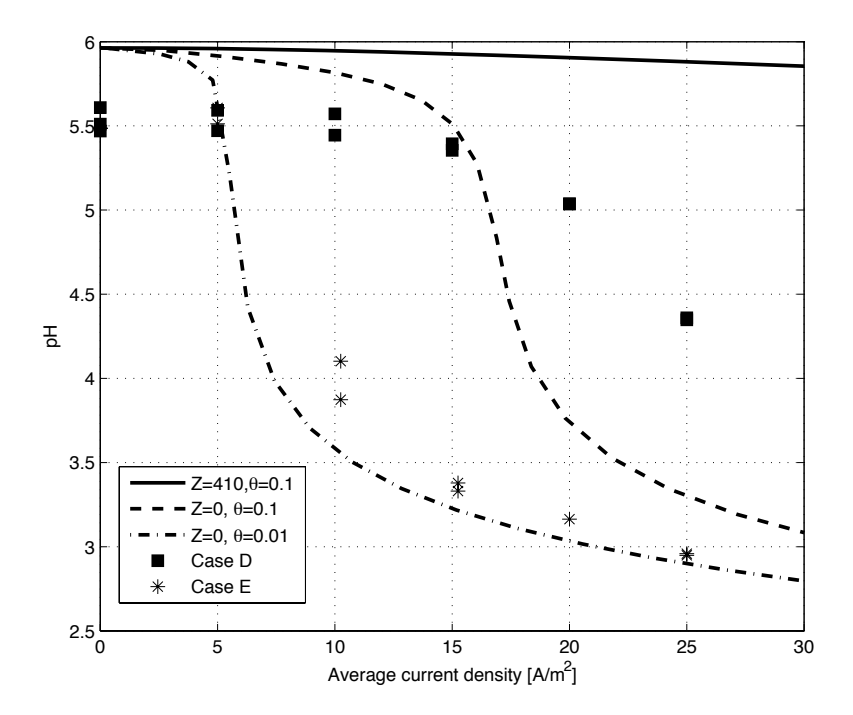


FIGURE 5.8. pH as a function of the applied current density. Comparison between simulations with different textiles and experimental results.

conductive spacer was not used. However, with the textile incorporated, the model did not predict the pH change obtained in the experiments. The reason for this is discussed, and the most likely explanation is that the contact between the textile and the membrane was not perfect in the experiments.

Then electroper mutation with a non-conductive textile as spacer in the feed compartment was investigated. This was done in order to point out the limitations of this process alternative. Only a very low current density could be applied before the limiting nitrate flux was obtained. Increasing the current further resulted in dissociation of water and as a result of this a dramatic change in pH. The effect of the water dissociation on the nitrate removal, product pH, current density distribution and pH distribution in both feed and concentrate compartments are discussed. In figure 5.9 the dimensionless nitrate concentration, averaged over the feed compartment thickness, is presented as a function of the streamwise coordinate for different values of χ . At low χ values the enhanced water dissociation can be neglected and the nitrate concentration drops though out the entire length of the feed compartment. For the highest

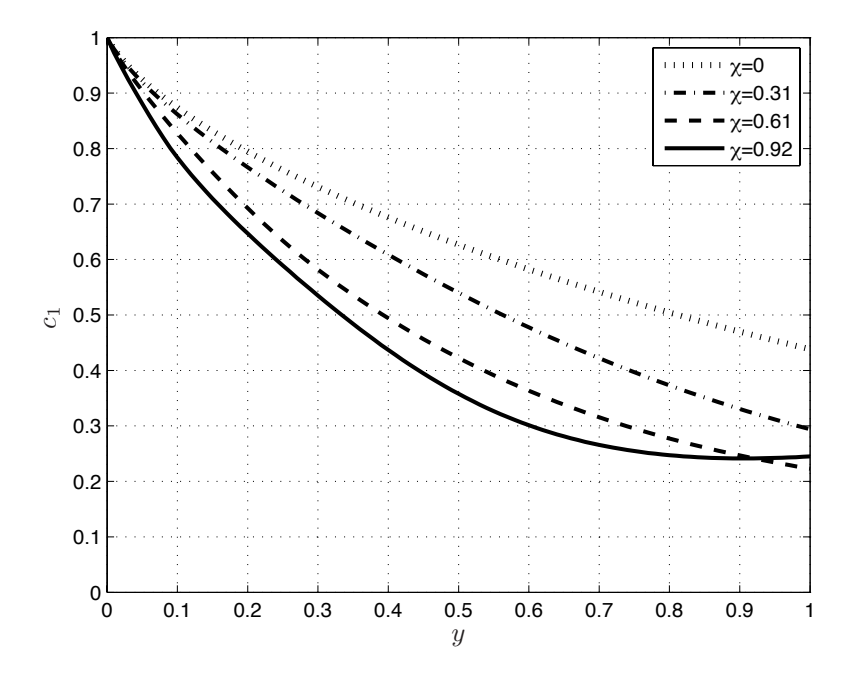


FIGURE 5.9. Nitrate concentration averaged over the F.C thickness as a function of streamwise coordinate. Theses curves were calculated for an inert textile, Z=0.

 χ value presented in figure 5.9 it is clear that nitrate level passes through a minimum inside the feed compartment.

To investigate the influence of a conductive spacer in the feed compartment simulations were performed with two different textile capacities. In figure 5.10 the nitrate concentration in the product scaled by the inlet concentration is presented as a function of χ for different values of Z, which is the capacity of the textile scaled with the nitrate concentration of the feed. It is clear that increasing the Z value leads to an improved more efficient nitrate removal. The optimal χ value is reduced when Z is increased in such a way that the product χ Z remains constant. Thus a higher Z value reduces the power consumption of the process by reducing the resistance of the feed compartment. The dissociation of water is reduced considerably by incorporation of a conductive textile. Very low levels on nitrate can be obtained when a conductive textile is used as the process can be operated at higher current densities. The inclusion of the conductive fibers transfers the mass transport limitation from the membrane surface to the much larger surface of the fiber phase.

The pH close to the membrane surface in the concentrate compartment was also investigated in the fourth article. It is known that metal hydroxides with

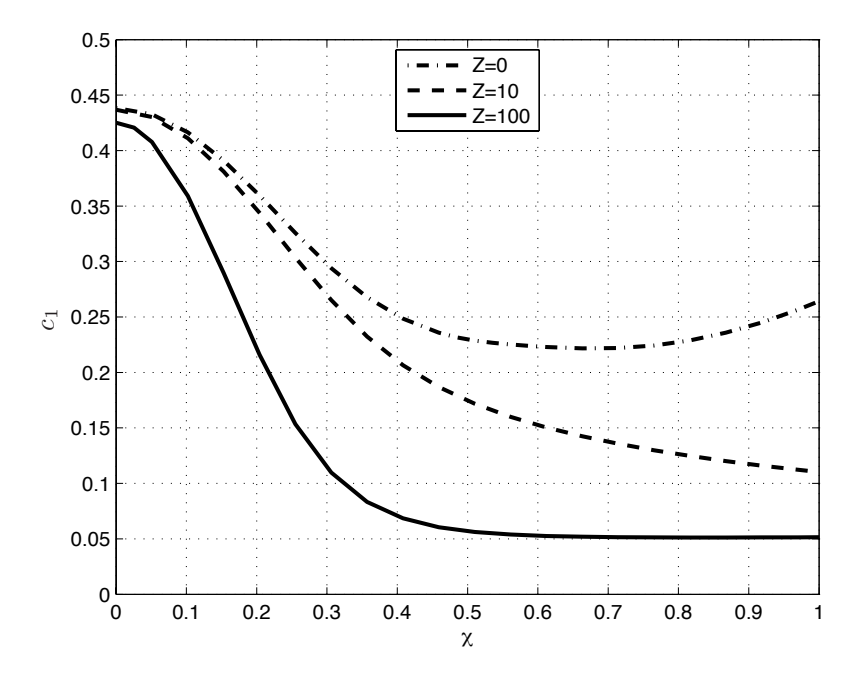


FIGURE 5.10. Nitrate concentration in the product as a function of the dimensionless parameter χ . Each line corresponds to a different textile capacity.

low solubility can precipitate and foul the membrane if the local pH becomes to high. Simulations, which allow the enhanced water dissociation to be captured, can be used to predict if such problem could be expected.

CHAPTER 6

Concluding Discussion and Outlook

Concluding Discussion

Nitrate removal from drinking water by electropermutation assisted by ion-exchange textiles has been investigated. The main advantage using the ion-exchange textile as conducting spacer is that the sheet shaped form of the textile makes it easy to assemble the electropermutation cell. Furthermore, the non-woven structure makes it possible to construct very porous structures with high permeability giving a low pressure drop over the feed compartment. These two features makes it possible to construct an electropermutation equipment in which the membranes and textiles could easily be replaced. This would extend the lifetime of the electropermutation cell and thereby reducing the investment cost.

A macro-homogeneous steady state model for nitrate removal by electropermutation assisted by ion-exchange textile as conducting spacer has been developed. The macro-homogeneous equations were obtained by taking the volume averages of the governing equations at the microscopic level. To obtain expressions for the macro-homogeneous fluxes it was assumed that the two phases that contribute to the mass transfer are in a parallel arrangement. The model equations were analyzed and appropriate simplifications were identified. The slender geometry of the domain was used to simplify the equations. The relatively small diameter (10 μ m) of the fibers in a typical ion-exchange textile made it possible to assume ion-exchange equilibrium between the phases.

From the experimental investigation it was concluded that a significant increase in the nitrate removal is obtained by using the ion-exchange textile, as conducting spacer. From an initial nitrate concentration of 1.7 mM in the feed water a product stream with 0.25 mM of nitrate could be obtained in a single pass mode of operation with an applied current density of $25 \, \text{A/m}^2$ and a flow velocity of $1.2 \, cm/s$. The nitrate level in the product stream was well below the limiting value of 50 ppm for drinking water and also under the recommended maximum level of 25 ppm of nitrate [2, 4]. The flow rate used corresponded to a production capacity of $20 \, \text{l/h/unit}$ cell. A stack with 50 elementary cells would, thus, be able to treat 1 m³ of water per hour. Nitrate removal from drinking water by ion-exchange assisted electropermutations has been shown to be an interesting alternative to conventional ion-exchange and electrodialysis. However, before one can put the ion-exchange assisted electropermutation

process for nitrate removal on the market, long time pilot experiments need to be conducted. The economy of the process needs to be evaluated and the reliability of the process tested on real ground waters.

The contact problem between the ion conducting spacer and the membranes was discovered during the experimental investigation of the process. If the contact was insufficient a poor nitrate removal was accomplished at the same time as intense water dissociation took place when the current density was increased. Increasing the pressure in the concentrate compartment reduced the contact problem. However, also in this case signs of intense water dissociation taking place were found at high current densities, in the form of low pH of the product water. In order to predict if, when and where enhanced water dissociation could be expected to take place, it was decided to include this effect in our model. Since, the actual mechanism behind the enhanced water dissociation is not fully understood a semi-empirical approach was taken for the model. Thus, a model that incorporated the enhanced water dissociation in the form of a heterogeneous surface reaction was formulated. One advantages of this was that it could rather easily be incorporated into the model of electropermutation that had already been developed.

A very powerful tool for investigating electropermutation processes with and without conducting spacer in the feed compartment was obtained by incorporating the enhanced water dissociation into the model. The model can be used to design the equipment as well as optimizing the operating conditions. Simulations performed with an ion-exchange textile incorporated into the feed compartment did not predict the change in pH as was obtained in the experiments. The most likely explanation for this is that the ideal contact between spacer and membrane assumed in the model was not established during the experiments. New experiments with reference electrodes located in the concentrate compartments should be carried out. This would provide more data that can be used to validate the models. Experiments should also be conducted as to try to determine the parameters of the enhanced water dissociation model.

One of the main conclusions of the work presented in this thesis is that the contact between the ion-conducting spacer and the membranes is very important for the performance of the process. In the experimental investigation it was found that the nitrate removal could be enhanced if the process was operated with a higher pressure in the concentrate compartments than in the feed compartment. This is however not a very elegant solution. CEDI equipments used for production of ultrapure water should be operated with a higher pressure in the dilute compartment in order to reduce problems with convective transport of impurities into the dilute compartment through the membranes. Instead one would like to find a way to "glue" to textiles against the membranes or at least against the membrane close to which the concentration in the liquid phase becomes very low. In the dilute compartment of an CEDI equipment the concentrations becomes very low at both membranes but then one would like the cation-exchange spacer to be attached to the cation permeable membrane and

vice versa. Ideal contact between the textile and the membranes makes it possible to operate the process at higher current densities. This would mean that thicker feed compartments could be considered, which would not only increase the production per membrane area, but it would also make the construction of equipment easier. If thicker frames were used, o-rings could be used to seal against the membranes, which would make the construction more reliable.

Extending the model as to be able to simulate continuous electrodeionisation would be an interesting step to take. Simulating layered bed CEDI would be rather straightforward with the model developed during the work presented in this thesis. Including the effect of the enhanced water dissociation would make it possible to capture the local pH within the dilute compartment of the CEDI cell. It would then be possible to investigate how the local pH within the compartment is affected by the configuration of the layered bed. The separation of weak acids in a CEDI cell would also be possible to study with such a model. There are several industrial applications where the separation of weak acids from dilute solutions is of great importance.

Ion-exchange assisted electromembrane processes are very interesting process alternatives when it comes to treating dilute solutions. In this thesis the main application in focus has been removal of nitrate from drinking water. There are numerous of other applications where these techniques show a great potential. Discharge of harmful substances can be reduced and expensive process chemical recovered. In order to develop the technique further there is a need for better theoretical understanding of the mechanisms involved and how they interact. The work presented in this thesis has been focused on the theoretical description of the electropermutation process, and hopefully the models presented can be used to develop the electromembrane devices of the future.

Acknowledgment

This work was financed by the VINNOVA competence center, FaxénLaboratoriet, with the main industrial partner in this project being Vattenfall AB.

I would like to thank my supervisors Docent Anders Dahlkild, Dr. Anna Velin and Dr. Mårten Behm for giving me the opportunity to work on this project. You have generously shared your knowledge, guided me through the work and believed in my ability for which I am greatly indebted. I appreciate the optimism and high spirit that have prevailed during our meetings.

The Iontex partners are greatly acknowledged. I want to thank them for all the exciting and interesting meetings.

I want to thank all my colleagues at the department for providing a good working atmosphere and interesting discussions during the coffee breaks.

The time spent in VUAB's electrochemistry lab would not been as enjoyable without the people working there. *Bosse*, thanks for helping me with the analysis and for all the interesting food which made the lunches at the lab ever so interesting. I also wish to thank *Anna*, *Noemi*, *Jinjin*, *Anders*2*, *Stefan* and *Leif*.

Prof. Fritz Bark, Prof. Gran Lindberg, Dr. Ann Cornell and everybody involved are acknowledged for their work with the electrochemistry group within FaxénLaboratoriet. I have appreciated the meetings with this group, which I think have been a good forum for discussing various problems.

Bernt Bengtsson at Ringhals has taught me about all kinds of plausible applications for the CEDI technology at a nuclear power plant. He also arranged for me so that I could spend some time at Ringhals to do some experimental work, for this I am very grateful. I also would like to thank Pernilla Svanberg and all the people at the chemistry group for reactor 1 and 2 at Ringhals, for helping me with analyzing my samples and for providing a friendly working atmosphere.

I would also like to thank all of my friends and family for their love and support.

Last but not least. Elin and Tage, thank you for all your love and support. Jag Älskar Er!

Bibliography

- A. Hult. Dricksvattensituationen i sverige. Technical report, VAV AB, 1998. 91-89182-11-1.
- [2] Council directive of 3 november 1998. Official J.Europ.Commun., L330, 05/12/1998 P. 0032 0054, 1998.
- [3] K. Kesore, F. Janowski, and V.A. Shaposhnik. Highly effective electrodialysis for selective elimination of nitrates from drinking water. *Desalination*, 127:17–24, 1997.
- [4] WHO. Guidlines for drinking water quality; recomendations i, geneva, 2004. 3rd Edition.
- [5] A. Kapoor and T. Viraraghavan. Nitrate removal from drinking water review. *Journal of Environmental Engineering*, pages 371–380, June 1997.
- [6] K. Salem, J. Sandeaux, J. Molnat, R. Sandeaux, and C. Gavach. Elimination of nitrate from drinking water by electrochemical membrane processes. *Desalination*, 101:123–131, 1995.
- [7] H. Schoebesberger, M. Einzmann, J. Schmidtbauer, P. Gayrine, and R. Martinetti. Iontex-viscose fibers with ion exchange properties. *Chemical Fibers International*, 54(2):101–111, Apr 2004.
- $[8]\ {\rm F.\ Helfferich}.\ Ion\ Exchange.\ Dover,\ 1995.\ ISBN\ 0-486-68784-8.$
- [9] M.S. Mintz. Electrodialysis, principles of process design. Industrial and engineering Chemistry, 55(6):18–28, June 1963.
- [10] S. Ezzahar, A. Cherif, J. Sandeaux, R. Sandeaux, and C. Gavach. Continuous electropermutation with ion-exchange textiles. *Desalination*, 104:227–233, 1996.
- [11] N. Kourda. lectropermutation sur textiles changeurs de Cations. PhD thesis, Universitet Montpellier II, 2000.
- [12] K. Basta, A. Aliane, A. Lounis, R. Sandeaux, J. Sandeaux, and C. Gavach. Electroextraction of Pb²+ ions from diluted solutions by a process combining ion-exchange textiles and membranes. *Desalination*, 120:175–184, 1998.
- [13] A. Smara, R. Delimi, C. Poinsignon, and J. Sandeaux. Electroextraction of heavy metals from dilute solutions by a process combining ion-exchange resins and membranes. Separation and Purification Technology, 44:271–277, 2005.
- [14] M. Paidar, I. Rousar, and K. Bouzek. Electrochemical removal of nitrate ions in waste solutions after regeneration of ion exchange columns. *Journal of Applied Electrochem-istry*, 29:611–617, 1999.
- [15] H. Strathmann. Ion-Exchange Membrane Separation Processes. Elsevier, 2004. ISBN 0-444-50236-X.
- [16] M. Hichour, F. Persin, J. Molenat, J. Sandeaux, and C. Gavach. Fluoride removal from diluted solution by donnan dialysis with anion-exchange membranes. *Desalina*tion, 122(1):53–62, 1999.
- [17] M. Hichour, F. Persin, J. Molenat, J. Sandeaux, and C. Gavach. Fluoride removal from waters by donnan dialysis. Separation and Purification Technology, 18(1):1–11, 2000.
- [18] T. Ruiz, F. Persin, M. Hichour, and J. Sandeaux. Modelisation of fluoride removal in donnan dialysis. *Journal of Membrane Science*, 212:113–121, 2003.

- [19] F. Durmaz, H. Kara, Y. Cengeloglu, and M. Eroz. Fluoride removal by donnan dialysis with anion-exchange membranes. *Desalination*, 177(1-3):51–57, 2005.
- [20] K. Brajter and K. Slonawska. Separation of noble metals by donnan dialysis. Separation Science and Technology, 23(4-5):321–331, 1988.
- [21] W.R. Walters, D.W. Weiser, and L.J. Marek. Concentration of radioactive aqueous waste, electromigration through ion-exchange membranes. *Industrial and Engineering Chemistry*, 47(1):61–67, January 1955.
- [22] E. Glueckauf. Electro-deionisation through a packed bed. British Chemical Engineering, pages 646–651, Dec 1959.
- [23] G.C. Ganzi, Y. Egozy, A.J. Giuffrida, and A.D. Jha. Deionization-high purity water by electrodeionization Performance of the ionpure continuous deionization system. *Ultra*pure Water, 4(3):43–48, 1987.
- [24] G. C. Ganzi, A. D. Jha, F. DiMascio, and J. H. Wood. Electrodeionization therory and practice of continuous electrodeionization. *Ultrapure Water*, 14(6):64–68, 1997.
- [25] L.S. Liang and L. Wang. Continuous electrodeionization processes for production of ultrapure water. Semiconductor, Pure Water and Chemicals Conference, 2001.
- [26] F. DiMascio, J. Wood, and J.M. Fenton. Continuous electrodeionization production of high-purity water without regeneration chemicals. *The Electrochemical Interface*, pages 26–29, 1998.
- [27] M. Hong, P. Changsheng, S. Shaoxian, and D. Dayo. Electro-regeneration mechanism of ion-exchange resins in electrodeionization. Surface Review and Letters, 11(6):1–7, 2004.
- [28] S. Thate, N. Specogna, and G. Eigenberger. Electrodeionization, a comparison of different EDI concepts used for the production of high-purity water. *Ultrapure Water*, 16(8):42–49, 1999.
- [29] E. Dejean, E. Laktionov, J. Sandeaux, R. Sandeaux, G. Pourcelly, and C. Gavach. Electrodeionization with ion-exchange textile for the production pf high resistivity water: Influence of the nature of the textile. *Desalination*, 114:165–173, 1997.
- [30] E. Dejean, J. Sandeaux, R. Sandeaux, and C. Gavach. Water demineralization by electrodeionization with ion-exchange textiles. comparison with conventional electrodialysis. Separation Science and Technology, 33(6):801–818, 1998.
- [31] E. Laktionov, E. Dejean, J. Sandeaux, C. Gavach, and G. Pourcelly. Production of high resistivity water by electrodialysis. influence of ion-exchange textiles as conducting spacers. Separation Science and Technology, 34:69–84, 1999.
- [32] E. Dejean. Electrodesionisation Sur Textiles Echangeurs D'Ions. PhD thesis, Universitet Montpellier II, 1997.
- [33] J. S. Newman. Electrochemical Systems. Prentice Hall, 2nd edition, 1991. ISBN: 0-13-248758-6.
- [34] S. Whitaker. The Method of Volume Averaging. Kluwer Academic Publisher, 1999. ISBN 0-7923-5486-9.
- [35] R.B. Bird, W.E. Stewart, and E.N. Lightfoot. Transport Phenomena. Wiley, 2nd edition, 2002.
- [36] D. Petruzzelli, A. Kalinitchev, V. S. Soldatov, and G. Trivavanti. Chloride/sulfate ion exchange kinetics on fibrous resins. two independent models for film diffusion control. *Ind. Eng. Chem. Res.*, 34:2618–2624, 1995.
- [37] L. Carlsson, B. Sandegren, D. Simonsson, and M. Rihovsky. Design and performance of a modular, mulit-purpose electrochemical reactor. *J. Electrochem. Soc.*, 130(2):342, 1983.
- [38] L. Carlsson, H. Holmberg, B. Johansson, and A. Nilsson. Techniques of Electroorganic Synthesis Part III, N.L. Weinberg & B.V. Tilak, chapter III. John Wiley & sons, 1982.
- [39] C. Bengoa, A. Montillet, P. Legentilhomme, and J. Legrand. Flow visualization and modelling of a filter-press type electrochemical reactor. *Journal of Applied Electrochem-istry*, 27:1313–1322, 1997.
- [40] F.A.L. Dullien. Porous Media, Fluid Transport and Pore Structure. Academic Press, 2nd edition, 1992.

- [41] G.W Jackson and D.F James. Permeability of fibrous porous media. Can. J. Chem. Eng., 64:364–374, 1986.
- [42] D. S. Clague, B. D. Kandhai, R. Zhang, and P. M. A. Sloot. Hydraulic permeability of (un)bounded fibrous media using lattice boltzmann method. *Physical Review E*, 61(1):616–625, January 2000.
- [43] A. Koponen, D. Kandhai, E. Hellén, A. Hoekstra, M. Kataja, K. Niskanen, P. Sloot, and J. Timonen. Permeability of three-dimensional random fiber webs. *Physical Review Letters*, 80(4):716–719, 1998.
- [44] K.S. Spiegler, R.L. Yoest, and M.R.J. Wyllie. Electrical potentials across porous plugs and membranes, ion-exchange resin-solution systems. *Disc. Faraday. Soc.*, 21:174, 1956.
- [45] K. Vuoriletho and A. Tamminen. Application of a solid ion-exchange electrolyte in threedimensional electrodes. *Journal of Applied Electrochemistry*, 27:749–755, 1997.
- [46] K.H. Yeon, J.H. Seong, S. Rengaraj, and S.H. Moon. Electrochemical characterization of ion-exchange resin beds and removal of cobalt by electrodeionization for high-purity water production. Separation Science and Technology, 38(2):443–462, 2003.
- [47] K.H. Yeon and S.H. Moon. A study on removal of cobalt from primary coolant by continuous electrodeionization with various conducting spacers. Separation Science and Technology, 38(10):2347–2371, 2003.
- [48] J.H. Song, K.H. Yeon, J. Cho, and S.H. Moon. Effects of the operating parameters on the reverse osmosis-electrodeionization performance in the production of high purity water. Korean J. Chem. Eng., 22(1):108–114, 2005.
- [49] V.I. Zabolotskii, V.V. Nikonenko, N.M Korzhenko, R.R Seidov, and K.Kh. Urtenov. Mass transfer of salt ions in an electromembrane system with violated electroneutrality in the diffusion layer: The effect of a heterolytic dissociation of water. *Russian Journal* of *Electrochemistry*, 38(8):810–818, 2002.
- [50] I. Rubinstein and B. Zaltzman. Electro-osmotically induced convection at a permselective membrane. Physical Review E, 62(2):2238–2251, 2000.
- [51] M. Taky, G. Pourcelly, F. Lebon, and C. Gavach. Polarization phenomena at the interfaces between an electrolyte solution and an ion exchange membrane part I. ion transfer with a cation exchange membrane. J. Electroanal. Chem., 336:171–194, 1992.
- [52] Yu. I. Kharkats. The mechanism of supralimiting currents at ion-exchange membrane electrolyte interfaces. Soviet Electrochemistry, 21:917–920, 1985.

Paper 1



Nitrate Removal by Continuous Electropermutation Using Ion-Exchange Textile

I. Modeling

Carl-Ola Danielsson, a,z Anders Dahlkild, Anna Velin, and Mårten Behma,*

^aFaxénLaboratoriet, Royal Institute of Technology, Stockholm, Sweden ^bVattenfall Utveckling AB, Stockholm, Sweden

This paper presents a steady-state model of the feed compartment of an electropermutation cell, used for nitrate removal, with ion exchange textiles incorporated as a conducting spacer. In the model the ion-exchange textile is treated as a porous medium and volume averaging is applied to obtain a macrohomogeneous two-phase model. The ion-exchange between the two phases is modeled assuming that the rate-determining step is the mass-transfer resistance on the liquid side of the phase interface. Analysis of the model equations reveals appropriate simplifications. The influence of the governing dimensionless numbers is investigated through simulations based on the model.

© 2006 The Electrochemical Society. [DOI: 10.1149/1.2170597] All rights reserved.

Manuscript submitted April 7, 2004; revised manuscript received December 13, 2005. Available electronically February 22, 2006.

Excessive use of fertilizers in agricultural activities has led to increased nitrate concentration in ground and surface waters. According to the *Guidelines for Drinking Water Quality* published by the World Health Organization, ¹ the nitrate level in drinking water should not exceed 50 ppm, and within the European Union there is a recommendation for less than 25 ppm² of nitrate in drinking water.

Nitrate can be removed from drinking water in a number of different ways; examples of such are biological treatment, ion exchange, reverse osmosis, electrodialysis, Donnan dialysis, and electrodeionization. Among these the membrane techniques appear to be the most suitable.³ Continuous electropermutation⁴ is an electromembrane process, which so far has not been considered for nitrate removal. The principle of continuous electropermuation is illustrated in Fig. 1, which shows a schematic of a setup with one feed compartment (FC), two concentrate compartments (CCs), and two electrode compartments (ECs). Two anion-permeable ion-exchange membranes delimit the FC. The feed water is passed through the FC. Under the influence of an applied electric field the anions in the cell migrate toward the anode. The anions present in the FC migrate over to the CC located on the anode side at the same time as they are replaced by anions coming from the CC on the cathode side of the FC. This way it is possible to replace the ions initially present in the feed by anions from the concentrate solution while the cations are preserved. In the schematic presented in Fig. 1 the nitrate ions migrate out of the FC over the right side membrane at the same time as chloride ion enters the FC over the left side membrane. The solution in the concentrate compartment in this example is a concentrated sodium chloride solution. Depending on the quality of the feed water the concentrate solution can be tailored, adjusting, for example, the pH by replacing the nitrate ions partially with hydroxide.

The low conductivity of the feed water may lead to a high voltage drop over the FC and hence, a high power consumption. Concentration polarization increases the power consumption even further and will lead to a limiting current density. Hence, to accomplish sufficient separation one might be required to operate at a low feed flow rate and/or use very large equipment together with a moderate dc current. To overcome the difficulties associated with the poor conductivity of the feed water the central compartment is filled with an ion-conducting medium. This ion-conducting medium can be an ion exchange resin bed, for example. In this study, however, the structure of a newly developed textile material with anion-exchange properties is considered in the model.

An electropermutation stack can be constructed by placing several repeating units consisting of one CC and one FC in series be-

tween one pair of electrodes. The advantage of this is that the irreversible power loss in the electrode reactions becomes negligible compared to the power required to drive the current through the stack. To prevent the nitrates that end up in the CC from being transferred into the next FC, the molar fraction of nitrate in the concentrate solution needs to be kept low. This requires that the concentration and flow rate of the concentrate solution is sufficiently high. Note that it is the relative nitrate concentration in the concentrate solution that should be kept low. The absolute nitrate concentration in the concentrate, however, can become much higher than in the initial feed solution.

Continuous electropermutation offers a continuous option for nitrate removal which adapts well to changes in production demand, feed water quality, and temperature. The capacity can easily be scaled by changing the numbers of repeating units in each stack and by operating stacks in parallel. The high conductivity of the concentrate solution makes the power consumption low compared to electrodialysis/electrodeionization. Furthermore, the selective replacement of the unwanted nitrate ions by suitable anions might be advantageous to the quality of the product. In the production of drinking water it is desirable to preserve some minerals in the product. The concentrate solution obtained is suitable for further treatment, e.g., by selective electrochemical reduction of nitrate to form harmless nitrogen.⁵

Hybrid ion-exchange/electromembrane processes, capable of treating solutions of low conductivity, have been investigated since the mid 1950s. The use of ion-exchange textiles instead of ordinary ion exchange resins has been proposed more recently. The main advantages are higher permeability, faster ion-exchange kinetics, better contact with the membranes, and easier handling.

Glueckauf was the first to investigate the theory of these hybrid processes in the late 1950s. ¹¹ He proposed a theoretical model where the process was divided into two stages: first the mass transfer to the surface of the ion-exchange resins, followed by the transfer of ions in a chain of ion-exchange resin beads. The actual ion-exchange reaction was considered to be in equilibrium, which is still a generally accepted assumption. A one-dimensional model along the flow direction, averaged over the width of the intermembrane spacing, was formulated and compared with experiments. Rubinstein 12 investigated electrodeionization with ion-exchange fibers and developed a model that was one-dimensional in the direction perpendicular to the flow. The objective of this study was to obtain voltage against current curves. An electrodeionization process with separated anion and cation exchange beds were investigated theoretically in a series of papers by Verbeek et al. ¹³ Based on longitudinal convection in the liquid phase and transverse migration in the solid phase a twodimensional model was formulated. The model also accounted for removal of silicate and carbon dioxide. Some results from simula-

^{*} Electrochemical Society Active Member.

^z E-mail: carl-ola@mech.kth.se

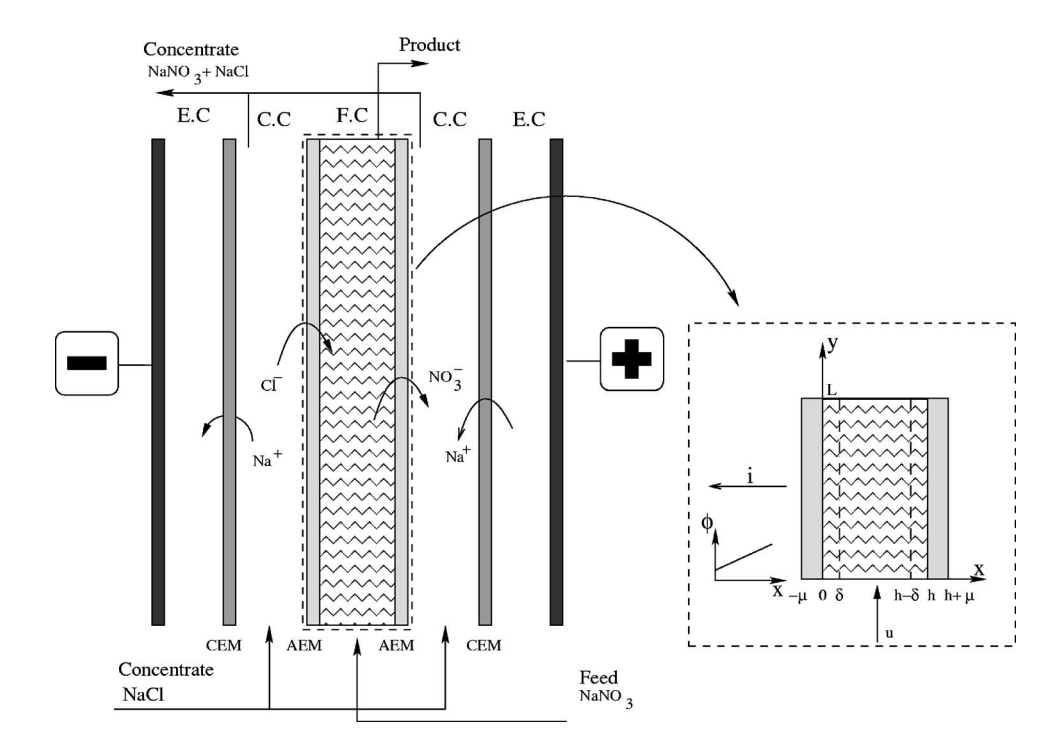


Figure 1. The principles behind nitrate removal by continuous electropermutation. The water to be treated is passed through the FC, which is separated from the CC by anion-permeable membranes on each side. The solution in the CC has a high concentration of chloride. Under the influence of an applied electric field the anions in the FC are exchanged for anions from the CC. To the right the domain included in the model is shown together with the coordinate system used.

tions are presented and compared to experimental results. The specific theory of continuous electropermutation has been studied by Johann and Eigenberger, ¹⁴ who developed a transient one-dimensional model, in the flow direction, for metal ion removal.

A theoretical model would give a fundamental understanding of the mechanisms of the process and their interactions. Simulations could be used to design the equipment and to optimize operation conditions. Furthermore, one can identify the important properties of the ion-exchange textile using the model. This paper presents a two-dimensional steady-state model of nitrate removal with continuous electropermutation using anion-exchange textile. The macrohomogeneous equations are derived from the microscopic scale by volume averaging. Dimensionless parameters that characterize the process are identified and their influence on the process is investigated via simulations.

The following paper presents an experimental study of the continuous electropermutation process using anion-exchange textile as conducting spacer. The model predictions and the experimental results are then compared in order to validate some results from the model.

The Problem Formulation

A steady-state model of the FC in an electropermutation cell is formulated and filled with an anion-exchange textile material. A schematic of the domain to be modeled together with the coordinate system used in the model is shown to the right in Fig. 1.

The feed water in the model contains low levels of sodium nitrate and sodium chloride. Thus, the ionic species that will be included in the model are NO₃, Cl⁻, and Na⁺.

The domain included in the model is divided into three different subdomains, i.e., the membrane on the cathodic side, the feed compartment, and the membrane on the anodic side. The liquid-saturated textile network is assumed to consist of three phases. The fluid which is flowing through the compartment is a liquid mobile phase denoted as the α -phase. The ion-exchange fibers are a solid stationary phase which will be treated as an isotropic porous material, designated as the β -phase. Finally, it is assumed that each fiber is surrounded by a stagnant fluid layer of thickness δ which is the γ -phase. A schematic of the porous medium is presented in Fig. 2. The conservation of mass of each species in each phase at the microscopic level, together with electroneutrality in each phase, forms

the basis for the model. The governing equations on the macroscopic level are obtained by volume averaging the equations on the microscopic scale.

Rubinstein¹² formulated two hypotheses, which also are used here: (H1) The overlap of the stagnant layers can be neglected, i.e., each individual fiber can be treated separately, interacting with other fibers only through the α phase. (H2) The ionic transfer along the fibers in the stagnant layer can be neglected compared to the ionic transfer in that direction in the other two phases. These two hypotheses require that the volume fraction of fibers in the feed compartment be sufficiently low. The second hypothesis allows us to reduce the model from three phases to two phases. A simplified Nernst diffusion layer model replaces the γ -phase in the model equations

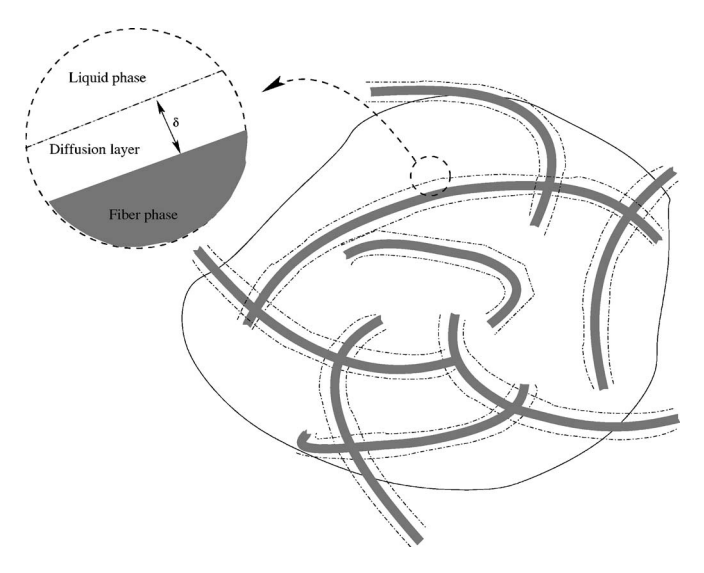


Figure 2. Schematic of the textile material. The fiber phase denoted as the β -phase is separated from the liquid phase, the α -phase, by a stagnant diffusion layer denoted as the γ -phase.

and the transport over the γ phase enters our model as the coupling between the liquid and the fiber phases. The volume fraction of the γ phase is small and is neglected.

Governing equations in the feed compartment.— Electroneutrality in the feed compartment gives

$$\sum z_i c_i = 0 \quad \text{in the } \alpha \text{ phase for } i = 1 - 3$$
 [1a]

$$\sum z_i \overline{c}_i + z_{\omega} \omega = 0 \quad \text{in the } \beta \text{ phase for } i = 1,2$$
 [1b]

where i is a number between 1 and 3 referring to NO $_3$, Cl $^-$, and Na $^+$, respectively, z_i is the valence of species i, z_{ω} is the valence of the fixed charges in the ion-exchange fibers, and ω is the concentration of functional groups in the ion-exchange fibers.

Conservation of species i at steady state in the α -phase gives

$$\nabla \cdot \mathbf{N}_i = 0 \text{ for } i = 1 - 3$$
 [2]

The fibers are treated as ideally selective ion exchangers and thus the mass balance equations in the fiber phase are given by

$$\nabla \cdot \overline{\mathbf{N}}_i = 0 \text{ for } i = 1,2$$
 [3]

The macrohomogeneous mass conservation equations are obtained by volume averaging the equations at the microscale. Applying the volume-averaging theorem¹⁵ allows the superficial averages of the mass conservation equations to be expressed as

$$\langle \nabla \cdot \mathbf{N}_i \rangle = \nabla \cdot \langle \mathbf{N}_i \rangle + \frac{1}{V} \int_{A_{\alpha,\gamma}} \mathbf{N}_i \cdot n_{\alpha,\gamma} dA \quad \text{for } i = 1-3 \quad \left[4 \right]$$

where the integral terms in Eq. 4 describes the flux over the phase interfaces

$$\frac{1}{V} \int_{A_{\alpha,\gamma}} \mathbf{N}_i \cdot n_{\alpha,\gamma} dA = S_i \quad \text{for } i = 1 - 3$$
 [5a]

$$\frac{1}{V} \int_{A_{\alpha,i}} \overline{\mathbf{N}}_i \cdot n_{\beta,\gamma} dA = \overline{S}_i \quad \text{for } i = 1 - 3$$
 [5b]

A consequence of the second hypothesis is that

$$S_i = -\overline{S}_i \quad \text{for } i = 1 - 3 \tag{6}$$

where $S_3 = 0$ due to the ideal selectivity of the β -phase.

The interfacial fluxes enter as sink/source terms in the macro-homogeneous equations

$$\langle \nabla \cdot \mathbf{N}_i \rangle = \nabla \cdot \langle \mathbf{N}_i \rangle - \overline{S}_i = 0 \quad \text{for } i = 1 - 3$$
 [7a]

$$\langle \nabla \cdot \overline{\mathbf{N}}_i \rangle = \nabla \cdot \langle \overline{\mathbf{N}}_i \rangle + \overline{S}_i = 0 \quad \text{for } i = 1, 2$$
 [7b]

The Nernst-Planck equation is used as the transport equation that describes the ionic fluxes at the microscopic scale in both phases. Expressing the superficial volume average of these fluxes in terms of the intrinsic volume averages of the concentrations and potentials turns out to be a complex problem. The structure of the porous medium influences the ionic transport through it. In the present model it is assumed that the two macrohomogeneous phases are in a parallel arrangement. ¹⁴ Thus, the volume-averaged fluxes are assumed to be described by

$$\langle \mathbf{N}_i \rangle = \mathbf{j}c_i - \mathcal{D}' \nabla c_i - z_i \frac{F}{RT} D_{i,e} c_i \nabla \Phi$$
 [8a]

and

$$\langle \overline{\mathbf{N}}_i \rangle = - \ \overline{D}_{i,e} \ \nabla \ \overline{c}_i - z_i \frac{F}{RT} \overline{D}_{i,e} \overline{c}_i \ \nabla \ \overline{\phi} \eqno{[8b]}$$

The superficial average of the fluid velocity, \mathbf{j} , is calculated as the flow rate divided by the cross-sectional area of the empty channel. c_i

and \bar{c}_i are the intrinsic averages of the concentrations of species i in the α and β -phases, respectively. $D_{i,e}$ and $\bar{D}_{i,e}$ are the effective diffusion coefficients of species i in the α and β phase, respectively. \mathcal{D}' is the hydrodynamic dispersion tensor.

The effective diffusion coefficients are modeled by 16,17

$$D_{i,e} = (1 - \epsilon)^{1+b} D_i$$
 [9a]

$$\bar{D}_{i,e} = \epsilon^{1+b} \bar{D}_i$$
 [9b]

where ϵ is the volume fraction of the fiber (β) phase and b is a constant taken to be equal to 0.5.

In a uniaxial flow along the y axis through an isotropic porous material the dispersion tensor is given by

$$\mathcal{D} = \begin{pmatrix} \mathcal{D}_T & 0 & 0 \\ 0 & \mathcal{D}_L & 0 \\ 0 & 0 & \mathcal{D}_T \end{pmatrix}$$
 [10]

where \mathcal{D}_L is known as the longitudinal coefficient of dispersion and \mathcal{D}_T as the transverse coefficient of dispersion. The values of \mathcal{D}_L and \mathcal{D}_T are determined experimentally and in the literature a number of correlations can be found. Usually it is the coefficient of hydrodynamic dispersion

$$\mathcal{D}_{\mathcal{L}}' = (\mathcal{D}_{\mathcal{L}} + D_{i,e})$$

which is given. Here, the following correlations will be used 18,19

$$\mathcal{D}_L' = 2.7 D_0 P e_{df}$$
 for $300 < P e_{df} < 10^4$ [11a]

where Pe_{df} is the Peclet number based on the diameter of the fibers in the β phase and D_0 is a reference molecular diffusivity

$$Pe_{df} = \frac{j_0 d_f}{D_0}$$

Less experimental data is available for the transverse dispersion coefficient. However, one could expect a similar relationship to Pe_{df} as for the longitudinal coefficient of dispersion. ¹⁸ For the ratio $\mathcal{D}_L/\mathcal{D}_T$ values from 3–24 ^{19,20} are found in the literature. Using a value of 10 for this ratio gives

$$\mathcal{D}_T' = 0.27 D_0 P e_{df}$$
 for $300 < P e_{df} < 10^4$ [11b]

A study of the ion-exchange kinetics on ion-exchange fibers made by Petruzzelli 21 suggests that the rate-determining step for the ion exchange is associated with the mass transfer over the $\gamma\text{-phase}.$ This mass transfer is included in the model through the sink/source terms in the volume-averaged mass balance equations. These are calculated from

$$\bar{S}_i = \langle N_i \rangle^* \mathfrak{S}_a$$
 [12]

where $\langle N_i \rangle^*$ is the average flux of species *i* over the fiber-phase interface. The specific surface area of the fibers, \mathfrak{G}_a , is taken to be

$$\mathfrak{S}_a = \frac{4}{d_f} \epsilon_{\beta} \tag{13}$$

where d_f is the fiber diameter.

The average flux over the phase interface is calculated by treating the γ -phase as a Nernst diffusion layer of thickness δ . The fluxes over the Nernst layer are expressed in terms of concentration differences over the layer as

$$\langle N_i \rangle^* = \frac{D_i}{\delta} \left[(c_i^* - c_i) + z_i \frac{F c_i^*}{RT} (\phi^* - \phi) \right] \text{ for } i = 1-3 \quad [14]$$

where the star indicates the average value taken on the liquid side of the phase interface. The assumed ideal selectivity of the β -phase gives

$$\langle N_3 \rangle^* = 0$$

Thus, the potential difference over the Nernst layer can be expressed as

$$(\phi^* - \phi) = -\frac{RT}{z_3 F c_3^*} (c_3^* - c_3)$$
 [16]

Using this in Eq. 14 gives

$$\langle N_i \rangle^* = \frac{D_i}{\delta} \left[(c_i^* - c_i) - \frac{z_i}{z_3} \frac{c_i^*}{c_3^*} (c_3^* - c_3) \right] \text{ for } i = 1-2 \quad [17]$$

To calculate the fluxes over the phase interface from Eq. 17, c_1^* , c_2^* , c_3^* , and ϕ^* need to be determined. Continuity of electrochemical potential for nitrate and chloride at the interface gives²²

$$\overline{c}_i = k_i c_i^* e^{-z_i F \Delta \phi / RT}$$
 for $i = 1-2$ [18]

where $\Delta \phi = \overline{\phi} - \phi^*$ is the Donnan potential at the interface and k_i is the partition coefficient of species i which is assumed to be constant. Eliminating the Donnan potential from the above expression give the separation factor, α_2^1

$$\alpha_2^1 = \frac{\overline{c}_1 c_2^*}{\overline{c}_2 c_1^*} = \frac{k_1}{k_2}$$
 [19]

which is a parameter often used to describe the selectivity of the ion-exchange material. In the present study it is assumed that the textile is nonselective so that $\alpha_1^1 = 1$.

Electroneutrality at the interface gives

$$c_1^* + c_2^* = c_3^*$$
 [20]

Equations 16, 18, and 20 provide four conditions with which the four unknown interface properties can be expressed in terms of the values in the α and β phases.

The thickness of the Nernst layer, δ , is assumed to be controlled by the hydrodynamics and hence, the same value is used for all ionic species. An estimate of the thickness of the stagnant layer is obtained from the following correlation

$$Sh = \frac{1.09}{\epsilon_{ca}} (Re_d Sc)^{1/3} = \frac{1.09}{\epsilon_{ca}} (Pe_d)^{1/3}$$
 [21]

where $Sh = (kd/D) = (d/\delta)$, $Sc = (\nu/D)$, and $Re_d = (jd/\nu)$. This correlation was obtained from experiments with a packed bed of spheres with a diameter d. To use this correlation for a fibrous bed, the diameter of a fictitious sphere having the same specific area as our fibers is used, i.e., $d = 3/2d_f$. The ion-exchange rate is thus expressed as

$$\bar{S}_{i} = \frac{8.72\epsilon_{\beta} P e_{df}^{1/3}}{3\epsilon_{\alpha} d_{f}^{2}} D_{i} \left(\Delta c_{i} - z_{i} \frac{c_{i}^{*}}{c_{3}^{*}} \Delta c_{3} \right) \quad \text{for } i = 1-3$$
 [22]

where $\Delta c_i = c_i^* - c_i$.

Close to the membranes the convective transport goes down to zero, at the same time as the mechanical dispersion vanishes. Thus, there will be a boundary layer in which the molecular diffusion becomes important. In the present model a Nernst diffusion layer model, similar to that used for the stagnant layer surrounding the fibers, is used for the boundary layer close to the membranes. Koch²⁴ presented the following estimate for the thickness of concentration boundary layers close to walls in porous beds

$$\delta_c = \xi \left(\frac{D}{D_{\infty}}\right)^{1/3} \sim \xi (0.27 Pe_{df})^{-1/3}$$
 [23]

where ξ is the characteristic length scale of the porous bed. The characteristic length is given by the square root of the permeability, κ , of the porous medium. In this paper it is assumed that the characteristic length of the textile is equal to the fiber diameter, $\xi = d_f$.

Governing equations in the membranes.— The membranes are treated as solid electrolytes with a homogeneous distribution of

fixed charges. Furthermore, it is assumed that the membranes are perfectly ideal so that the co-ion flux through the membranes can be neglected.

Throughout the model it is assumed that electroneutrality prevails. In the membrane this gives

$$\sum_{i} z_{i} c_{i}^{m} + z_{0}^{m} c_{0}^{m} = 0 \quad \text{for } i = 1, 2$$
 [24]

with i equal to 1 and 2, referring to NO $_3^-$ and Cl $^-$, respectively. z_0^m and c_0^m are the valence and concentration of the fixed charges in the membranes. The superscript m refers to values in the membranes.

Conservation of mass in the membranes at steady state gives

$$\nabla \cdot \mathbf{N}_i^m = 0 \quad i = 1, 2 \tag{25}$$

The fluxes in the membrane are described by the Nernst-Planck equation

$$\mathbf{N}_{i}^{m} = -D_{i}^{m} \nabla c_{i}^{m} - z_{i} u_{i}^{m} c_{i}^{m} \nabla \Phi^{m} + c_{i}^{m} \mathbf{u}^{m}$$
 [26]

The convection through the membranes can be described by Schlögl's equation. ²⁵ In the present model it is, however, assumed that the convection in the membranes can be neglected, i.e., $\mathbf{u}^m = 0$.

Boundary conditions.—The composition of the feed water has to be specified. This gives the boundary conditions at the inlet boundary

$$c_i|_{0 \le x \le h, y=0} = c_{i0}$$
 for $i = 1-3$ [27]

The change of the composition in the flow direction is taken to be negligible at the outlet boundary

$$\frac{\partial c_i}{\partial y} \bigg|_{0 \le x \le h, y = L} = 0 \quad \text{for } i = 1 - 3$$
 [28]

The composition of the solution on the concentrate side of the membrane is assumed to be known and constant along the length of the channel. This can be justified by having concentrations, c_{icc} , many times higher than in the feed. It is assumed that ion-exchange equilibrium prevails at the interface between membrane and the concentrate compartment. Furthermore, the potential in the membranes at the interface with the concentrate compartments are prescribed. This gives the necessary boundary conditions at $x = -\mu$ and $x = h + \mu$

$$c_1^m|_{x=-\mu,h+\mu,0 \le y \le L} = \frac{\alpha_2^{m_1} c_{1cc}}{c_{2cc} + \alpha_2^{m_1} c_{1cc}} c_0^m$$
 [29a]

$$c_2^m|_{x=-\mu,h+\mu,0\leq y\leq L} = \frac{c_{2cc}}{c_{2cc} + \alpha_2^{m1} c_{1cc}} c_0^m$$
 [29b]

$$\phi^m|_{x=-\mu,0 \le y \le L} = 0$$
 [29c]

$$\phi^m|_{x=h+\mu,0 \le y \le L} = \phi_0$$
 [29d]

where c_0^m is the concentration of functional groups in the ion-exchange membrane. α_2^{m1} is the separation factor of the ion-exchange membrane. In the present study it is assumed that $\alpha_2^{m1} = 1$. At the internal boundaries between the membranes and the two phases of the feed compartment all ionic fluxes and electrochemical potentials are continuous.

Analysis

To analyze the equations and identify possible simplifications the model equations are made dimensionless. A number of dimensionless parameters, which characterize the process, are defined. The significance of these parameters are further investigated in the Results and Discussion section.

Feed compartment equations.— The equations in the feed compartment are made dimensionless by introducing the following dimensionless variables

$$\widetilde{x} = \frac{x}{h}, \quad \widetilde{y} = \frac{y}{L}, \quad \widetilde{\mathbf{j}} = \frac{\mathbf{j}}{j_0}, \quad X_i = \frac{c_i}{c_{10}}$$

$$Y_i = \frac{\widetilde{c}_i}{\omega}, \quad \Phi = \frac{\Phi}{\Phi_0}, \quad \widetilde{\Phi} = \frac{\Phi}{\Phi_0}, \quad \epsilon = \epsilon_\beta = (1 - \epsilon_\alpha)$$
 [30]

together with the dimensionless diffusion coefficients

$$\tilde{D}_i = \frac{D_i}{D_0} \quad \tilde{\bar{D}}_i = \frac{\bar{D}_i}{D_0}$$
 [31]

Values of the diffusion coefficients in the pure liquid, D_i , can be found in the literature. The mobility of ions inside the fibers is lower due to the friction caused by the backbone of the fibers and the electrostatic attractions of the fixed groups. ²⁶ In the analysis of the model equations the following relationship between the diffusion coefficients is used

$$\bar{D}_i = 0.15D_i$$
 [32]

The flow through the textile is treated as a plug flow in the y direction and thus, $\tilde{\mathbf{j}} = (0, \tilde{j}_{\nu}, 0)$.

The nondimensional electroneutrality conditions in the feed compartment are given by

$$X_1 + X_2 = X_3 ag{33}$$

and

$$Y_1 + Y_2 = 1 ag{34}$$

Using the dimensionless variables and coefficients the macrohomogeneous conservation of mass equations can be expressed as

$$\begin{split} \widetilde{j}_{y} \frac{\partial X_{i}}{\partial \widetilde{y}} &- 2.7 \vartheta \frac{\partial^{2} X_{i}}{\partial \widetilde{y}^{2}} - 0.27 \frac{\vartheta}{\sigma^{2}} \frac{\partial^{2} X_{i}}{\partial \widetilde{x}^{2}} - z_{i} \frac{\mathcal{V}(1 - \epsilon)^{1.5} \widetilde{D}_{i}}{\sigma^{2} P e} \left[\frac{\sigma^{2} \partial}{\partial \widetilde{y}} \left(X_{i} \frac{\partial \Phi}{\partial \widetilde{y}} \right) \right. \\ &+ \left. \frac{\partial}{\partial \widetilde{x}} \left(X_{i} \frac{\partial \Phi}{\partial \widetilde{x}} \right) \right] - \frac{8.72 \epsilon P e_{df}^{1/3} \widetilde{D}_{i}}{3(1 - \epsilon) \vartheta^{2} P e} \widetilde{\widetilde{S}}_{i} = 0 \quad \text{for } i = 1 - 3 \quad [35a] \end{split}$$

and

$$-z_{i}\frac{0.15\mathcal{V}\epsilon^{1.5}Z\widetilde{D}_{i}}{\sigma^{2}Pe}\left[\frac{\sigma^{2}\partial}{\partial\widetilde{y}}\left(Y_{i}\frac{\partial\widetilde{\Phi}}{\partial\widetilde{y}}\right) + \frac{\partial}{\partial\widetilde{x}}\left(Y_{i}\frac{\partial\widetilde{\Phi}}{\partial\widetilde{x}}\right)\right]$$

$$-\frac{0.15\epsilon^{1.5}Z\widetilde{D}_{i}}{\sigma^{2}Pe}\left(\frac{\sigma^{2}\partial^{2}Y_{i}}{\partial\widetilde{y}^{2}} - \frac{\partial^{2}Y_{i}}{\partial\widetilde{x}^{2}}\right) + \frac{8.72\epsilon Pe_{df}^{1/3}\widetilde{D}_{i}}{3(1 - \epsilon)\vartheta^{2}Pe}\widetilde{\widetilde{S}}_{i} = 0$$
for $i = 1, 2$ [35b]

where

$$\widetilde{\widetilde{S}}_i = \Delta X_i - z_i \frac{X_i^*}{X_{Na^+}^*} \Delta X_{Na^+}$$
 [36]

Above, the following dimensionless parameters were introduced

$$\sigma = \frac{h}{L}, \quad \vartheta = \frac{d_f}{L}, \quad \mathcal{V} = \frac{F\phi_0}{RT}, \quad Z = \frac{\omega}{c_{10}}, \quad Pe = \frac{j_0 L}{D_0}$$
 [37]

The long and slender geometry can be used to simplify the equations. Consider the limit when $\sigma^2 \to 0$ at the same time as $\vartheta \to 0$ so that $(\vartheta/\sigma^2) = \theta = \text{constant}$. Furthermore, $Pe \to \infty$ in such a way that $\sigma^2 Pe = \widetilde{P}e = \text{constant}$. The parameters \mathcal{V} , ϵ , and \widetilde{D}_i are kept constant as $\sigma^2 \to 0$. In this limit the mass balance equations with $\widetilde{j} = 1$ can be written as

$$\frac{\partial X_{i}}{\partial \tilde{y}} - 0.27\vartheta \frac{\partial^{2} X_{i}}{\partial \tilde{x}^{2}} - z_{i} \frac{\mathcal{V}(1 - \epsilon)^{1.5}}{\tilde{P}e} \tilde{D}_{i} \frac{\partial}{\partial \tilde{x}} \left(X_{i} \frac{\partial \Phi}{\partial \tilde{x}} \right) \\
- \frac{8.72 \epsilon P e_{df}^{1/3}}{3(1 - \epsilon)\sigma^{2} \theta^{2} \tilde{P}e} \tilde{D}_{i} \tilde{\tilde{S}}_{i} = 0$$
[38a]

$$-\frac{0.15\epsilon^{1.5}Z}{\widetilde{P}e}\widetilde{D}_{i}\frac{\partial^{2}Y_{i}}{\partial\widetilde{x}^{2}}-z_{i}\frac{0.15\mathcal{V}\epsilon^{1.5}Z}{\widetilde{P}e}\widetilde{D}_{i}\frac{\partial}{\partial\widetilde{x}}\left(Y_{i}\frac{\partial\widetilde{\Phi}}{\partial\widetilde{x}}\right) + \frac{8.72\epsilon Pe_{df}^{1/3}}{3(1-\epsilon)\sigma^{2}\theta^{2}\widetilde{P}e}\widetilde{D}_{i}\widetilde{\overline{S}}_{i} = 0$$
 [38b]

where

$$\theta = \frac{\vartheta}{\sigma^2} = \frac{d_f L}{h^2}$$
 and $\tilde{P}e = \sigma^2 P e = \frac{j_0 h^2}{D_0 L}$ [39]

The model equations have now become parabolic instead of elliptic. Thus, all the boundary conditions at $\tilde{y}=0$ and $\tilde{y}=1$ cannot be fulfilled without reinstating the streamwise diffusion close to the inlet and the outlet of the feed compartment. This problem is, however, not considered in this paper. The parabolic nature of the model equations is used to simplify the numerical solution procedure. Instead of solving the full two-dimensional problem, one can march through the feed compartment solving a sequence of one-dimensional problems at each streamwise position. The upstream solution provides the boundary condition at the next downstream position. By doing this the boundary condition at $\tilde{y}=1$ is not needed.

For the equations above to be balanced as $\sigma^2 \to 0$ it is necessary that $\tilde{\tilde{S}}_i \to 0$. Thus, the liquid phase is assumed to be in ion-exchange equilibrium with the textile phase, which gives

$$Y_2 = \alpha_2^1 \frac{Y_1 X_2}{X_1}$$
 [40]

and that the potential gradients in the two phases are related through

$$\frac{\partial \widetilde{\Phi}}{\partial \widetilde{x}} = \frac{\partial \Phi}{\partial \widetilde{x}} + \frac{1}{\mathcal{V}} \frac{\partial}{\partial \widetilde{x}} \left(\ln \frac{Z}{X_1 + X_2} \right)$$
 [41]

Hence, it is sufficient to solve three differential equations.

Eliminating $\bar{\mathcal{S}}_i$ from the mass conservations equations above gives

$$\frac{\partial X_i}{\partial \widetilde{y}} = 0.27\theta \frac{\partial^2 X_i}{\partial \widetilde{x}^2} + z_i \chi (1 - \epsilon)^{1.5} \widetilde{D}_i \frac{\partial}{\partial \widetilde{x}} \left(X_i \frac{\partial \Phi}{\partial \widetilde{x}} \right) + \frac{0.15 \epsilon^{1.5} Z}{\widetilde{P}_e} \widetilde{D}_i \frac{\partial^2 Y_i}{\partial \widetilde{x}^2}$$

$$+ z_i 0.15 \chi \epsilon^{1.5} Z \tilde{D}_i \frac{\partial}{\partial \tilde{x}} \left(Y_i \frac{\partial \tilde{\Phi}}{\partial \tilde{x}} \right) \quad \text{for } i = 1, 2$$
 [42]

$$\frac{\partial X_3}{\partial \widetilde{v}} = 0.27\theta \frac{\partial^2 X_3}{\partial \widetilde{x}^2} + z_3 \chi (1 - \epsilon)^{1.5} \widetilde{D}_3 \frac{\partial}{\partial \widetilde{x}} \left(X_3 \frac{\partial \Phi}{\partial \widetilde{x}} \right)$$
 [43]

where

$$\chi = \frac{\Phi_0 F D_0 h^2}{R T j_0 L} = \frac{\mathcal{V}}{\sigma^2 P e} = \frac{\mathcal{V}}{\tilde{p}_e}$$
 [44]

The governing equations in the feed compartment include the five dimensionless parameters θ , χ , ϵ , $\tilde{P}e$, and Z. θ , χ , and $\tilde{P}e^{-1}$ relate dispersion, migration, and diffusion in the x direction to convection in the y direction, respectively.

Membrane equations.— The equations in the membranes are made dimensionless by introducing the following dimensionless variables

$$\widetilde{x}^m = \frac{x}{\mu}, \quad -\mu \le x \le 0 \ \widetilde{x}^m = \frac{x-h}{\mu}, \quad h \le x \le h + \mu$$

$$\tilde{y} = \frac{y}{L}, \quad X_i^m = \frac{c_i^m}{c_0^m}, \quad \Phi^m = \frac{\Phi^m}{\Phi_0}$$
 [45]

and dimensionless diffusion coefficients

$$\tilde{D}_i^m = \frac{D_i^m}{D_0^m} \tag{46}$$

The concentrations in the membrane are scaled with the concentration of the fixed charges. This means that the nondimensional electroneutrality condition in the membrane can be expressed as

$$X_1^m + X_2^m = 1 ag{47}$$

The dimensionless form of the mass-conservation equations, using the flux scale, $j_0c_0h/L\mu$, is given by

$$\widetilde{D}_{i}^{m} \left[\frac{\gamma}{\widetilde{P}e} \frac{\partial^{2} X_{i}^{m}}{\partial \widetilde{x}^{m2}} + z_{i} \gamma \chi \frac{\partial}{\partial \widetilde{x}^{m}} \left(X_{i}^{m} \frac{\partial \Phi^{m}}{\partial \widetilde{x}^{m}} \right) \right] = 0$$
 [48]

where

$$\gamma = \frac{D_0^m c_0^m h}{D_0 c_{10} \mu}$$
 [49]

Since the membranes are very thin, $\mu \ll L$, all derivatives along the cell are neglected in Eq. 48, analogous to the treatment of the equations in the feed compartment. The physical interpretation of the new dimensionless parameter γ is that it relates the flux by diffusion through the membrane to the diffusion in the feed compartment. It is clear that γ can be eliminated from Eq. 48; however, γ enters the model when ensuring continuity of the ionic fluxes over the membrane surfaces as is shown later. The relative importance of the diffusion through the membrane compared to the convective transport in the FC is reflected by the ratio between γ and $\widetilde{P}e$

$$\Gamma = \frac{\gamma}{\widetilde{P}e}$$
 [50]

In this paper Γ , rather than $\widetilde{P}e$, is used as the independent parameter together with γ .

Dimensionless boundary conditions.— The dimensionless boundary conditions are given by

$$X_1^m|_{\bar{x}^{m}=-1} = \frac{\alpha_2^{m_1} c_{1cc}}{c_{2cc} + \alpha_2^{m_1} c_{1cc}}, \quad X_1^m|_{\bar{x}^{m}=1} = \frac{\alpha_2^{m_1} c_{1cc}}{c_{2cc} + \alpha_2^{m_1} c_{1cc}}$$
[51a]

$$X_2^m|_{\widetilde{x}^{m}=-1} = \frac{c_{2cc}}{c_{2cc} + \alpha_2^{m1}c_{1cc}}, \quad X_2^m|_{\widetilde{x}^{m}=1} = \frac{c_{2cc}}{c_{2cc} + \alpha_2^{m1}c_{1cc}}$$
 [51b]

$$\Phi^m|_{\tilde{x}^m = -1} = 0 \tag{51c}$$

$$\Phi^m|_{\tilde{x}^{m}=1}=1$$
 [51d]

The nondimensional inlet boundary condition is given by

$$X_i|_{y=0} = \frac{c_{i0}}{c_{10}}$$
 for $i = 1-3$ [52]

At the internal boundaries between the membranes and the feed compartment ion-exchange equilibrium is assumed to hold

$$\frac{X_1^m}{X_1^*} = \alpha_2^{m1} \frac{X_2^m}{X_2^*} \tag{53}$$

where the stared concentrations are taken to be in the liquid phase at the membrane surface. It is assumed that the Donnan potential jump, at the membrane surface, is given by

$$\frac{c_0^m}{(X_1^* + X_2^*)c_0} = \exp[\mathcal{V}(\Phi^m - \Phi^*)]$$
 [54]

Since the ratio c_0^m/c_0 appears at both membrane interfaces its value is not needed, i.e., in the model it is sufficient to use

$$\frac{1}{(X_1^* + X_2^*)} = \exp[\mathcal{V}(\Phi^m - \Phi^*)]$$
 [55]

The fluxes of the counter ions, 1 and 2, are continuous and the flux of the co-ion, 3, is zero over the membrane surfaces. In the appendix it is shown that the slenderness ratio, σ , is needed to ensure continuity of the fluxes at the internal boundaries. This is the final parameter needed to describe the continuous electropermutation process.

Results and Discussion

From the analysis of the model equations it was found that the continuous electropermutation process, using ion-exchange textile as conducting spacer, can essentially be described by the following dimensionless parameters: θ , χ , γ , Γ , Z, ϵ , and σ . The relative importance of mechanical dispersion and migration in the feed compartment, compared to convection, is described by θ and χ , respectively. Γ gives information about the relative importance of diffusion through the membranes compared to the convection in the feed compartment. γ relates the flux by diffusion through the membrane to diffusion in the feed compartment and is usually fairly large. Z represents the ratio between the intrinsic averages of the concentration of functional groups in the ion-exchanger to the feed water concentration. This is a design parameter of the ion-exchange material, which essentially is the dimensionless ion-exchange capacity of the textile. ϵ is another design parameter of the ion-exchange textile defined as the volume fraction of the fibers. The slenderness ratio, σ , is a design parameter of the cell defined as the thickness-to-length

ratio of the FC. Reasonable magnitudes of the nondimensional parameters were obtained by estimating typical values of the physical quantities. A typical feed water concentration was obtained by considering a 1.6 mM NaNO₃ (100 ppm NO₃). The concentrate solution was chosen as a solution with 0.2 M NaCl and 0.02 M NaNO₃. A typical length of the cell was chosen to be L = 0.3 m, and a typical thickness of the feed compartment is h = 3 mm. This gave a slenderness ratio, $\sigma = 0.01$, which is small enough for our simplification of the model equations to be justified. The average fiber diameter in the textile was assumed to be $d_f = 12 \mu m$, and the volume fraction of fibers in the textile was taken to be $\epsilon = 0.15$. The membranes were assumed to have a thickness $\mu = 0.2$ mm and a concentration of fixed charges of 1.5 M. The diffusivities in the membrane are typically two orders of magnitude smaller than in the solution. Thus, based on these estimates the values of $\theta = 0.4$ and $\gamma = 140$ were kept constant in the simulations presented in this paper. A consequence of keeping γ constant is that $\tilde{P}e$ and Γ no longer can be treated as two independent dimensionless parameters. The model equations were simplified in the limit of high Pe. Typical values for the velocity of the flow in the FC lies in the interval $j_0 = 0.01$ -0.1 m/s. This gives values of Pe in the interval $10^6 - 10^7$, which is large enough for the approximations made to be justified. The corresponding values of Γ are in the range 0.047–0.47. The value of χ was varied in the interval 0–0.2, for which the upper limit would give a potential drop of 1.5 V at the lower flow rate, j_0 = 0.01 m/s. However, for the higher flow rate, j_0 = 0.1 m/s, χ = 0.2 would correspond to a potential drop of 15 V, which might be unreasonably high. The parameter values used in the simulations are summarized in Table I.

The model equations were discretized using a conservative finite volume scheme, which was second-order accurate in the x direction and first-order accurate in the y direction. The nonlinear system of equations obtained was solved using the fsolve routine in Matlab. The number of node points was gradually increased in order to

Concentrations	
c ₁₀	1.6 (mM)
c ₃₀	1.6 (mM)
c_{1cc}	0.2 (M)
c_{2cc}	0.2 (M)
Physical parameters	
D_0	$1 \times 10^{-9} (\text{m}^2 \text{s}^{-1})$
D_1	$1.902 \times 10^{-9} (\text{m}^2 \text{ s}^{-1})^{17}$
D_2	$2.032 \times 10^{-9} (\text{m}^2 \text{s}^{-1})^{17}$
D_3	$1.334 \times 10^{-9} (m^2 s^{-1})^{17}$
\mathbf{D}_0^m	$1 \times 10^{-11} (\text{m}^2 \text{s}^{-1})$
D_1^m	$2.8 \times 10^{-11} (\text{m}^2 \text{s}^{-1})^{27}$
D_2^m	$3.9 \times 10^{-11} (\text{m}^2 \text{s}^{-1})^{27}$
Nondimensional parameters	
	1
$rac{lpha_2^1}{lpha_2^{m1}}$	1
É	0.15
γ	140
σ	0.01
θ	0.4
χ	0-0.2
\hat{z}	1, 100, 620, 1500
Γ	0.047, 0.094, 0.47

obtain grid-independent solutions with 40 nodes in the x direction and 80 nodes in the y direction.

The distribution of nitrate in the feed compartment is shown in Fig. 3 for a simulation with $\chi=0.1,~\Gamma=0.094,$ and Z=620. The anode is located on the right side of the feed compartment. Due to the applied electric field the nitrate concentration is shifted towards the membrane on the anodic side of the compartment.

The current density in the cell may vary from the inlet to the outlet depending on the composition of the solution. In an electrodialysis cell one would expect the current density to decrease as one moves toward the outlet, since the conductivity of the solution decreases with increasing streamwise position. With electropermutation this is not the case as can be seen in Fig. 4, where the current density distribution is presented. The current density increases as

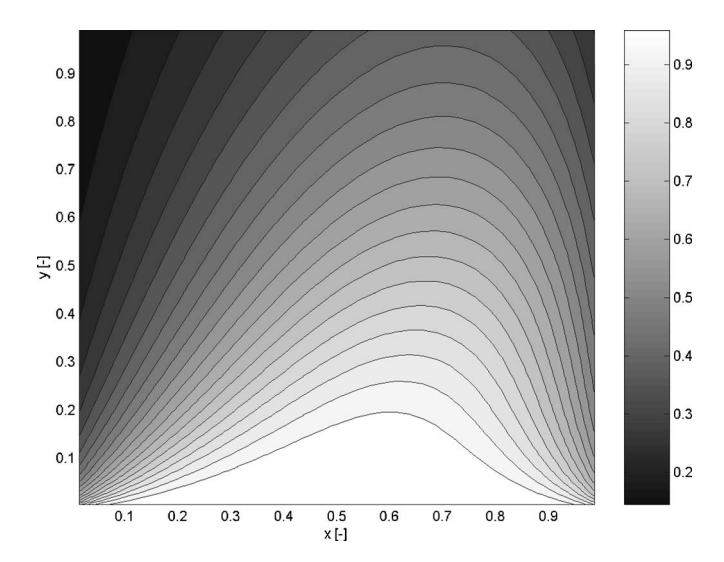


Figure 3. The nitrate concentration distribution in the feed compartment at steady state for $\chi=0.10$, $\Gamma=0.094$, and Z=620. The anode is located on the right side of the feed compartment. It is clear that the nitrate distribution in the feed compartment is shifted toward the anode. The same plot with $\chi=0$, i.e., Donnan dialysis, shows a perfectly symmetric concentration distribution.

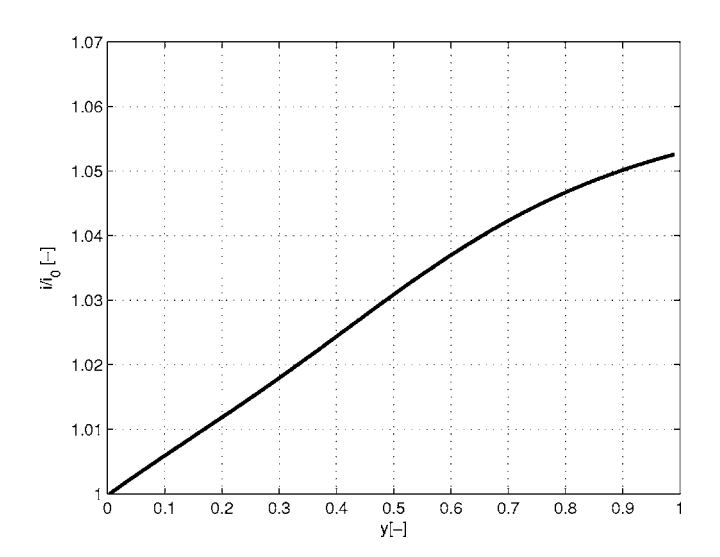


Figure 4. The current density distribution in the cell as a function of streamwise coordinate for $\chi = 0.10$, $\Gamma = 0.094$, and Z = 620.

one moves from the inlet toward the outlet. This can be explained by the gradual replacement of nitrate ions for the slightly more mobile chloride ions.

In Fig. 5 the concentration of nitrate in the product is plotted as a function of χ . The different curves in Fig. 5 represent different values of Γ with a constant Z value of 620. It is clear that the nitrate concentration in the product decreases with increasing χ until the limit of the separation possible to achieve is reached. The value of χ where the nitrate concentration in the product reaches the requirements set on the product represents the optimal value of χ . This gives the optimal relationship between the applied potential and the flow rate through the feed compartment. For example, if it is required that 90% of the nitrate is removed, one finds from Fig. 5 that the optimal χ value is between 0.12 and 0.14 for all values of Γ . The potential difference needed to obtain this value of χ for the highest flow rate, estimate $j_0 = 0.1$ m/s, is found to be $\varphi_0 \approx 10$ V. This might be an unrealistically high value for the potential difference.

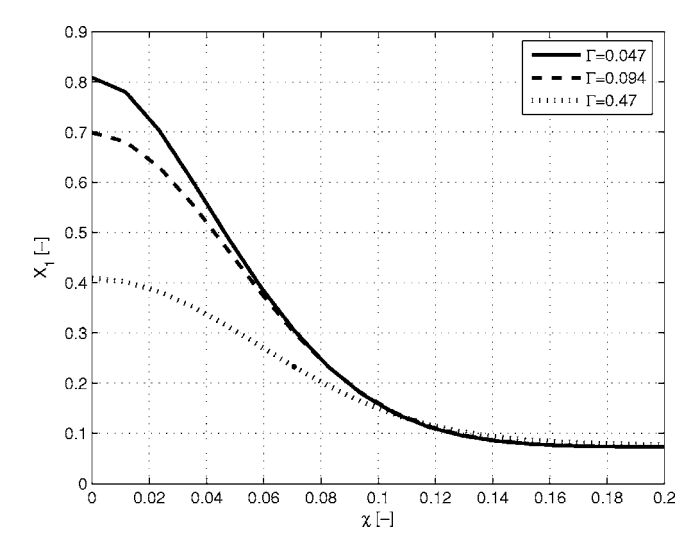


Figure 5. Nitrate concentration in the product as a function of χ obtained from simulations of continuous electropermutation. The different curves represent different values of the dimensionless number Γ as indicated in the figure. The value of Z in these simulations was 620.

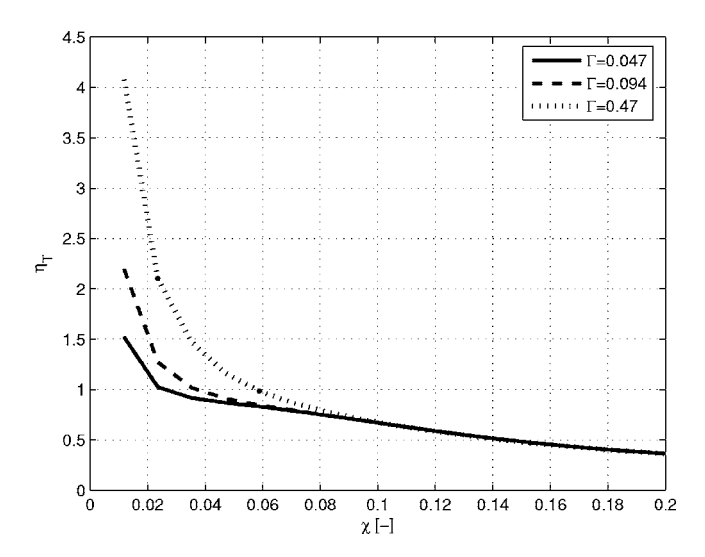


Figure 6. Overall current efficiency as a function of χ . The different curves represent simulations with different values of Γ . The value of Z was 620.

Instead one has to adjust the flow rate and/or the thickness of the feed compartment according to the maximum potential difference acceptable.

From Fig. 5 it is clear that nitrate is removed from the feed compartment even when χ is zero. The reason for this is the Donnan dialysis effect, 28 and its relative importance is indicated by the dimensionless parameter $\Gamma.$ It is found that the nitrate removal due to Donnan dialysis increases with increasing $\Gamma.$ High Γ values represents a configuration where membranes with high conductivity are used in a long and slender cell operated at low flow rate. In the simulations presented here the value of Γ was changed by varying the flow rate through the feed compartment.

The fraction of the current used to remove nitrate is given by the overall current efficiency, η_T . The following definition of η_T is used

$$\eta_T = \frac{Fc_{10}\Delta X_1 h j_0}{L \int_0^1 |i_T| d\tilde{y}}$$
 [56]

where $\Delta X_1 = X_1(\text{Feed}) - X_1(\text{Product})$ and $|i_T|$ is the absolute value of the current density in the feed compartment. In Fig. 6 the overall current efficiency has been plotted against χ for different Γ values. The definition of the current efficiency gives very high values of the efficiency at low values of χ where the Donnan dialysis effect removes nitrate without contributing to the current density. The curves for different Γ values collapse as χ is increased. This indicates that migration becomes the dominating transport mechanism in the membranes as the value of χ increases. From Fig. 6 it is clear that an increased χ value leads to a decreased overall current efficiency.

An alternative way to illustrate the effect of χ presented in Fig. 5 is given in Fig. 7, where the nitrate concentration, averaged over the thickness of the FC, is given as a function of streamwise position in the feed compartment. Each line in the plot corresponds to a specific value of χ at a constant Γ value of 0.094 and Z value of 620. The slope of the curves in Fig. 7 illustrates the contribution to the nitrate removal from different parts of the feed compartment. For low χ values the nitrate concentration decreases almost linearly from the inlet to the outlet. This indicates that nitrate removal takes place over the total length of the feed compartment. Increasing the value of χ gives a concentration profile that levels off toward the end of the cell, indicating a decrease in the nitrate removal efficiency. At $\chi=0.2$, essentially only the first half of the feed compartment is contributing to the removal of nitrate.

The decrease in nitrate removal efficiency with streamwise position can also be shown by looking at the local current efficiency, η , defined as

$$\eta = -\frac{Fhj_0c_{10}}{L|i_T|}\frac{\partial}{\partial \widetilde{y}}\left(\int_0^1 X_1 d\widetilde{x}\right)$$
 [57]

In Fig. 8 the local current efficiency, η , is presented as a function of streamwise position. The current efficiency is high in the beginning

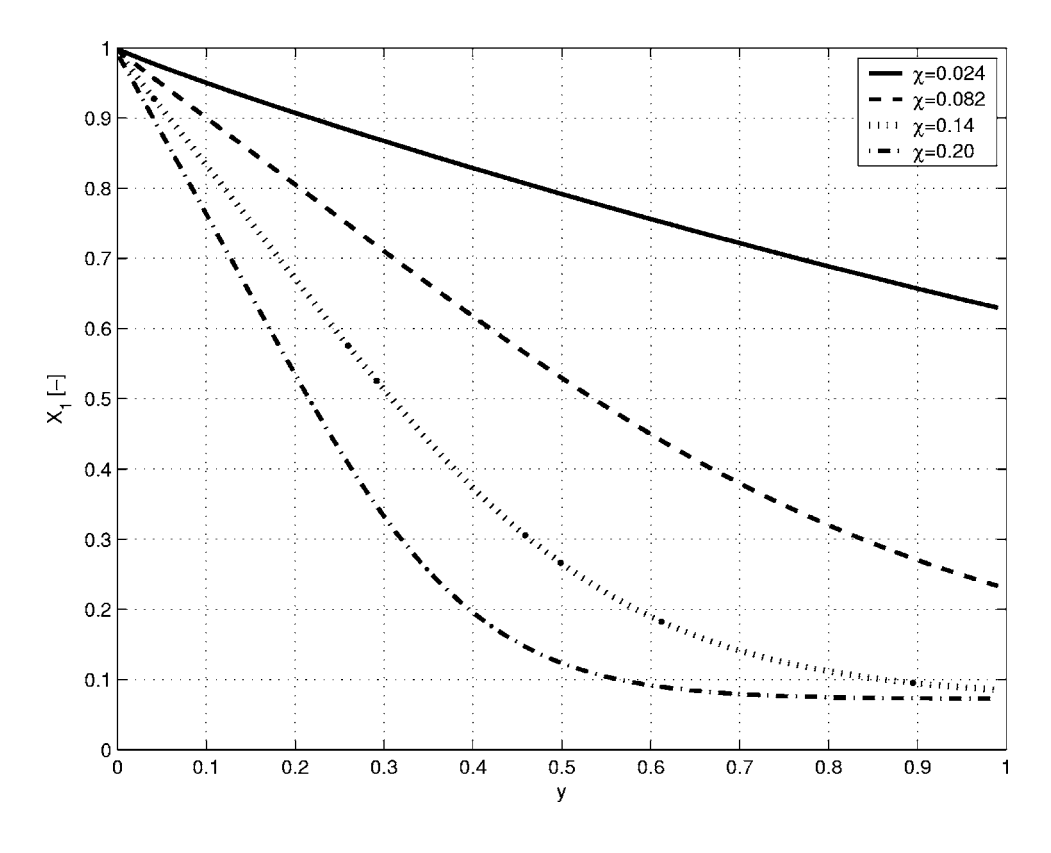


Figure 7. Nitrate concentration in the liquid phase, averaged over the gap between the membranes, as a function of streamwise coordinate for different values of χ . The Z value was 620 and Γ was 0.094.

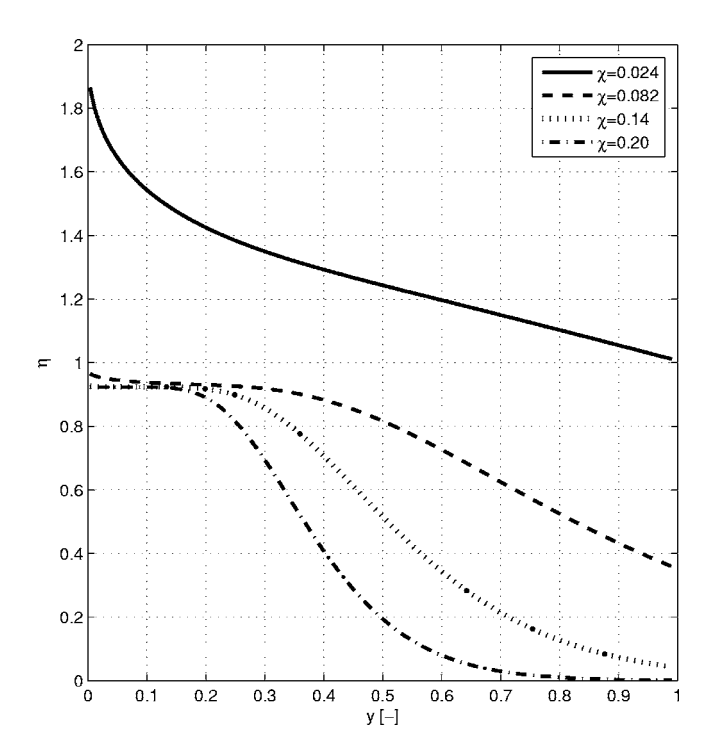


Figure 8. Local current efficiency as a function of streamwise position, \tilde{y} .

of the feed compartment, where the concentration of nitrate is still high compared to chloride, for all values of χ . Marching downstream through the feed compartment the nitrate ions are gradually replaced by chloride ions. Finally, as nitrate carries the same fraction of the current over both membranes, the local current efficiency becomes zero.

If $\chi=0$ and an infinitely long cell is used, nitrate separation continues until the concentrate and feed solutions are in Donnan equilibrium over the membrane. Assuming that the separation coefficient of the ion-exchange membrane is one and independent of the concentrations, then this limit is given by

$$\frac{X_1}{X_2} = \frac{X_{1cc}}{X_{2cc}}$$
 [58]

Thus, the maximum separation possible to achieve with Donnan dialysis is determined directly by the composition of the concentrate solution. In the simulations presented in this paper the feed solution at the inlet was taken to be free from chloride, i.e., $X_{10} = X_{30} = 1$. Thus, the above expression can, using the electroneutrality condition, be rewritten as

$$X_1 = \frac{X_{1cc}}{X_{1cc} + X_{2cc}} = 0.1$$
 [59]

Looking at the result presented in, e.g., Fig. 5, it is clear that the nitrate concentration obtained in the product is lower than this value for the simulations with high χ values independent of the value of Γ .

Another expression for the minimum nitrate concentration possible to reach is obtained by considering the case when χ and Z are high. In this case migration can be assumed to be the dominating transport mechanism in the membranes. In the feed compartment migration in the textile phase is dominating the transport. Again an infinitely long cell is considered. The transport of nitrate and chloride through the membranes then has to equal the transport through the feed compartment. Forming the ratio of the nitrate flux to the chloride flux in the membrane and setting it equal to the corresponding ratio in the feed compartment gives

$$\frac{D_1^m X_1^m}{D_2^m X_2^m} = \frac{\bar{D}_1 Y_1}{\bar{D}_2 Y_2}$$
 [60]

Assuming the separation factor, $\alpha_2^{1m} = 1$, and using electroneutrality in the textile phase gives the nitrate concentration in the textile

$$Y_1 = \frac{\bar{D}_2 D_1^m X_{1cc}}{\bar{D}_2 D_1^m X_{1cc} + \bar{D}_1 D_2^m X_{2cc}}$$
 [61]

The corresponding concentrations in the product are obtained by considering the ion-exchange equilibrium between the liquid and the textile with $\alpha_2^1=1$, whereby

$$\frac{X_1}{X_2} = \frac{Y_1}{1 - Y_1} \approx \text{Constant}$$
 [62]

The above equation also holds for the averages over the feed compartment, i.e., it holds for the concentrations of the product. Furthermore, electroneutrality for the product gives that

$$X_1 + X_2 = X_3 ag{63}$$

In the simulations presented in this paper X_3 in the product equals 1. This gives that

$$X_1 = Y_1 = \frac{\bar{D}_2 D_1^m X_{1cc}}{\bar{D}_2 D_1^m X_{1cc} + \bar{D}_1 D_2^m X_{2cc}}$$
 [64]

With the values of the diffusion coefficients and the composition of the concentrate used in the simulations presented in this paper, the minimum value of X_1 would be 0.0072. Comparing this with the results presented, e.g., in Fig. 5, it is found to correspond very well to the lowest nitrate concentration obtained. One might argue that this limit is not that much lower than the limit (Eq. 59) obtained for pure Donnan dialysis. However, one should remember that theses limits are obtained for infinitely long cells. As illustrated in Fig. 7, the limit is approached much faster as χ is increased. It can be concluded that the maximum nitrate separation possible to accomplish generally will depend on the selectivity of the membrane and ion-exchange textile, the diffusivities in the membrane and textile, and of course, on the composition of the concentrate solution.

The dimensionless number *Z*, defined in Eq. 37, represents the ratio between the intrinsic concentration of the fixed ion-exchange groups in the fiber-phase and the concentration of nitrate in the feed. The idea behind incorporating an ion-conductive spacer in the feed compartment is to increase the effective conductivity, which reduces the power consumption of the process. Furthermore, the transport of nitrate ions from the solution to the ion-exchange phase takes place over a much larger area, i.e., the surface area of the spacer and membrane. This reduces problems associated with concentration polarization. Hence, a much higher current can be applied before the limiting current density is reached. The analogy to the use of porous electrodes for metal ion removal is close at hand. Increasing the value of *Z* leads to a higher contribution from the textile to the separation process and hence, a faster separation.

In Fig. 9 the concentration of nitrate in the product is plotted as a function of χ for different values of Z. This illustrates the influence of the fiber phase ion-exchange capacity on the nitrate removal. A realistic value of the capacity of the anion-exchange textiles available today is about 1 meq/g. Assuming that the density of the fibers is roughly 1000 kg/m³, one finds that a textile with a density of 150 kg/m³ would have a volume fraction of fiber, ϵ , equal to 0.15. A textile with the above-mentioned density and capacity would have a concentration of functional groups, ω , of 1 M. Using such a textile to treat a 100-ppm nitrate solution would give a Z value of 620. If the same textile would have an ion-exchange capacity of 2.4 meq/g, a reasonable value for ion-exchange resins, the corresponding Z value would be 1500. A Z-value of 1 corresponds to the case where the concentration of functional group in the textile is the same as the nitrate concentration at the inlet. In such a case the textile phase has

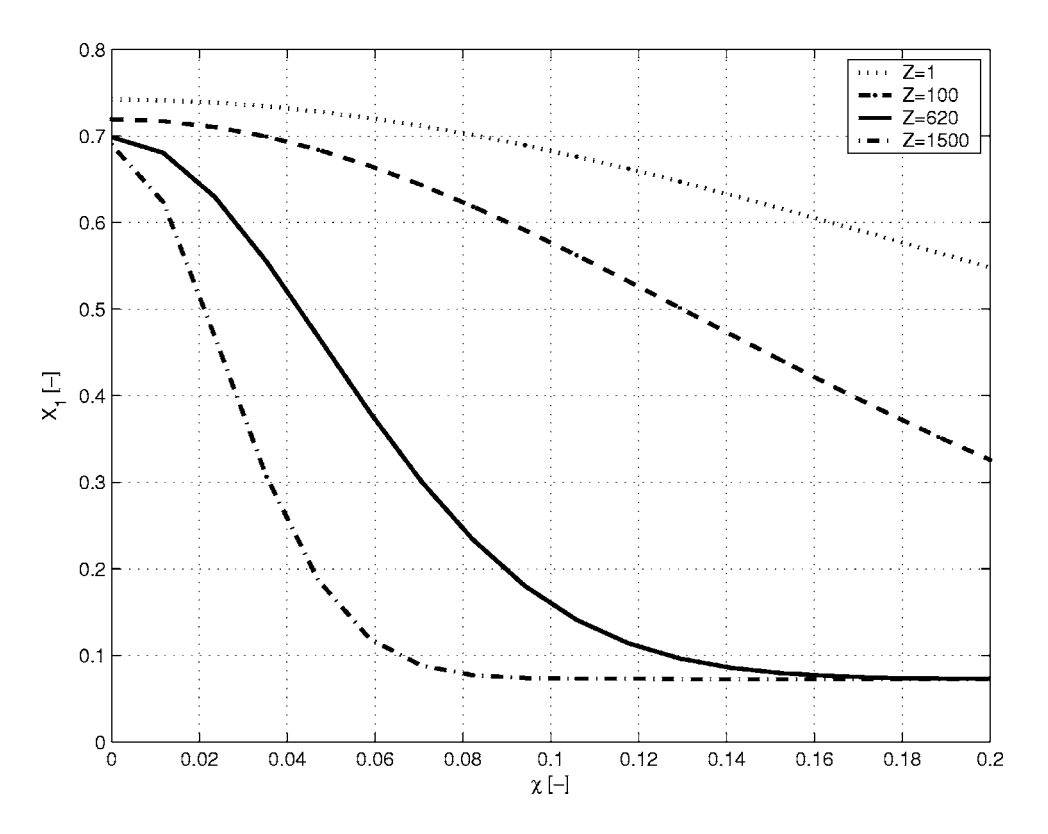


Figure 9. Concentration of nitrate in the product as a function of the dimensionless parameter χ , plotted for different values of the dimensionless parameter Z as indicated in the figure. The value of Γ in these simulations was 0.094.

a lower conductivity than the liquid phase and its main contribution to the process will merely be as an effective "turbulence" promoter.

It is found that the amount of nitrate removed by Donnan dialysis, $\chi = 0$, increases only slowly with Z. This indicates that the mass transfer to the membrane surface in the fiber-phase increases with increasing Z value. However, the mass transfer through the membrane is the rate-determining step in Donnan dialysis, hence, the rather weak influence of Z on the separation at $\chi = 0$.

The importance of the ion-exchange capacity of the textile phase is illustrated when the electric field is applied. As can be seen, the nitrate concentration in the product decreases quickly when χ increases in the simulations with high Z values. It is clear that increasing the value of Z makes the optimal value of χ lower. Thus, when the capacity of the conducting spacer used is increased one can operate at a higher flow rate at a given potential drop or decrease the applied potential at a given flow rate. Making the same assumption as when estimating the maximum nitrate separation possible, i.e., migration in the textile is the dominating transport mechanism, one can argue from Eq. 42 that the product $Z\chi$ sets the criteria for reaching the limit concentration. One finds from Fig. 9 that for the two highest capacities the limit is reached at $Z\chi \approx 124$ in both cases.

If the capacity of the textile is low, a higher value of χ is required to remove a sufficient amount of nitrate. Increasing χ by raising the potential difference might lead to concentration polarization at the surface of the membrane located closest to the anode. If the concentration close to the membrane surface becomes sufficiently low the concentrations of hydroxide and oxonium ions can no longer be neglected. The hydroxide ions in the water will then participate in the transfer of electric charge over the membrane. To replace the hydroxide ions that are transferred over the membrane, water starts to dissociate into its ionic products. This leads to a pH change in the feed and concentrate compartments. The present model cannot capture this effect. However, it is an important task for future work to incorporate the effect of water dissociation and the resulting change in pH.

Conclusions

This paper presented a macrohomogeneous steady-state model for nitrate removal by continuous electropermutation using an ionexchange textile as conducting spacer. The macrohomogeneous equations were obtained by taking the volume averages of the governing equations at the microscopic level. To obtain expressions for the macrohomogeneous fluxes it was assumed that the two phases that contribute to the mass-transfer are in a parallel arrangement. The model equations and boundary conditions were made dimensionless and appropriate simplifications were identified. The slender geometry of the domain was used to simplify the equations. Up to this point the model would have been equally valid for a configuration where an ion-exchange resin bed is used as conducting spacer. However, the relatively small diameter (10 µm) of the fibers in a typical ion-exchange textile made it possible to assume ionexchange equilibrium between the phases. This reduced the number of unknowns in the model. From the analysis of the dimensionless model equations and boundary conditions it was found that the following parameters characterizes the process: $\theta,\,\chi,\,\gamma,\,\Gamma,\,Z,\,\varepsilon,$ and $\sigma.$

The influence of χ , Γ , and Z on the process was investigated by solving the model equations numerically. The dimensionless number χ , defined in Eq. 44, was found to be the key number to study when the operating conditions are to be optimized. The optimal relation between the applied potential and the flow rate through the feed compartment is found by studying χ and its influence on the process. The relative importance of the removal due to the Donnan dialysis effect was found to be reflected by the dimensionless number Γ as defined in Eq. 50. It was found that a significant amount of nitrate could be removed by Donnan dialysis. Assuming that γ is kept constant, Γ has no influence on the nitrate concentration in the product for high χ values.

Z is the parameter that represents the ratio between the intrinsic concentrations in the ion-exchanger and in the solution, i.e., it can be thought of as the dimensionless capacity of the ion-exchange textile. Simulations gave that increasing the Z value reduces the

value of the optimal χ in such a way that $Z\chi \approx \text{constant}$. When Z is raised the conductivity of the feed compartment increased and a lower potential drop is required to drive a specific current density.

It has been shown that simulations based on the developed model can provide valuable information that is useful for optimizing the process parameters as well as in the stage of designing the equipment. The water considered in the simulations presented was typically a 100 ppm nitrate solution. Using the equipment, membranes, and textile considered it should be possible to obtain a product with about 10 ppm nitrate at a flow rate of 0.01 m/s and a potential drop of 1.0 V. The nitrate level in the concentrate solution was taken to be 1000 ppm, which is high enough for a further electrochemical treatment to produce harmless nitrogen. The limitation to the nitrate separation possible to achieve is determined by the composition of the concentrate solution, membrane selectivity, and the diffusivities of the ions in the membrane. The results from the simulations should be compared to experimental results in order to validate the model.

Acknowledgment

The work was financed by the VINNOVA competence center, FaxénLaboratoriet, with the main industrial partner in this project being Vattenfall AB.

Royal Institute of Technology assisted in meeting the publication costs of $this\ article.$

Appendix

Continuity of the counter ion fluxes over the internal membrane surfaces can be

$$N_i^{\text{FC}} = N_i^{bl} = N_i^m$$
 at $\tilde{x} = 0, 1$ for $i = 1-3$ [A-1]

where NFC, Nbl, and Nm are the fluxes in the feed compartment, in the Nernst diffusion layer, and in the membrane, respectively.

The flux in the FC scaled with $j_0c_0\sigma$ is given by

$$N_i^{\rm FC} = \left[-0.27\theta \frac{\partial X_i}{\partial \widetilde{x}} - z_i \chi \widetilde{D}_i X_i \frac{\partial \Phi}{\partial \widetilde{x}} - 0.15 Z \widetilde{D}_i \left(\frac{\Gamma}{\gamma} \frac{\partial Y_i}{\partial \widetilde{x}} + z_i \chi Y_i \frac{\partial \overline{\Phi}}{\partial \widetilde{x}} \right) \right] \qquad [\text{A-2}]$$
 and the flux in the membrane using the same scale is given by

$$N_i^m = \widetilde{D}_i^m \left[-\Gamma \frac{\partial X_i^m}{\partial \widetilde{x}^m} - z_i \gamma \chi X_i^m \frac{\partial \Phi}{\partial \widetilde{x}^m} \right]$$
 [A-3

The algebraic expressions for the fluxes of counterions through the Nernst diffusion layer scaled with $j_0c_0\sigma$ is given below. The zero flux of the coin through the diffusion layer is used to eliminate the potential gradient in the Nernst layer

$$\begin{split} N_{i}^{bl} &= -\frac{0.27^{1/3}}{\sigma(\tilde{Pe}\theta)^{2/3}} \tilde{D}_{i} \left[\Delta X_{i} + \frac{X_{i}^{*}}{X_{3}^{*}} \Delta X_{3} \right] - \frac{0.27^{1/3}}{\sigma(\tilde{Pe}\theta)^{2/3}} 0.15Z \tilde{D}_{i} \left[\Delta Y_{i} + \frac{Y_{i}}{X_{3}^{*}} \Delta X_{3} \right] \\ &+ \frac{Y_{i}\Gamma}{\chi \gamma} \frac{(\Delta X_{1} + \Delta X_{2})}{(X_{1} + X_{2})} \end{split}$$
 [A-4]

In the above expression ΔX_i , ΔY_i , and $\Delta (Y_i X_i^{-1})$ are given by

$$\Delta X_i|_{\widetilde{x}=0} = (X_i - X_i^*)$$
 [A-5]

$$\Delta X_i|_{\widetilde{x}=1} = (X_i^* - X_i)$$
 [A-6]

$$\Delta Y_i|_{\widetilde{x}=0} = (Y_i - Y_i^*)$$
 [A-7]

$$\Delta Y_i|_{\widetilde{Y}=1} = (Y_i^* - Y_i)$$
 [A-8]

Thus, the slenderness ratio of the cell σ enters the equations as a parameter that needs to be specified in order for the counter ion fluxes to be continuous over the membrane surface. In principle, as the analysis is performed in the limit when σ^2 goes to zero, σ goes to zero also, although not as fast as σ^2 (see Analysis section). Then, since in Eq. A-4 Z, $\tilde{P}e = (\gamma/\Gamma)$, and θ are of order one as $\sigma^2 \to 0$, the fluxes in the Nernst layer, N_i^{bl} , are finite only if $\Delta X_i \sim \Delta Y_i \sim \sigma$. Thus, in the limit $\sigma \to 0$ the concentrations difference over the Nernst layer are all zero. However, in our estimates of typical parameters in the Results and Discussion section $\sigma \approx$ 0.01, which together with θ = 0.4, γ = 140, and $\Gamma = 0.047 - 0.47$ give $\sigma[(\tilde{P}e\theta)^{2/3}/0.27^{1/3}] = \sigma[\gamma^{2/3}\theta^{2/3}/\Gamma^{2/3}0.27^{1/3}] \approx 0.6 - 2.7$ for the denominator of Eq. A-4, i.e., numerical values that are not truly small. Therefore, the asymptotic limit $\sigma \to 0$ is not applied in Eq. A-4, and results of the calculations with $\sigma = 0.01$ in Eq. A-4 give ΔX_i and $\Delta Y_i \neq 0$.

- 1. World Health Organization, Guidelines for Drinking Water Quality; Recomendations I, 3rd ed., (2004).
- European Community, Council directive of Nov 3, 1998, Official J. Europ. Commun., L330, 0032 (1998)
- 3. K. Salem, J. Sandeaux, J. Molénat, R. Sandeaux, and C. Gayach, Desalination, 101, 123 (1995).
- S. Ezzahar, A. Cherif, J. Sandeaux, R. Sandeaux, and C. Gavach, Desalination, 104, 227 (1996).
- M. Paidar, I. Rousar, and K. Bouzek, *J. Appl. Electrochem.*, **29**, 611 (1999). W. R. Walters, D. W. Weiser, and L. J. Marek, *Ind. Eng. Chem.*, **47**, 61 (Jan 1955).
- E. Dejean, Ph.D. Thesis, Universitet Montpellier II (1997).
- E. Dejean, E. Laktionov, J. Sandeaux, R. Sandeaux, G. Pourcelly, and C. Gavach, Desalination, 114, 165 (1997).
- E. Dejean, J. Sandeaux, R. Sandeaux, and C. Gavach, Sep. Sci. Technol., 33, 801 (1998).
- 10. E. Laktionov, E. Dejean, J. Sandeaux, C. Gavach, and G. Pourcelly, Sep. Sci. Technol., 34, 69 (1999).
- 11. E. Glueckauf, Br. Chem. Eng., 4, 646 (1959).
- 12. I. Rubinstein, J. Chem. Soc., Faraday Trans. 1, 73, 528 (1977).
- 13. H. M. Verbeek, L. Frst, and H. Neumeister, Comput. Chem. Eng., 22, 913 (1998).
- J. Johann and G. Eigenberger, Cem.-Ing.-Tech., 1, 75 (1993).
- S. Whitaker, The Method of Volume Averaging, Kluwer Academic, Dordrecht, The Netherlands (1999).
- R. B. Bird, W. E. Stewart, and E. N. Lightfoot, Transport Phenomena, Wiley, New York (2002).
- 17. J. S. Newman, Electrochemical Systems, Prentice Hall, New York (1991).
- J. Bear, Dynamics of Fluids in Porous Media, Dover, Mineola, NY (1998)
- F. A. L. Dullien, Porous Media, Fluid Transport and Pore Structure, Academic, New York (1992).
- 20. R. A. Greenkorn, Flow Phenomena in Porous Media, Dekker, New York (1983),
- 21. D. Petruzzelli, A. Kalinitchev, V. S. Soldatov, and G. Trivavanti, Ind. Eng. Chem. Res., 34, 2618 (1995).
- V. Nikonenko, K. Lebedev, J. A. Manzanares, and G. Pourcelly, Electrochim. Acta, **48**, 3639 (2003).
- 23. E. J. Wilson and C. J. Geankoplis, Ind. Eng. Chem. Fundam., 5, 9 (1966).
- D. L. Koch and J. F. Brady, J. Fluid Mech., 154, 399 (1985)
- R. Schlögl and U. Schöedel, Z. Phys. Chem. (Munich), 2, 372 (1955).
- F. Helfferich, Ion Exchange, Dover, Mineola, NY (1995)
- A. Elattar, A. Elmidaoui, N. Pismenskaia, C. Gavach, and G. Pourcelly, J. Membr. Sci., 143, 249 (1998).
- 28. M. Mulder, Basic Principles of Membrane Technology, Kluwer Academic, Dordrecht, The Netherlands (1996).

Paper 2

2



Nitrate Removal by Continuous Electropermutation Using Ion-Exchange Textile

II. Experimental Investigation

Carl-Ola Danielsson, a,z Anna Velin, Mårten Behm, a,* and Anders Dahlkilda

^aFaxénLaboratoriet, Royal Institute of Technology, Stockholm, Sweden ^bVattenfall Utveckling AB, Stockholm, Sweden

Water with nitrate concentrations above 100 ppm has been treated with continuous electropermutation which partially substitutes the nitrate with chloride. The performance of a textile anion exchanger as conducting spacer in the feed compartment of an electropermutation cell was investigated. Experiments with and without textile are compared and the influence of the textile is discussed. The process could, using the textile, successfully treat feed water with 105 ppm nitrate to produce a water with less than 25 ppm nitrate. The importance of establishing a good contact between the membranes and the textile spacer was pointed out. The experimental results were compared to model predictions and a good agreement was found.

© 2006 The Electrochemical Society. [DOI: 10.1149/1.2170659] All rights reserved.

Manuscript submitted April 7, 2005; revised manuscript received December 13, 2005. Available electronically February 22, 2006.

Increased nitrate levels in the groundwater have made many wells unsuitable as drinking water sources. There are a number of available techniques for removal of nitrate for production of drinking water, such as biological methods, ion exchange, and electrodialysis. In the first part of this series of paper nitrate removal by electroextraction or continuous electropermutation (CEP)³⁻⁵ was investigated theoretically. A steady-state model of the CEP technique, with an anion-exchange textile incorporated as a conducting spacer in the feed compartment, was derived. The parameters describing the process were identified. The maximum nitrate separation possible to accomplish was discussed. Furthermore, it was found that the separation of nitrate at zero current, i.e., by Donnan dialysis, could be quite substantial.

In the present paper nitrate removal by CEP is investigated experimentally for the first time. A new nonwoven textile with strong anion-exchange properties is tested as a conducting spacer in the feed compartment. The advantages of using this ion-exchange textile compared to conventional ion-exchange resins are faster ion-exchange kinetics, easier handling, and lower pressure drop. 6

The purpose of the work presented in this paper is to:

- 1. Investigate the performance of continuous electropermutation for nitrate removal.
- 2. Investigate the influence of using an ion-exchange textile as conducting spacer in the feed compartment as compared to a non-conducting net-type spacer.
- 3. Compare the experimental results with the predictions made by the steady-state model presented in part one of this series of papers.²

Experimental

The cell used in this study was composed of five compartments separated by ion-exchange membranes; a schematic is presented in Fig. 1. The electrode compartments were taken from an ElectroSynCell. A DSA electrode, titanium coated with iridium-oxide, was used as anode and a nickel electrode as cathode. The electrode and concentrate compartments were separated by cation-permeable membranes to prevent chloride ions from being transfered into the electrode compartments. This minimizes the risk of chlorine evolution in the electrode reactions. The feed and concentrate compartments were 3-mm-thick and separated by anion-permeable membranes. Net-type (PE) spacers were used to provide mechanical support to the membranes. When the ion-exchange textile was used, it replaced the net-type spacer in the feed compart-

ment. Each compartment was 0.28 m in the streamwise direction and 0.15-m wide, giving an active membrane area of 0.04 m².

The concentrations of nitrate, chloride, and sulfate ions were determined by ion chromatography, using the Dionex Ag17 and As17 columns, and pH was measured with a pH electrode from Radiometer.

Ion-exchange materials.— The characteristics of the textile and membranes used are given in Table I. The Neosepta standard-grade membranes AMX and CMX from Tokuyama Soda were used to separate the compartments.

The ion-exchange textile used was developed within the EU-funded research project Iontex. It is a nonwoven felt made of cellulose fibers with ion-exchange groups introduced by electrobeam grafting. The selectivity of a textile similar to that used in this study was investigated by Passounaud et al. It was found that the separation factor between nitrate and chloride, $\alpha_{\text{Cl}^-}^{\text{NO}_3}$, for this type of textile was around 2. The separation factor is defined as

$$\alpha_{\text{Cl}^{-}}^{\text{NO}_{3}^{-}} = \frac{[\overline{\text{NO}_{3}^{-}}][\text{Cl}^{-}]}{[\text{NO}_{3}^{-}][\bar{\text{Cl}}^{-}]}$$
[1]

where the bars indicate concentrations in the textile phase. The textile was not specially designed to be nitrate-selective.

Operating conditions.—Before the textile was introduced into the cell it was washed carefully with deionized water to remove any excess chemicals remaining from the grafting process, and it was turned into chloride form by treating the textile with a sodium chloride solution.

A synthetic sodium nitrate solution served as feed. The level of nitrate in the feed was 105 ppm, which corresponds to 1.7 mM. The initial solution in the concentrate container was 20 L of 0.2 M sodium chloride, which was recirculated. The level of nitrate in the concentrate solution gradually increased and the chloride concentration decreased during the experiments. The concentrate solution was sampled before and after every experiment to determine the composition of the solution. When the nitrate concentration in the concentrate was higher than 5% of the chloride concentration or the pH of the concentrate solution exceeded 8.5 the concentrate solution was replaced.

The initial solution in the electrode container was 10 L of 0.3 M sodium sulfate, which was recirculated. Samples of this solution were taken before and after every experiment to make sure that no chloride or nitrate ions had leaked over to the electrode compartment. This could happen if the cation-permeable membranes were damaged.

^{*} Electrochemical Society Active Member.

^z E-mail: carl-ola@mech.kth.se

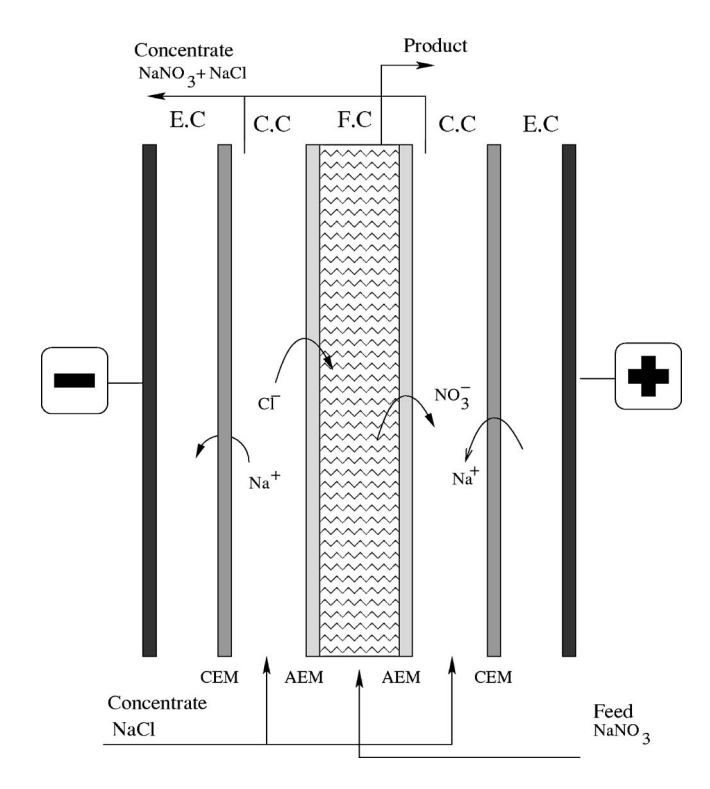


Figure 1. A schematic of the principle of continuous electropermutation used for nitrate removal. The nitrate in the feed water is replaced by another anion, in this case chloride, under the influence of an applied electric field.

The current passed through the cell was varied between 0 and 1 A, corresponding to an average current density of 0–25 A/m². A single-pass mode of operation was used for the feed. The product water was collected at the outlet of the feed compartment. A true steady state did not exist for this setup since the composition of the concentrate solution changed continuously. This change, however, was very slow, and a quasi-steady state was established at each value of the current after some time of operation. It was found that at least 30 min of operation was needed each time the current had been changed before the quasi-steady state was reached.

Experiments were carried out with and without the ion-exchange textile in the feed compartment and with different pressure drops applied over the feed, concentrate, and electrode compartments. The different experiments presented here are denoted cases A–E and are presented in Table II.

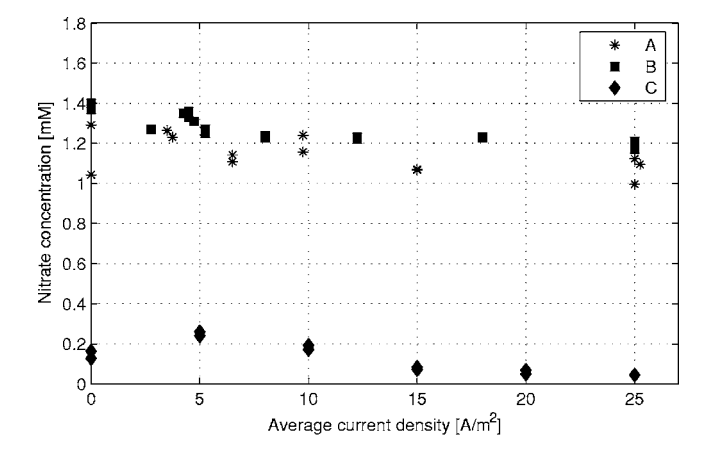
Results and Discussion

In the first experiments carried out, cases A and B, the same pressure drops were employed over all compartments. The pressures were adjusted so that the same flow rate was obtained both with and without the textile. In case A, with the textile included, the applied pressure drop was 0.17 bar and in case B, without the textile, it was 0.13 bar. The superficial flow velocity through the feed compartment in these experiments was 1.7 cm/s.

In Fig. 2 the concentrations of nitrate and chloride in the product at different average current densities are presented for cases A and

Table I. Properties of ion-exchange textile and membrane used.

	Textile	AMX	CMX
Type	Anion-exchange	Anion-permeable	Cation-permeable
	Textile	membrane	membrane
Thickness (mm)	3.0-3.3	0.16 - 0.18	0.17 - 0.19
Capacity (meq/g)	0.5-0.7	1.4 - 1.7	1.5-1.8



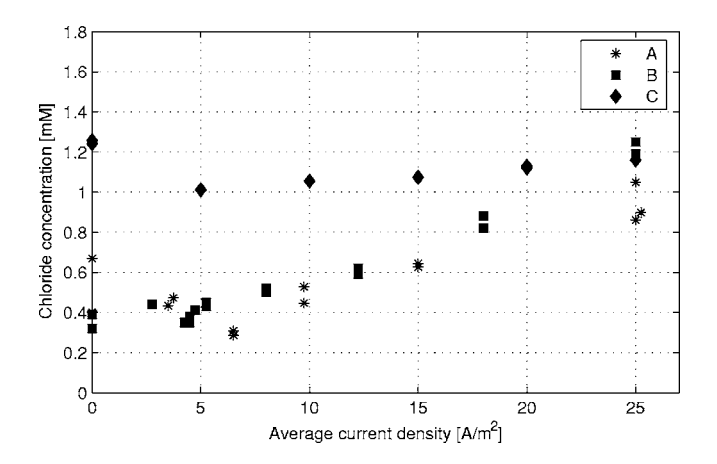


Figure 2. Nitrate and chloride concentrations as function of average current density. In case A the ion-exchange textile was incorporated and in case B a polyethylene net-type spacer was used. The mean velocity in the feed compartment in these cases was 1.7 cm/s. In case C the textile was incorporated and the pressure outside of the feed compartment was increased in order to press the membranes against the membrane. This led to a decreased flow through the feed compartment and the mean velocity was only 0.4 cm/s.

B. The initial concentration of nitrate in the feed was 1.7 mM. In case A the nitrate level is decreased to 1.2 mM at zero current and in case B it is decreased to 1.4 mM at zero current. The difference in chemical potential over the membranes for chloride makes the chloride ions diffuse into the feed compartment. A transport of nitrate in the opposite direction, driven by an electrical potential difference, then has to take place to ensure that the electroneutrality condition is fulfilled. This separation process, which uses ion-exchange membranes without applying an external electric field, is called Donnan dialysis. ¹⁰

The separation of nitrate, defined as

Table II. The different test cases. FC refers to feed compartment. EC and CC refer to electrode compartments and concentrate compartments, respectively.

Cases	A	В	C	D	Е
Spacer	Textile	Net-type	Textile	Textile	Net-type
$\Delta P EC (bar)$	0.17	0.13	0.15	0.30	0.10
ΔP EC and CC (bar)	0.17	0.13	0.25	0.40	0.20
Mean velocity in FC (m/s)	0.017	0.017	0.004	0.012	0.012

Table III. The separation of nitrate, as defined by Eq. 2, by Donnan dialysis and continuous electropermentation for the different cases reported.

Cases	A	В	C	D	Е
$R_{\text{NO}_{3}^{-}}$ (0 A/m ²)	0.24	0.18	0.91	0.57	0.21
$R_{\text{NO}_{2}^{-}}$ (25 A/m ²)	0.35	0.29	0.97	0.86	0.40

$$R = \frac{\mathrm{C_{NO_3^-}(Feed)} - \mathrm{C_{NO_3^-}(Product)}}{\mathrm{C_{NO_3^-}(Feed)}}$$
 [2]

is given in Table III. In case A, with the textile, the nitrate separation increases from 24% at zero current up to 32% at 5 A/m². Raising the current density further does not lead to an increased nitrate removal. The same behavior is seen in case B, without the textile. It seems that raising the current density does not lead to an increased nitrate removal. To consider the electropermutation as a successful process a nitrate separation of 75–80% should be accomplished. This would translate into a product water with about 25 ppm nitrate, which is the recommended upper limit of nitrate for drinking water. Thus, these first experiments cannot be considered successful.

The concentration of chloride in the product, however, increases with the average current density, as is seen in the lower part of Fig. 2. The poor improvement of nitrate removal as the current density increases is believed to be due to dissociation of water taking place in the feed compartment. This produces hydroxide and oxonium ions that will compete with the nitrate ions in carrying the current. The pH of the product water, presented in Fig. 3, decreases from 5.7 at 5 A/m^2 to 3–3.5 as the current density is increased to 25 A/m^2 . This indicates that water dissociation takes place in the feed compartment and the generated hydroxide ions are transferred over the membrane instead of the nitrate ions. The results from cases A, with textile, and B, without textile, are almost identical. This would indicate that the performance of the ion-exchange textile as a conducting spacer is very poor. The slightly higher nitrate separation obtained in case A, with the textile included in the cell, can be explained by an increased mechanical dispersion provided by the textile compared to the net-type spacer.

One possible explanation for the poor performance of the textile is the creation of preferential flow paths between the membrane and the ion-exchange textile. This problem was described in the thesis of Dejean⁶ and leads to insufficient contact between the membrane and

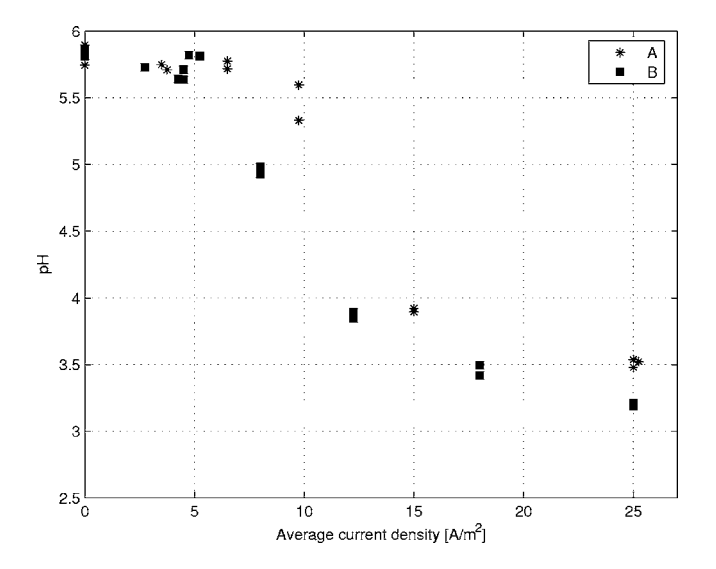
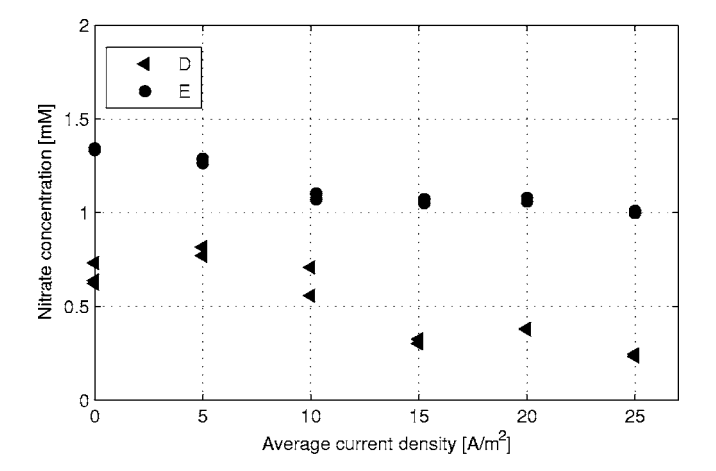


Figure 3. pH in product as a function of average current density. Case A is with ion-exchange textile incorporated and case B is without textile.



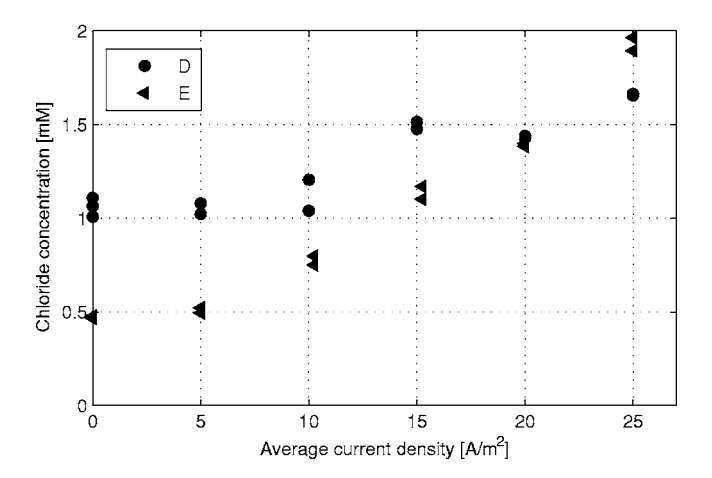


Figure 4. The concentration of nitrate and chloride in the product as a function of average current density for cases D and E. In these cases the mean velocity in the feed compartment was 1.2 cm/s. The textile was incorporated in case D and in case E the net-type spacer was used.

the textile. In order to utilize the ion-exchange character of the textile it is important to ensure that a satisfactory contact between textile and membranes is established.

In the experimental setup used, the pressure difference over the membranes could not be determined. However, the pressure drop over each compartment, i.e., the pressure difference between the inlet and outlet, could be controlled independently. In case C the pressure drop over the concentrate and electrode compartments was increased to 0.25 bar whereas the pressure drop over the feed compartment was set to 0.15 bar. The idea was to press the membrane against the textile by increasing the pressure outside of the textile-filled compartment.

The velocity of the feed solution through the feed compartment obtained in case C decreased from 1.7 to 0.4 cm/s. This indicates that resistance for the flow in the feed compartment increased as a consequence of the increased pressure outside of the feed compartment. As can be seen in Table III and Fig. 2, a nitrate separation of about 90% was obtained by Donnan dialysis in case C. Thus, applying the electric field seems unnecessary in this case.

In order to study the influence of the applied electric field it was necessary to increase the flow rate through the feed compartment. In cases D and E, with and without textile incorporated, respectively, the linear flow velocity of the feed was 1.2 cm/s. In both cases D and E the pressure drop over the feed compartment was adjusted to be 0.1 bar lower than over the other compartments, as was done in case C.

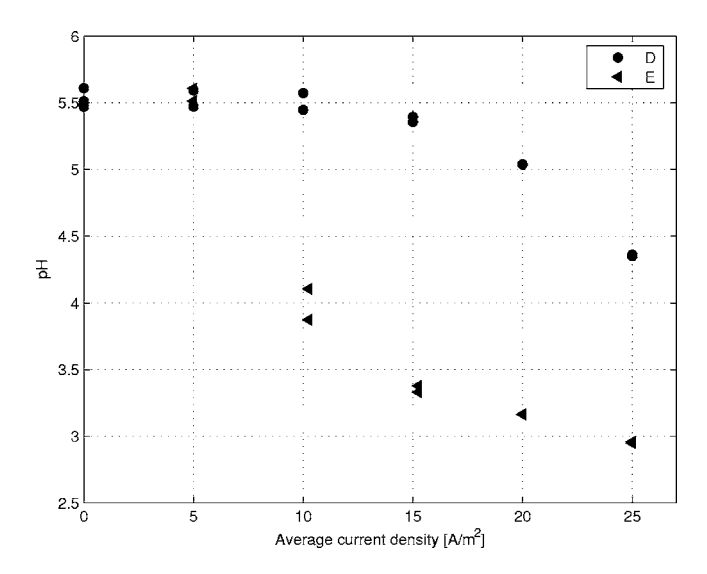


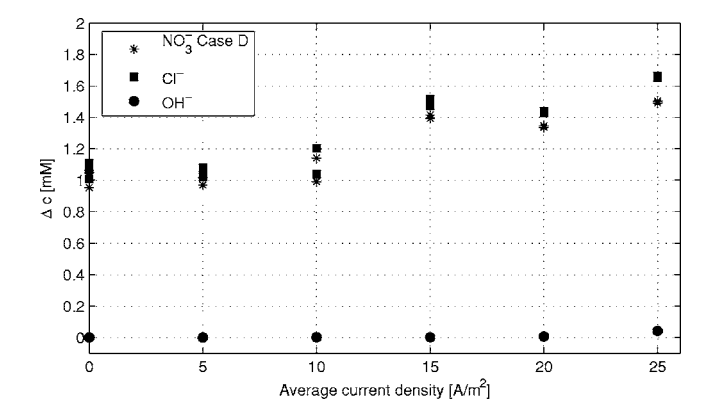
Figure 5. The pH of the product as a function of average current density for cases D and E.

The concentrations of nitrate and chloride in the product for cases D and E are shown in Fig. 4. The nitrate removal by Donnan dialysis is much higher in case D, with textile incorporated, compared to case E, without textile. In case D a nitrate concentration of 0.7 mM was obtained with the current switched off, compared to 1.35 mM in case E. Thus, the textile improves the mass transfer to the membranes. Results obtained from simulations² showed that the capacity of the ion-exchange textile only had a weak influence on the nitrate removal by Donnan dialysis. However, the structure of the textile material generates an effective mixing of the liquid phase in the feed compartment (FC), which reduces the thickness of the diffusion layers at the membranes. This can explain the improved nitrate removal by Donnan dialysis with the textile.

In case D the nitrate removal increased as the current density increased; this is presented in Fig. 4. At 25 A/m² the nitrate separation was 86%, corresponding to a reduction from 1.7 mM (105 ppm) to 0.25 mM (15 ppm). This is well below the regulated maximum level of 50 ppm for drinking water and also below the recommended maximum of 25 ppm. ^{11,12} This indicates that continuous electropermutation could successfully be used as a method for production of drinking water from nitrate-contaminated sources. The composition of the concentrate solution can be changed depending on the quality of the feed water. For example, if the pH of the feed is low one can accomplish a pH adjustment at the same time as the nitrate is removed by using a concentrate solution with a high pH.

Increasing the current density above 10 A/m² in case E, without the textile, does not result in an increased nitrate removal. Instead water dissociation becomes important and hydroxide ions are removed from the feed compartment instead of nitrate. Hence, it can be concluded that the use of an ion-conductive spacer in the feed compartment makes it possible to operate the process at a higher current and remove more nitrate at a given flow rate. The ionexchange textile used in the present study made it possible to increase the current density to 25 A/m² before water dissociation became influential. The result obtained for case E resembles those obtained for case B. Thus, the increased pressure outside of the feed compartment did not affect the separation for the cases without ionexchange textile incorporated. This supports the idea that the difference between cases A and D is explained by an improved contact between the membrane and the textile. A good contact between the conducting spacer and the membranes is necessary for the continuous electropermutation process to be successful.

It is expected that the change in pH should be less in case D compared with case A, in which the textile was also incorporated,



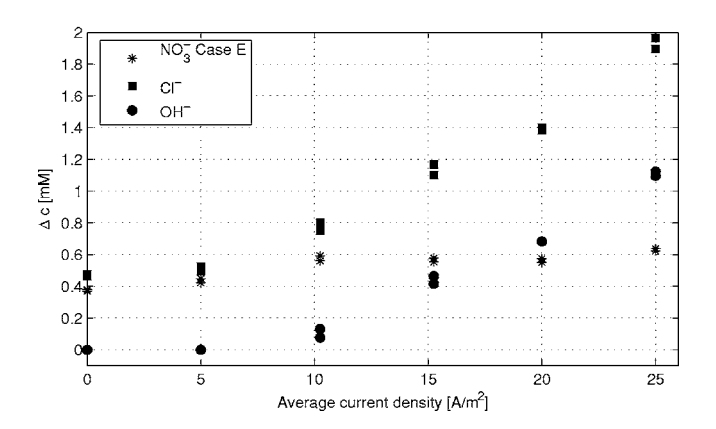


Figure 6. Changes in concentration over the feed compartment for case D with textile incorporated to the left and case E without textile to the right. The amount of nitrate removed is plotted at the top. In the center the increase in chloride concentration is plotted and at the bottom the decrease in hydroxide concentration is plotted against the average current density.

since nitrate is removed instead of hydroxide. That this is also the case is illustrated in Fig. 5, where the pH values for case D, with textile, and case E, without textile, are presented. In case D the pH went down to 4.4 at a current density of 25 A/m² compared to 3.5 in case A. In the corresponding experiments without textile incorporated the pH decreased to 3.2 in case B and to just under 3 in case E. This difference can be explained by the longer residence time in case E compared to case B.

In Fig. 6 the nitrate removed, chloride introduced, and hydroxide removed by the transport through the membranes are shown for cases D on the top and E at the bottom. The amount of hydroxide removed is calculated from the change in pH over the feed compartment. The change in pH in case E, where the textile was not incorporated, is more significant than when the textile was used. This is also reflected in the net introduction of chloride, which is higher in case E. In case D a higher degree of the current over the membrane on the anode side of the feed compartment is carried by chloride ions and thus does not lead to a net increase of the chloride concentration in the product water. The total ionic strength of the product is higher for case E due to the water splitting taking place, giving a production of ions in the feed compartment.

The experiments in case D seem to best represent the assumptions of the model presented in the first part of this series of papers and are compared to the model predictions. In the model it is the potential difference, ϕ_0 , over the feed compartment that is varied, since it is this potential difference that naturally enters the equations. In the experimental setup this potential difference was not possible to measure. This means that the dimensionless parameter χ , defined

Table IV. Parameter values used in the simulations. All parameters are defined in the first part of this series of papers.²

Nondimensional	parameters

α_2^1	2
$egin{array}{c} lpha_2^1 \ lpha_2^{m1} \end{array}$	1
E	0.15
γ	178
Γ	0.49
$ ilde{P}e$	360
σ	0.01
θ	0.4
χ	0–2
Z	410
Physical parameters	
D_1	$1.902 \times 10^{-9} (\text{m}^2 \text{s}^{-1})^{14}$
D_2	$2.032 \times 10^{-9} \; (\text{m}^2 \; \text{s}^{-1})^{14}$
$D_3 \ D_1^m$	$1.334 \times 10^{-9} \; (\text{m}^2 \; \text{s}^{-1})^{14}$
D_1^m	$2.8 \times 10^{-11} (\text{m}^2 \text{s}^{-1})^{13}$
D_2^m	$3.9 \times 10^{-11} (\text{m}^2 \text{s}^{-1})^{13}$
z_1, z_2	-1 [-]
z_3	1 [-]
Feed and	
concentrate	
X_{01}	1.0
X_{02}	0
X_{03}	1.0
X_{cc1}	0.05
X_{cc2}	0.95

$$\chi = \frac{\Phi_0 F}{RT} \frac{D_0 L}{j_0 h^2}$$
 [3]

in the model could not be determined. Instead the calculated average current density was used when comparing the model predictions with the experimental results. In the expression above, F is Faraday's constant, R is the gas constant, T is the temperature, D_0 is a typical scale for the ionic diffusivities, j_0 is the linear velocity of the flow through the feed compartment, L is the length of the cell, and h is the thickness of the feed compartment.

Values of the diffusion coefficients in the membrane, membrane thickness, and capacity of the membrane, used to determine the model parameters, were taken from the literature. ¹³ The volume

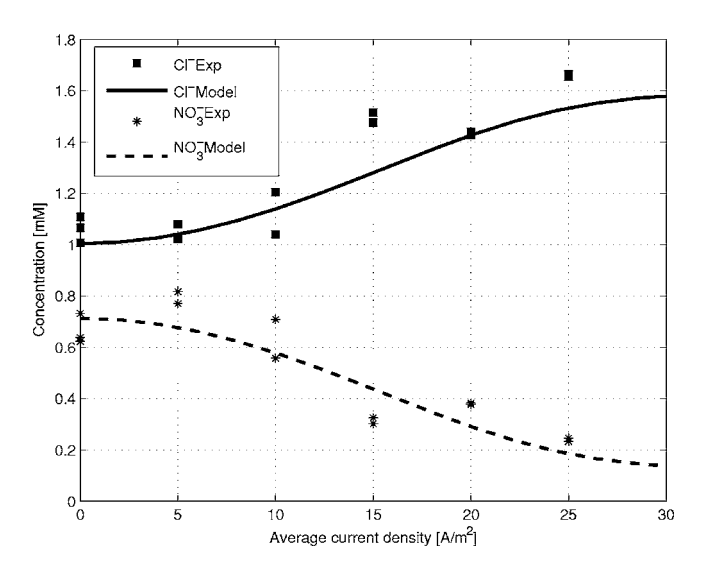


Figure 7. The model predictions for the outlet concentrations of chloride and nitrate plotted against the average current density together with the experimental results from case D.

Table V. χ values corresponding to the experimental data in case D. These values are not measured in the experiments but rather calculated with the model.

<i>i</i> (A/m ²)	χ
0	0
5	0.026
10	0.052
15	0.078
20	0.10
25	0.13

fraction of fibers in the textile was estimated to be $\epsilon=0.15$ from the density of the textile. The average fiber diameter was estimated from information given by the textile supplier to be $d_f=12~\mu m$. The model parameters used in the simulation are given in Table IV. The subscripts 1, 2, and 3 in Table IV refer to nitrate, chloride, and sodium, respectively.

The model predictions for the concentrations of nitrate and chloride are plotted together with the experimental results in Fig. 7. In Table V the χ value corresponds to the current densities at which the samples were taken in case D. It is found that the model predictions agree well with the experimental results.

An alternative way to illustrate the performance of the process that was presented in the modeling paper is to look at the overall current efficiency, η_T . This quantity was defined as

$$\eta = \left| \frac{F\Delta chWj_0}{I_T} \right|$$
 [4]

where Δc is the change in nitrate concentration between feed and product, I_T is the total current passed through the cell, and W is the width of the feed compartment. In Fig. 8 the current efficiency from case D is presented together with the current efficiency obtained in a simulation. An excellent agreement between the model and the experiment is found.

Conclusions

Nitrate removal from drinking water by continuous electropermutation was investigated. Experiments were conducted with and without a new anion-exchange textile incorporated as conducting spacer. It was shown that a significant increase in the nitrate removal was obtained by using the ion-exchange textile as conducting spacer. From an initial nitrate concentration of 1.7 mM in the feed water a

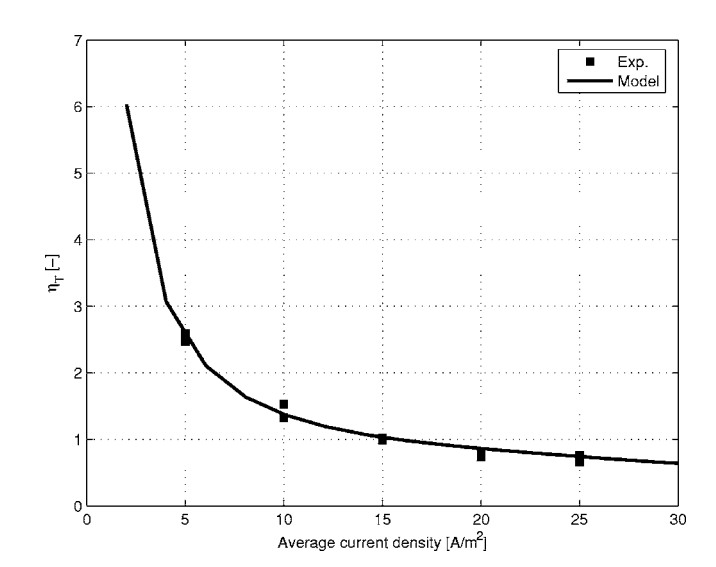


Figure 8. The current efficiency as predicted by the model compared to the experimental values determined from case D.

product stream with 0.25 mM of nitrate could be obtained in a single pass mode of operation with an applied current density of 25 A/m² and a flow velocity of 1.2 cm/s. The nitrate level in the product stream was well below the limiting value of 50 ppm for drinking water and also under the recommended maximum level of 25 ppm of nitrate. 11,12 The flow rate used corresponded to a production capacity of 20 L/h/unit cell. A stack with 50 elementary cells would be able to treat 1 m³ of water per hour.

It was pointed out that it is essential to have a good contact between membrane and ion-exchange textile. If the pressure in the feed compartment is too high compared to the adjacent concentrate compartments, preferential flow paths can be created between the membranes and the textile. The advantage of using the ion-exchange textile is then reduced and the process behaves similarly to the case with no textile incorporated. When the pressure drops over the concentrate and electrolyte compartments were increased to ensure contact between membrane and textile a dramatically improved nitrate removal was obtained. In case A, with insufficient contact, the maximum nitrate removal obtained was 35%, and in case D, with satisfactory contact, a nitrate removal of 86% was reached. Part of this difference is, however, explained by the different flow rates.

Incorporation of the ion-exchange textile improved the nitrate removal by Donnan dialysis. The importance of Donnan dialysis, which was discovered during the theoretical investigation, was confirmed by the experiments. Nitrate removal by Donnan dialysis is, however, slow compared to continuous electropermutation. In order to increase the flow rate it is necessary to apply the electric field to improve the nitrate removal rate.

Comparisons between predictions of a previously presented mathematical model and the experimental data were made to validate some results of the model and the assumptions made. A good agreement between the experimental results and the model predictions was obtained. Further improvement of the model would be to include the effects of water dissociation.

Nitrate removal for drinking water production by continuous electropermutation using ion-exchange textile shows great potential.

Continued development of the ion-exchange textiles will hopefully provide textiles with higher capacity. This would make it possible to use higher current densities before water dissociation becomes important and the production per unit cell can be increased. Development of nitrate-selective ion-exchange textiles would also have a positive influence on the performance of the process. Further studies are needed in order to investigate the energy consumption of the process.

Acknowledgment

The work was financed by the VINNOVA competence center, FaxénLaboratoriet, with the main industrial partner in this project being Vattenfall AB.

Royal Institute of Technology assisted in meeting the publication costs of this article.

- A. Kapoor and T. Viraraghavan, J. Environ. Eng., 123, 371 (1997).
 C. O. Danielsson, A. Dahlkild, A. Velin, and M. Behm, J. Electrochem. Soc., 153, D51 (2006).
- S. Ezzahar, A. Cherif, J. Sandeaux, R. Sandeaux, and C. Gavach, Desalination, 104 227 (1996)
- 4. K. Basta, A. Aliane, A. Lounis, R. Sandeaux, J. Sandeaux, and C. Gavach, Desalination, 120, 175 (1998).
- 5. N. Kourda, Ph.D. Thesis, Universitet Montpellier II (2000).
- E. Dejean, Ph.D. Thesis, Universitet Montpellier II (1997)
- L. Carlsson, B. Sandegren, D. Simonsson, and M. Rihovsky, J. Electrochem. Soc., 130, 342 (1983).
- 8. H. Schobesberger, M. Einzmann, J. Schmidtbauer, P. Gayrine, and R. Martinetti, Chemical Fibers International, 54, 101 (2004).
- M. Passounaud, J. C. Bollinger, B. Serpaud, and S. Lacour, Environ. Technol., 21, 745 (2000).
- 10. H. Strathmann, Ion-Exchange Membrane Separation Processes, Elsevier, Amsterdam (2004).
- 11. European Community, Official J. Europ. Commun., L330, 0032 (1998).
- 12. World Health Organization, Guidlines for Drinking Water Quality; Recommendations I, 3rd ed. (2004).
- 13. A. Elattar, A. Elmidaoui, N. Pismenskaia, C. Gavach, and G. Pourcelly, J. Membr.
- 14. J. S. Newman, Electrochemical Systems, Prentice Hall, New York (1991).

Paper 3

3

A Model for the Enhanced Water Dissociation On Monopolar Membranes

By Carl-Ola Danielsson¹, Anders Dahlkild¹, Anna Velin² & Mårten Behm³

To be submitted

A model for the enhanced water dissociation that takes place at the membrane interface in electromembrane processes is presented. The mechanisms behind the enhanced water dissociation are poorly understood and therefore a semi-empirical approach is suggested. The enhanced water dissociation is introduced as a heterogeneous surface reaction similar to the well established Butler-Volmer law for electrode reactions. In the model there are two parameters that need to be determined through experiments. A 1-D diffusion boundary layer problem is presented and solved in order to show that a sufficient rate of water dissociation can be obtained with the model. The advantage of the presented model is that is can easily be incorporated into simulations of electromembrane processes such as electrodialysis and electropermutation. The influence of the enhanced water dissociation on these processes can then be studied.

1. Introduction

It is known that concentration polarization and water dissociation takes place close to the membranes in the dilute compartment of an electrodialysis cell operating at high current densities. Generally dissociation of water is an unwanted phenomenon in electromembrane processes. It reduces the current efficiency and brings about a change of the pH in the concentrate and dilute compartments. Besides affecting the quality of the product, this pH change can cause problems such as precipitation of metal-hydroxides, which can foul the membranes.

However, there are examples of processes in which the dissociation of water is desired or even a necessity [1]. Electrodeionization is a electromembrane process that is capable of separating weak acids, such as silica acid and boric acid [2]. Local pH variations, due to water dissociation, within the dilute

¹Department of Mechanics, KTH, SE-100 44 Stockholm, Sweden.

²Vattenfall Utveckling AB, SE-162 87 Stockholm, Sweden.

 $^{^3{\}mbox{Department}}$ of Chemical Engineering and Technology, Applied Electrochemistry, KTH, SE-100 44 Stockholm, Sweden.

compartment of an electrodeionization cell are believed to be part of the mechanisms behind this separation. In electro-membrane processes with bipolar membranes the dissociation of water produces the ions that carries the current through the membrane under reverse bias operation. This way bipolar membranes are used to produce acid and bases [3].

In a previous article [4] we presented an experimental investigation of nitrate removal by electropermutation assisted by ion-exchange textile. It was found that the incorporation of the ion-exchange textile as conducting spacer was necessary in order to obtain sufficient mass transfer rates. Concentration polarization and intense water dissociation made the process very inefficient if a conducting spacer was not used. However, also in the cases where the textile was incorporated, water dissociation was starting to become important at the highest current density, 25 A/m^2 , considered in the study. Thus, in order to be able to accurately simulate the performance of an electropermutation process we decided that the effect of water dissociation should be included in the model. This work is the first step towards that goal.

The mechanisms behind the dissociation of water at the rates observed in electro-membrane processes are poorly understood. A number of different characteristic features of water dissociation in electromembrane processes have been reported, some of which were summarized by Jialin *et. al* [5]:

- Enhanced water dissociation behavior is found to be far more intense at the surface of anion-exchange membranes compared to cation-exchange membranes
- The water dissociation taking place in bipolar membranes is even more intense than at the surface of anion-exchange membranes .
- For anion-exchange membranes with quaternary ammonium groups, water dissociation develops after some of operation. It is believed that the quaternary ammonium groups at the membrane interface have degraded to tertiary form during electrolysis in the strong electric field present at the membrane interface. The water dissociation can be eliminated again by treating the membrane with methyl iodide.
- Water dissociation at the surface of cation-exchange membranes can suddenly become violent when some cations such as Mg(II) were present in dilute NaCl solution.

At present day there exist no theoretical model for the enhanced water dissociation that can explain all of these experimental findings. One theory that has been put forward to try to explain the accelerated water dissociation taking place in a bipolar membrane is the second wien effect (SWE), which predicts an increase in the degree of dissociation of weak acids at high electric fields strengths. A kinetic model for this effect was developed by Onsager [6]. There are some drawbacks associated with predicting the increased water dissociation in electromembrane processes by the second wien effect. The main limitation would be that it predicts a similar water dissociation behavior for mono-polar cation and anion exchange membranes. This is not in accordance

with the experimental results. Furthermore, the SWE theory has not been experimentally validated at the high electric field strengths, $E\approx 5\cdot 10^8$ V/m, present in, e.g., the space charge region of an bipolar membrane. Finally, the model presented by Onsager was developed for weak acids in water, and might not be directly applicable for dissociation of water molecules in water.

The water dissociation at cation and anion exchange membranes was studied by Simons [7, 8, 9] who proposed that the fixed charges groups in the membranes are involved in the water dissociation process. The produced protons and hydroxyl ions are believed to be the result of a protonation/deprotonation reaction according to the following schemes:

$$B + H_2O \underset{k_{-2}}{\overset{k_2}{\rightleftharpoons}} BH^+ + OH^-$$

$$BH^+ + H_2O \underset{k_{-3}}{\overset{k_3}{\rightleftharpoons}} B + H_3O^+$$

where BH⁺ refers to the catalytic active center for the proton-transfer reaction. The functional groups in some anion-exchange membrane act as these catalytic centers. A similar reaction could also be written for cation-exchange membranes according to:

$$A + H_2O \stackrel{k_4}{\underset{k_{-4}}{\rightleftharpoons}} AH^+ + OH^-$$

$$AH^{+} + H_{2}O \underset{k_{-5}}{\overset{k_{5}}{\rightleftharpoons}} A + H_{3}O^{+}$$

where AH is an acid group located at the surface of a cation-exchange membranes. This mechanism is called the chemical reaction (CHT) model [10]. The kinetics obtained with CHT model is to slow to explain the rate of water dissociation found in experiments. However, if the rate constants in the CHT model are assumed to increase in the strong electric field found in the space charge region membrane then a sufficient rate of dissociation can be predicted. Two different approaches have been proposed to explain the increased reaction rate under the influence of a strong electric field. First the SWE effect was again considered. This time it was not applied to an isolated water molecule, but to the dissociation reaction between the fixed charge group and the water molecules. The other approach is to use an empirical expression according to

$$\frac{k_d(E)}{k_d(0)} = \exp\left(\frac{\alpha F}{RT}E\right) \tag{1}$$

where α is a fitting parameter with the dimension of length [11]. Mafé tried to give α a physical interpretation from statistical arguments about the orientation of the polar water molecules in a strong electric field [12].

Yet another approach to explain the accelerated dissociation of water taking place in bipolar membranes was taken by Hurwitz and Dibiani [13, 14]. They looked at the reaction from a slightly different perspective. The ions

that are produced in the reaction are displaced to different sides of a reaction layer, and thus becomes separated in space. A consequence of this is that there exists a potential difference between the ionic products. This way the change in electrochemical potential between the reactant and the products, i.e. the change in Gibbs free energy, will depend on the potential difference over the reaction layer.

In the present paper a one dimensional three layer problem, known as the Kharkats problem [15] is solved with water dissociation/recombination taken into account. The enhanced water dissociation at the surface of the ion-exchange membrane is modeled as a heterogeneous surface reaction. The approach taken to capture the enhanced water dissociation in a surface reaction is similar to that taken by Hurwitz and Dibiani [13, 14]. Thus, a reaction layer is assumed to be located in a narrow region close to the solution/membrane interface. The differences in the water dissociation rates found with different types of membranes and with different electrolytes enter the model via the reaction rate constants and a symmetry factor. These parameters have to be determined from experiments. The main advantages of this model is that it can be used to incorporate the effect of water dissociation into simulations of electrodialysis, electropermutation and electrodeionisation in an efficient way. This makes it possible to model the pH of the solution in the dilute and concentrate compartments.

2. Problem formulation

A mono-polar ion-exchange membrane together with adjacent diffusion layers, as depicted in figure 1 is modeled. The solution in the compartments on both sides of the membrane is continuously replaced and thus the bulk concentrations on both sides are taken to be constant. The membrane in this study is an anion-permeable membrane with no selectivity towards any specific anion.

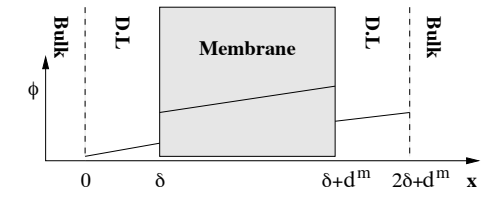


FIGURE 1. The domain included in the model. The concentration in the bulk of the dilute and concentrate compartments are assumed to be constant and known.

The solutions on both sides of the membrane are water with dissolved sodium chloride ions. Thus the following ions are included in the model Na⁺, Cl⁻, H⁺ and OH⁻ these will be referred to as specie 1-4 respectively. A one-dimensional steady state, model based on the conservation of mass of each of the species is formulated. The mass balance equations in the diffusion layers

are given by,

$$\nabla \cdot \mathbf{N}_i = R_i \quad i = 1 - 4, \tag{2}$$

where the fluxes, N_i , are given by Nernst-Plancks equation,

$$\mathbf{N}_{i} = \mathbf{u}c_{i} - D_{i}\nabla c_{i} - \frac{z_{i}F}{RT}D_{i}c_{i}\nabla\phi. \tag{3}$$

Furthermore, it is assumed that the electrolyte in the diffusion layers are stagnant, i.e., $\mathbf{u}=0$. The coordinate system is, as indicated in figure 1, chosen so that the diffusion layers are located between $0 \le x \le \delta$ and $\delta + d^m \le x \le 2\delta + d^m$, where d^m is the thickness of the membrane.

The only chemical reaction that is considered in the model is the auto protolysis of water

$$H_2O \underset{k_b}{\overset{k_f}{\rightleftharpoons}} H^+ + OH^-, \tag{4}$$

where $k_f = 2.7 \cdot 10^{-5} \text{ [s}^{-1} \text{]}$ and $k_b = 1.5 \cdot 10^{11} \text{ [M}^{-1} \text{s}^{-1} \text{]}$ are the forward and backward rate constants respectively. The concentration of water can be assumed to be constant since it is very high compared to the ionic concentrations, $c_{H_2O} \approx 55.5 \text{ [M]}$. The reaction rate is expressed as

$$R_{3,4} = k_f c_{H_2O} - k_b c_3 c_4 = k_b K_w \left(1 - \frac{c_3 c_4}{K_w} \right)$$
 (5)

where $K_w = \frac{k_f c_{H_2O}}{k_b}$.

The mass balance equations in the diffusion layers can be written as

$$D_{i}\frac{\mathrm{d}}{\mathrm{d}x}\left(\frac{\mathrm{d}c_{i}}{\mathrm{d}x} + z_{i}\frac{F}{RT}c_{i}\frac{\mathrm{d}\phi}{\mathrm{d}x}\right) = 0 \quad i = 1, 2$$
 (6a)

$$D_i \frac{\mathrm{d}}{\mathrm{d}x} \left(\frac{\mathrm{d}c_i}{\mathrm{d}x} + z_i \frac{F}{RT} c_i \frac{\mathrm{d}\phi}{\mathrm{d}x} \right) = k_b K_w \left(\frac{c_3 c_4}{K_w} - 1 \right) \quad i = 3, 4$$
 (6b)

The membrane is assumed to be ideally selective i.e. $c_1^m = c_3^m = 0$. Furthermore, no water dissociation/recombination is assumed to take place in the membrane. Thus, the mass balance equations in the membrane are

$$\nabla \cdot \mathbf{N}_i^m = 0 \quad i = 2, 4 \tag{7}$$

The fluxes in the membrane are described by Nernst-Plancks equations

$$\mathbf{N}_{i}^{m} = -D_{i}^{m} \nabla c_{i}^{m} - \frac{z_{i} F}{RT} D_{i}^{m} c_{i}^{m} \nabla \phi^{m}, \tag{8}$$

where any convective flux in the membrane is neglected. Thus, the mass balance equations in the membrane is given by,

$$D_i^m \frac{\mathrm{d}}{\mathrm{d}x} \left(\frac{\mathrm{d}c_i^m}{\mathrm{d}x} - \frac{F}{RT} c_i^m \frac{\mathrm{d}\phi^m}{\mathrm{d}x} \right) = 0 \quad i = 2, 4.$$
 (9)

The thickness of the membrane is $d^m[m]$ and the membrane is located between $x = \delta$ and $x = \delta + d^m$.

Electroneutrality is assumed to hold in the membrane and the diffusion layers adjacent to the membrane,

$$\sum_{i=1}^{4} z_i c_i = 0 \quad \text{in the diffusion layers,} \tag{10a}$$

$$z_2 c_2^m + z_4 c_4^m = z_w w \quad \text{in the membrane.} \tag{10b}$$

where z_w and w are valence and concentration of the functional groups in the membrane. Close to the membrane surface there is a thin layer in which the electroneutrality assumption is not valid. This layer is not resolved in the model and the changes of concentration and potential taking place over this region is incorporated into the model by internal boundary conditions. It is known that violent water dissociation can take place at the surface of an ion-exchange membrane, and a surface reaction is introduced as a mean of including the production of H^+ and OH^- ions at the membrane surface.

2.1. Boundary conditions

The concentration of all species in the bulk of both dilute compartment and the concentrate compartment are prescribed together with the applied potential difference.

$$c_i|_{x=0} = c_0, \ i = 1, 2$$
 $c_i|_{x=0} = \sqrt{K_w}, \ i = 3, 4$ (11)

$$\phi|_{x=0} = 0 \tag{12}$$

and

$$c_i|_{x=2\delta+d^m} = c_0 \ i = 1, 2$$
 $c_i|_{x=2\delta+d^m} = \sqrt{K_w} \ i = 3, 4$ (13)

$$\phi|_{x=2\delta+d^m} = \phi_0 \tag{14}$$

2.1.1. Internal boundary conditions

At the interface between the membrane and the electrolyte it is assumed that there exist a reaction layer. In the reaction layer the enhanced water dissociation reaction is taking place, which is modeled by a surface reaction term. A schematic of the reaction layer is presented in figure 2. The water molecules

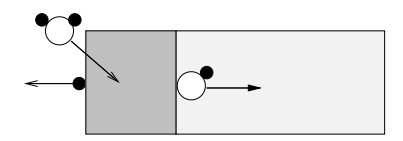


FIGURE 2. The reaction layer at the surface of the membrane. The ionic products are displaced to opposite sides of the reaction layer by the electric field.

in the reaction layer dissociate and the ionic products are transported out of the reaction layer on opposite sides. Thus, the concentration of OH^- , on the membrane side of the reaction layer, c_4^m , and the concentration of H^+ on the

diffusion layer side, c_3 , enters the expression for the reaction rate. The following overall water dissociation reaction is considered,

$$H_2O \underset{k'_h}{\overset{k'_f}{\rightleftharpoons}} H^+ + OH^{m-}, \tag{15}$$

The difference in Gibbs free energy, ΔG , of the water dissociation reaction (eq. 15) is affected by the difference in the electrical potential experienced by the product ions, $\Delta \phi_r$. Adopting the activated complex theory for the reaction kinetic gives,

$$k_f^{'} = k_f^{'0} \exp\left(\frac{\alpha F}{RT} \Delta \phi_r\right) \tag{16}$$

$$k_b^{'} = k_b^{'0} \exp\left(-\frac{(1-\alpha)F}{RT}\Delta\phi_r\right)$$
 (17)

where α is a symmetry factor. $k_f^{'0}$ and $k_b^{'0}$ are the surface reaction rate constants at zero potential difference over the reaction layer. Using these rate constants for the overall reaction rate of the water dissociation gives

$$R_{s} = k_{f}^{'0} c_{H_{2}O} \exp\left(\frac{\alpha F \Delta \phi_{r}}{RT}\right) - k_{b}^{'0} c_{4}^{m} c_{3} \exp\left(-(1-\alpha)\frac{F \Delta \phi_{r}}{RT}\right). \tag{18}$$

 R_s expresses the reaction rate per unit area and $\Delta\phi_r$ is the potential jump over the reaction layer. At equilibrium the forward and backward reaction rates are equal which defines the equilibrium potential according to

$$\Delta \phi_{eq} = \frac{RT}{F} \ln \left[\frac{k_b^{'0} c_3 c_4^m}{k_f^{'0} c_{H_2O}} \right]. \tag{19}$$

The reaction layer is assumed to be thin so that the water dissociation reaction is slow compared to the transport through the reaction layer. Thus, it is assumed that each species is in electrochemical equilibrium over the reaction layer. The potential difference over the reaction layer can then be expressed as a Donnan potential,

$$\Delta \phi_r = \frac{RT}{F} \ln \left[\frac{c_2^m}{c_2} \right] = \frac{RT}{F} \ln \left[\frac{c_4^m}{c_4} \right]. \tag{20}$$

Using electroneutrality and the second equality above makes it possible to write,

$$\Delta \phi_r = \frac{RT}{F} \ln \left[\frac{w}{c_2 + c_4} \right]. \tag{21}$$

Combining equation 18 and 20 gives,

$$R_s = K_w' k_b^{'0} \exp\left(\frac{\alpha F}{RT} \Delta \phi_r\right) \left(1 - \frac{c_3 c_4}{K_w'}\right)$$
 (22)

where $K_w' = \frac{k_f'^0 c_{H_2O}}{k_b'^0}$. The value of K_w' must be equal to K_w , for the reaction term to be zero at equilibrium. A further simplification is obtained by using

eq. 21 in eq. 22,

$$R_s = K_w k_b^{'0} \left[\frac{w}{c_2 + c_4} \right]^{\alpha} \left(1 - \frac{c_3 c_4}{K_w} \right). \tag{23}$$

This is the form of the heterogeneous surface reaction that is implemented in the present paper.

It is also possible to formulate the surface reaction rate by defining an equilibrium reaction rate r_0 and a reaction overpotential η . This gives a formulation that is similar to the well known Butler-Volmer expression for electrode reactions. The equilibrium reaction rate is defined as the forward or backward reaction rate at equilibrium,

$$r_0 = k_f^{'0} c_{H_2O} \exp\left(\frac{\alpha F \Delta \phi_{eq}}{RT}\right) = k_b^{'0} c_4^m c_3 \exp\left(-\frac{(1-\alpha)F \Delta \phi_{eq}}{RT}\right). \tag{24}$$

Using eq. 20 in eq. 24 one finds that the equilibrium reaction rate is concentration dependent according to

$$r_0 = k_b^{'0} {}^{\alpha} k_f^{'0} {}^{(1-\alpha)} c_{H_2O}^{(1-\alpha)} (c_3 c_4^m)^{\alpha} = K_w k_b^{'0} \left(\frac{c_3 c_4^m}{K_w}\right)^{\alpha}.$$
 (25)

A standard equilibrium reaction rate, $r_0^0 = K_w k_b^{\prime 0}$, can be defined as the exchange reaction rate when $c_3 c_4^m = K_w$.

$$r_0 = r_0^0 \left(\frac{c_3 c_4^m}{K_w}\right)^{\alpha} \tag{26}$$

Defining the overpotential, η , as

$$\eta = \Delta \phi_r - \Delta \phi_{eq} \tag{27}$$

makes it possible to express the surface reaction rate as

$$R_s = r_0 \left[\exp\left(\frac{\alpha F}{RT}\eta\right) - \exp\left(-\frac{(1-\alpha)F}{RT}\eta\right) \right]. \tag{28}$$

This form of the reaction rate is identical to the Butler-Volmer expression used to describe the reaction kinetics of electrode reactions. One main difference here, however, is that the overpotential cannot be controlled, which makes this formulation less powerful in this application.

The fluxes at the internal boundary at $x = \delta$ are related according to,

$$N_1|_{-} = 0 (29)$$

$$N_2|_- = N_2^m|_+ \tag{30}$$

$$N_3|_{-} = -R_s$$
 (31)

$$N_4|_- = N_4^m|_+ - R_s (32)$$

(33)

and at $x = \delta + d^m$, where the enhanced water dissociation can be neglected,

$$0 = N_1|_+$$
 (34)

$$N_2^m|_- = N_2|_+ \tag{35}$$

$$0 = N_3|_+$$
 (36)

$$N_4^m|_- = N_4|_+ (37)$$

. (38)

The +/- signs indicates that the flux is on the right/left side of the interface respectively. Together with the continuity of the electrochemical potential expressed by equation 20 this specifies the necessary internal boundary conditions.

3. Dimensionless form

The model equation are made dimensionless by introducing the following dimensionless variables,

$$\tilde{c}_{i} = \frac{\tilde{c}_{i}}{c_{0}} \quad i = 1 - 2, \ \tilde{c}_{i} = \frac{c_{i}}{\sqrt{K_{w}}} \quad i = 3 - 4, \ \tilde{c}_{i}^{m} = \frac{c_{i}^{m}}{w} \quad i = 2, 4$$

$$\tilde{x} = \frac{x}{\delta}, \quad \text{for } 0 \le x \le \delta,$$

$$\tilde{x} = \frac{x - \delta + d^{m}}{\delta} \frac{\delta}{d^{m}}, \quad \text{for } \delta \le x \le \delta + d^{m},$$

$$\tilde{x} = \frac{x + \delta - d^{m}}{\delta}, \quad \text{for } \delta + d^{m} \le x \le 2\delta + d^{m}$$

$$\tilde{\phi} = \frac{F\phi}{RT}, \ \tilde{\phi}^{m} = \frac{F\phi^{m}}{RT},$$
(39)

and dimensionless parameters,

$$\gamma = \frac{\sqrt{K_w}}{c_0}, \ \zeta = \frac{d^m}{\delta}, \ \kappa = \frac{\delta^2 K_w k_b}{D_0 c_0 \gamma}, \ Z = \frac{w}{c_0}.$$
(40)

With this choice of the dimensionless coordinate \tilde{x} the diffusion layers are located between $\tilde{x}=0-1$ and $\tilde{x}=2-3$ and the membrane is located between $\tilde{x}=1-2$. The dimensionless diffusion coefficients are defined by,

$$\tilde{D}_i = \frac{D_i}{D_0} \quad \tilde{D}_i^m = \frac{D_i^m}{D_0^m},\tag{41}$$

where D_0 and D_0^m are typical orders of magnitudes of the diffusion coefficients in the solution and membrane respectively.

Using these non-dimensional quantities the mass balance equations in the diffusion layer can be expressed as,

$$\frac{\mathrm{d}}{\mathrm{d}\tilde{x}}\tilde{D}_{i}\left(\frac{\mathrm{d}\tilde{c}_{i}}{\mathrm{d}\tilde{x}}+z_{i}\tilde{c}_{i}\frac{\mathrm{d}\tilde{\phi}}{\mathrm{d}\tilde{x}}\right)=0 \quad i=1,2,$$
(42a)

and

$$\frac{\mathrm{d}}{\mathrm{d}\tilde{x}}\tilde{D}_{i}^{m}\left(\frac{\mathrm{d}\tilde{c}_{i}}{\mathrm{d}\tilde{x}}+z_{i}\tilde{c}_{i}\frac{\mathrm{d}\tilde{\phi}}{\mathrm{d}\tilde{x}}\right)=\kappa(\tilde{c}_{3}\tilde{c}_{4}-1) \quad i=3,4.$$
(42b)

The electroneutrality in the diffusion layers in dimensionless form is given by,

$$\tilde{c}_1 - \tilde{c}_2 = \gamma(\tilde{c}_3 - \tilde{c}_4). \tag{43}$$

The mass balances in the membrane are expressed as,

$$\frac{\mathrm{d}}{\mathrm{d}\tilde{x}} \left(\frac{\mathrm{d}\tilde{c}_{i}^{m}}{\mathrm{d}\tilde{x}} - \tilde{c}_{i}^{m} \frac{\mathrm{d}\tilde{\phi}^{m}}{\mathrm{d}\tilde{x}} \right) = 0 \quad i = 2, 4, \tag{44}$$

and electroneutrality in the membrane gives,

$$\tilde{c}_2^m + \tilde{c}_4^m = 1. (45)$$

The dimensionless fluxes are given by

$$\tilde{N}_{i} = \tilde{D}_{i} \left(-\frac{\partial \tilde{c}_{i}}{\partial \tilde{x}} - z_{i} \tilde{c}_{i} \frac{\partial \tilde{\phi}}{\partial \tilde{x}} \right) \quad i = 1 - 4, \tag{46}$$

in the diffusion layers and by

$$\tilde{N}_{i}^{m} = \tilde{D}_{i}^{m} \left(-\frac{\partial \tilde{c}_{i}}{\partial \tilde{x}} - z_{i} \frac{\partial \tilde{c}_{i}}{\partial \tilde{x}} \right) \quad i = 2, 4, \tag{47}$$

in the membrane.

The dimensionless current density, \tilde{i} , is defined as,

$$\tilde{i} = \tilde{N}_1 - \tilde{N}_2 + \gamma (\tilde{N}_3 - \tilde{N}_4).$$
 (48)

Furthermore, the partial currents \tilde{i}_s and \tilde{i}_w are defined according to

$$\tilde{i}_s = \tilde{N}_1 - \tilde{N}_2 \quad \text{and} \quad \tilde{i}_w = \gamma(\tilde{N}_3 - \tilde{N}_4),$$

$$(49)$$

thus $\tilde{i} = \tilde{i}_s + \tilde{i}_w$.

3.1. Dimensionless boundary conditions

The dimensionless boundary conditions are given by,

$$\tilde{c}_i|_{\tilde{x}=0} = 1$$
 $\tilde{\phi}|_{\tilde{x}=0} = 0$ (50)

$$\tilde{c}_i|_{\tilde{x}=3} = 1 \qquad \qquad \tilde{\phi}|_{\tilde{x}=3} = \tilde{\phi}_0 \tag{51}$$

The dimensionless formulation of the continuity of the fluxes over membrane surface at $\tilde{x} = 1$ is given by,

$$\tilde{N}_1|_{-} = 0 \tag{52}$$

$$\tilde{N}_2|_- = \Theta \tilde{N}_2^m|_+ \tag{53}$$

$$\tilde{N}_3|_{-} + \kappa \Upsilon \left(\frac{Z}{(\tilde{c}_2 + \gamma \tilde{c}_4)}\right)^{\alpha} \left(1 - \tilde{c}_3 \tilde{c}_4\right) = 0 \tag{54}$$

$$\tilde{N}_4|_{-} = \frac{\Theta}{\gamma} \tilde{N}_4^m|_{+} - \kappa \Upsilon \left(\frac{Z}{(\tilde{c}_2 + \gamma \tilde{c}_4)}\right)^{\alpha} \left(1 - \tilde{c}_3 \tilde{c}_4\right)$$
(55)

and at $\tilde{x} = 2$

$$0 = \tilde{N}_1|_+ \tag{57}$$

$$\Theta \tilde{N}_2^m|_- = \tilde{N}_2|_+ \tag{58}$$

$$0 = \tilde{N}_3|_{+} \tag{59}$$

$$\frac{\Theta}{\gamma}\tilde{N}_4^m|_{-} = \tilde{N}_4|_{+} \tag{60}$$

(61)

where Θ and Υ are defined by

$$\Theta = \frac{D_0^m Z}{D_0 \zeta} \text{ and } \Upsilon = \frac{k_b^{'0}}{k_b \delta}.$$
 (62)

The dimensionless form of the Donnan equilibrium at the membrane surface, which was expressed in eq. 20 is given by,

$$\Delta \tilde{\phi}_r = \ln \left[Z \frac{\tilde{c}_2^m}{\tilde{c}_2} \right] = \ln \left[\frac{Z}{\gamma} \frac{\tilde{c}_4^m}{\tilde{c}_4} \right] = \ln \left[\frac{Z}{(\tilde{c}_2 + \gamma \tilde{c}_4)} \right]$$
 (63)

From the non-dimensional form of the model equations it is found that seven dimensionless parameters needs to be specified to solve the model equations. These are Z, $\tilde{\phi}_0$, κ , γ , Θ , Υ and α . The two last parameters Υ and α includes the information about the enhanced kinetics of the water dissociation reaction over the reaction layer.

4. Results and Discussion

The model equations were solved using the commercial finite element package COMSOL MultiphysicsTM 3.2. A number of different parametric studies were performed in order to study the influence of the different parameters in the model.

To obtain reasonable values of the model parameters the following base case was considered. The concentration of the salt in the bulk was taken to be 1 mM on both sides of the membrane. Together with a typical concentration of functional groups in an anion-exchange membrane of about 2 M [16] this gave a Z value of 2000. This Z value has been used in all simulations presented

in this paper. The rate constants for the dissociation and recombination of water, k_f and k_b , were taken to be $2.7 \cdot 10^{-5}$ s⁻¹ and $1.5 \cdot 10^{11}$ M⁻¹s⁻¹ [17] respectively. Together with a concentration of water, 55.5 M, this gave a K_w value of 10^{-14} M², and hence γ was 10^{-4} . The length scale of the diffusion layer, δ , was taken to be $100~\mu\mathrm{m}$ [18, 15, 19] and the diffusivity scale, D₀, was fixed at 10^{-9} m²s⁻¹, which gave a κ value of $1.5 \cdot 10^5$. The diffusivity scale in the membrane was assumed to be $2 \cdot 10^{-11}$ m²s⁻¹ [16] and the thickness of the membrane was taken to be $200~\mu\mathrm{m}$. This gave a Θ value of 20. For the two remaining parameters, α and Υ it is harder to estimate reasonable values, since the mechanisms behind the enhanced water dissociation at the membrane surface are unknown. However, by definition α lies in the interval 0-1. The first estimate of the surface reaction rate constant, k_b^0 , is given by the reaction rate in the bulk k_b multiplied by the thickness of the reaction layer i.e.

$$k_b^{'0} = k_b \lambda \tag{64}$$

The thickness of the reaction layer is assumed to be in the range 1-100 nm [8]. This gives that Υ is in the range 10^{-5} - 10^{-3} . The values of the dimensionless parameters and coefficients used in the simulations in this paper are summarized in table 1.

\tilde{D}_1	1.334 [20]
\tilde{D}_2	2.034[20]
\tilde{D}_3	9.02 [20]
\tilde{D}_4	5.26 [20]
Z	2000
α	0.01,0.1,0.3,0.5,0.7
γ	$10^{-5}, 10^{-4}, 10^{-3}$
κ	$1.5 \cdot 10^5$
Θ	20
Υ	$10^{-5}, 10^{-4}, 10^{-3}, 0.1, 1, 10$
$ ilde{\phi}_0$	0-200

TABLE 1. Values of the non dimensional parameters and coefficients used in the simulations presented in this paper.

Simulations were performed in order to investigate if the proposed model could predict dissociation rates that are commensurable with those found in experiments. First the influence of the symmetry factor, α was investigated. Polarization curves for different values of α , with $\Upsilon=10^{-4}$, and are presented in figure 3. The typical limiting current plateau is clearly visible, furthermore an overlimiting current density is obtained for the higher values of α . This gives the characteristic s-shape of the polarization curve found in experiments [21, 22]. It is stated in the literature that the slope of the polarization curve in the overlimiting region is somewhat less than the slope at sublimiting current densities [21, 23]. In figure 3 the curve representing the highest α value show

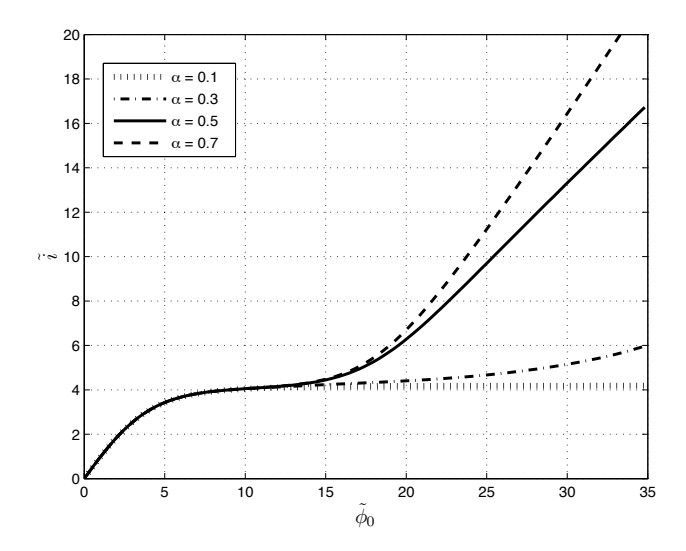


FIGURE 3. Current against voltage curves for different values of α . The Υ value in these simulations was 10^{-4} .

the opposite behavior. Thus, from the polarization curves presented in figure 3 it seems as if the proposed model is capable of predicting a sufficiently intense water dissociation at the membrane interface. The value of α will depend on the actual reaction mechanism of the dissociation reaction. If $\alpha=0$ then the strong electric field at the membrane surface does not affect the rate of water dissociation at all, instead the rate of the recombination reaction is decreased. If $\alpha=0.5$ half of the potential jump over the reaction layer helps increasing the rate of the dissociation, whereas the other half reduces the rate of the recombination.

In figure 4 the polarization curve for $\alpha=0.5, \ \gamma=10^{-4}$ and $\Upsilon=10^{-4}$ is shown together with the partial currents carried by the salt ions, \tilde{i}_s , and the ionic products of water, \tilde{i}_w . It is clear that at low potential differences the current is carried exclusively by the salt ions. When the voltage increases concentration polarization taking place at the membrane surface leads to a limiting current density behavior. As the voltage is further increased the accelerated water dissociation reaction, taking place at the membrane surface, makes the partial current carried by the ionic products of water, \tilde{i}_w , increase. The increased flux of H⁺ and OH⁻ also leads to an increased flux of the salt ions. This can be seen by the non zero slope of the dash-dotted curve, representing the partial current carried by the salt ions, in figure 4. This effect is known as the exaltation effect and was discovered by Kharkats [24]. It should be pointed out that the overlimiting current density captured in these simulations, is due to dissociation of water and the exaltation effect. It is stated in the literature that the contribution to the overlimiting current density from

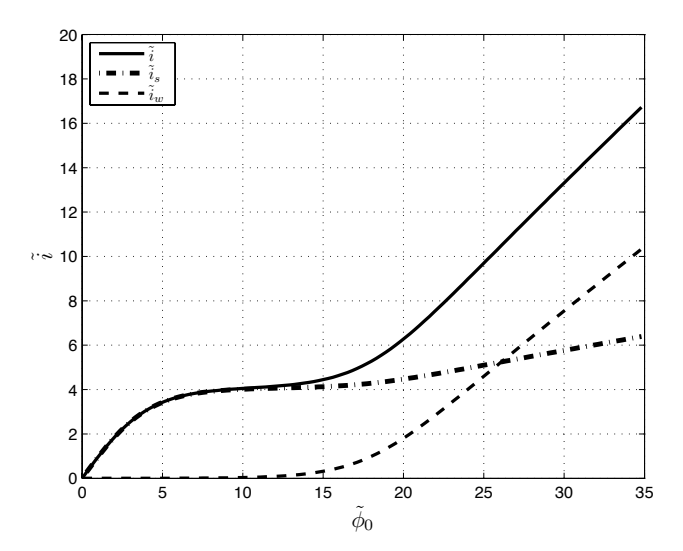


FIGURE 4. Current against voltage curves for α =0.5 and Υ = 10^{-4} . The different curves show the total current density as the solid line, the dotted line is the current density carried by the salt ions Na⁺ and Cl⁻ and the dashed line show the current density carried by the ion products of water.

the water dissociation products is small [25, 19, 26, 21], especially at the surface of cation-exchange membranes. Electroosmotic convection arising in the space charge region and leading to a mixing of the "unstirred" layer next to the membrane have been put forward as a mechanism for the overlimiting current in absence of intense water decomposition [27, 23, 28]. To capture this effect in the model one need to allow for deviation from electroneutrality by solving the Poisson equation for the potential. Furthermore, one would have to allow for electrosmotic convection to arise. This is, however, outside the scope of the present paper.

The fraction of the current carried by the salt ions and the dissociation products of water respectively are presented in figure 5 as a function of the potential drop. At low potentials the salt ions essentially carries the whole current. As the potential difference is increased and concentration polarization starts to take place the water dissociation reaction rate is enhanced. This is seen as the rapid increase in the fraction of the current carried by the ionic products of water. At very high applied potentials this fraction of the current approached the asymptotic value given by the exaltation effect. The expression for the total current density, obtained by adding the partial current from water

dissociation and the exaltation effect to the limiting current, is given by [19],

$$\tilde{i} = \tilde{i}_{lim} + \frac{\tilde{D}_2}{\tilde{D}_3} \tilde{i}_w + \tilde{i}_w. \tag{65}$$

At very high current densities the limiting current can be neglected and hence,

$$\frac{\tilde{i}_s}{\tilde{i}} = \frac{\tilde{D}_2}{\tilde{D}_2 + \tilde{D}_3} \approx 0.18 \quad \frac{\tilde{i}_w}{\tilde{i}} = \frac{\tilde{D}_3}{\tilde{D}_2 + \tilde{D}_3} \approx 0.82. \tag{66}$$

The curves in figure 5 approaches this asymptotic limit.

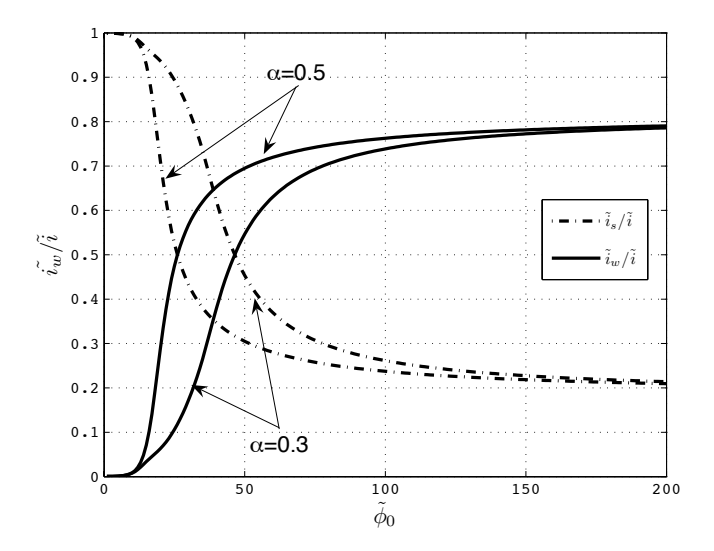


FIGURE 5. The fraction of the current carried by \tilde{i}_w and \tilde{i}_s as a function of $\tilde{\phi}_0$ for two different values of α . $\Upsilon=10^{-4}$ and $\gamma=10^{-4}$.

Enhanced water dissociation can only occur if the homogeneous reaction in the diffusion layers is not in equilibrium. Thus, both the heterogeneous surface reaction and the homogeneous reaction will contribute to the total rate of water dissociation. To determine where the water dissociation takes place the dimension less flux of hydroxide through the domain is presented in figure 6, for two different applied potentials.

The lowest potential presented in figure 6, $\dot{\phi}_0 = 5$, corresponds to the situation close to the limiting current. In this case the non-dimensional hydroxide flux through the membrane is quite low and the effect of the homogeneous reaction is clearly seen in both diffusion layers. The slope of the curves gives the rate of water dissociation. In the diffusion layer on the left hand side of the membrane water recombination takes place in the closest to the bulk and dissociation close to the membrane. The water dissociation due to the surface

reaction is relatively strong compared to the homogeneous reaction in the diffusion layer. In the diffusion layer on the right hand side of the membrane water recombination takes place through out the whole diffusion layer.

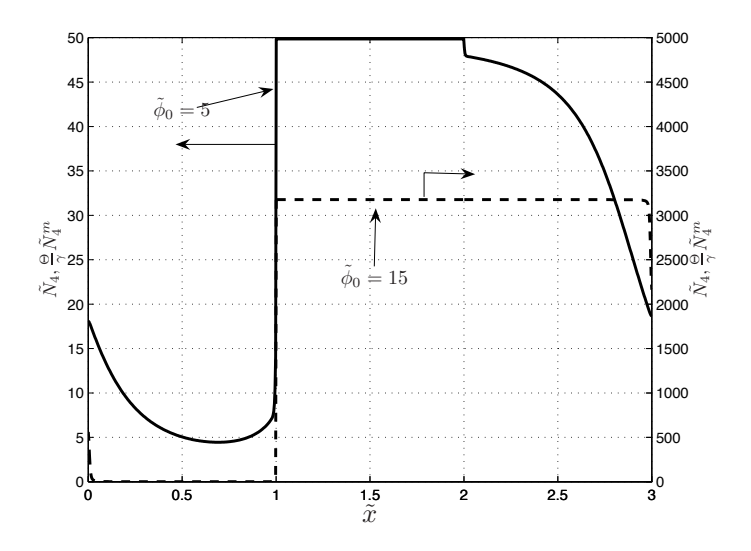


FIGURE 6. The dimensionless flux of hydroxide through the domain for two different potentials. These curves were obtained from simulations with $\Upsilon=10^{-4}$ and $\alpha=0.5$. Solid line, $\tilde{\phi}_0=5$, hydroxide flux given on the left y-axis. Dashed line, $\tilde{\phi}_0=15$, hydroxide flux given on the right y-axis.

Increasing the applied potential will give more intense water dissociation. The higher potential, $\tilde{\phi}_0 = 15$, corresponds to a point where the hydroxide flux through the membrane has started to be important compared to the chloride flux. Compared to the case where, $\tilde{\phi}_0 = 5$, the hydroxide flux has now increased almost two orders of magnitude. In this case the rate of water dissociation by the homogeneous reaction can be neglected. Only about 1% of the produced hydroxide ions at the surface of the membrane emerges from the homogeneous reaction in the diffusion layer. Close to the bulk in both diffusion layers there are thin reaction layers where intense water recombination takes place.

In order to study the influence of the surface reaction rate, polarization curves for different values of Υ are presented in figure 7 and 8. The α value in these simulations was 0.3 and 0.01 respectively, and the other parameter values were the same as in the base case presented above. In the case $\alpha=0.3$, the range of Υ -values were obtained from the assumption of a surface reaction rate k_b^0 proportional to the bulk reaction rate, k_b , multiplied with a reaction layer thickness λ of 1, 10 and 100 nm (eq. 64). As can be seen in figure 7, increasing Υ makes the dissociation of water faster.

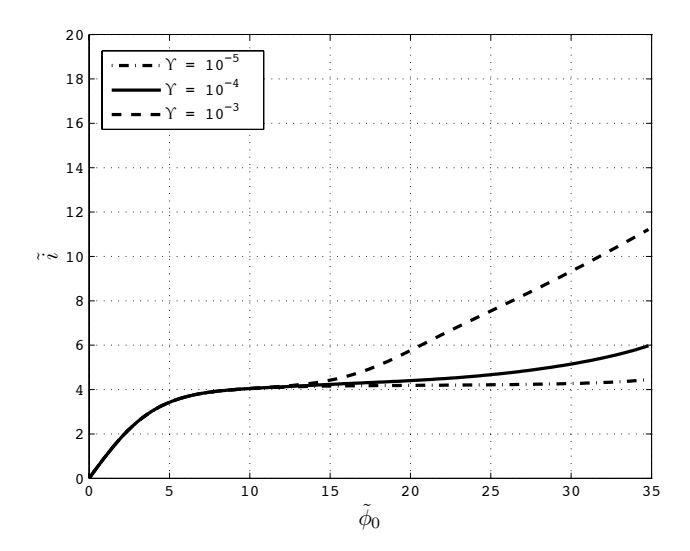


FIGURE 7. Current against voltage curves for different values of Υ . The symmetry factor, α , was equal to 0.3 in this case.

The case α =0.01 in figure 8 represents another assumption for the reaction mechanism. According to Simons [7, 8, 9] the effective reaction rate at the membrane surface can be several orders of magnitude larger than in the bulk solution even without the enhancement of the electric field. As was discussed in the introduction, Simons proposed that the difference between the water dissociation rates at the surface of anion- and cation-exchange membranes is explained by a catalytic effect of the functional groups in the anion exchange membranes. This is represented by the high Υ values in figure 8. Υ increases with the pK_b value of the catalytic groups as shown in appendix A. The value of α chosen in these simulations, α = 0.01, is reported by Hurwitz [14] for the water dissociation taking place in a bipolar membrane. From the results presented in figure 8 it is clear that the water dissociation rate increases with Υ also in this case.

The dash-dotted curve in figure 8 represents the case where $\Upsilon=0.1$. This polarization curve has two plateaus. The first one is given by the mass transport limitation of the salt ions in the bulk, i.e. what is referred to as the limiting current density, and the second plateau is due to the finite reaction rate of the water dissociation reaction. Increasing the potential difference over the reaction layer will only have a very small effect on the water dissociation in this case due to the very small α value. For the cases where Υ is high the reaction is sufficiently fast and the current density obtained is determined by the transport of the produced ions through the membrane and diffusion layer. Thus, there is a relatively small difference between the polarization curves obtained for Υ equal to 1 and 10 in the range of current densities presented in

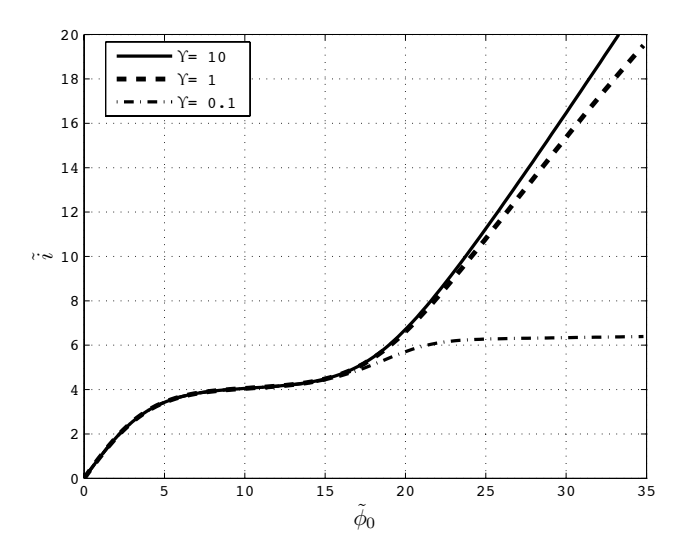


FIGURE 8. Current against voltage curves for different values of Υ . The symmetry factor α =0.01 in this case.

figure 8, i.e. up to 5 times the limiting current density in this case. Thus, if the reaction rate is sufficiently fast the mass transfer rather than the reaction rate will determine the rate of dissociation. For the nitrate removal application previously studied [29, 4] the situation is very similar to the base case presented here. It is therefore likely that the exact values of Υ and α will not be very important, over the relevant rage of current densities, as long as Υ can be assumed to large enough. The rate of water dissociation will be determined by the transport of the ionic products away from the reaction layer instead of the reaction rate constants.

Nikonenko et al. [30] investigated generation of H⁺ and OH⁻ at the surface of monopolar membranes. They concluded that the rate of waster dissociation can be described by the degree to which the membrane and the solution deviates from its critical stage, i.e. by the ratio i/i_{cr} . The critical stage is defined as the point when water starts to undergo a noticeable dissociation, which is claimed to be close to the limiting current density, $i_{cr} \approx i_{lim}$.

A linear relationship between $\log\frac{\tilde{i}_w}{\tilde{i}_{lim}}$ and $\sqrt{\frac{\tilde{i}}{i_{lim}}-1}$ was proposed. It was also stated that this relationship is only valid when the deviation from the critical state is not too large. The curve in figure 9 represents $\log\frac{\tilde{i}_w}{\tilde{i}_{lim}}$ calculated with our model as a function of $\sqrt{\frac{\tilde{i}}{\tilde{i}_{lim}}-1}$. The non-dimensional limiting current used to obtain this plot is given by,

$$\tilde{i}_{lim} = 2\tilde{D}_2. \tag{67}$$

The black squares in figure 9 are the experimental data presented in the paper by Nikonenko et.al~[30]. These data were obtained from a number of experiments with different sodium chloride solutions $(0.002\text{-}0.05\,\mathrm{M})$ and with different flow rates corresponding to different diffusion layer thicknesses. The scaling of the currents will however allow a direct comparison with our simulations. All

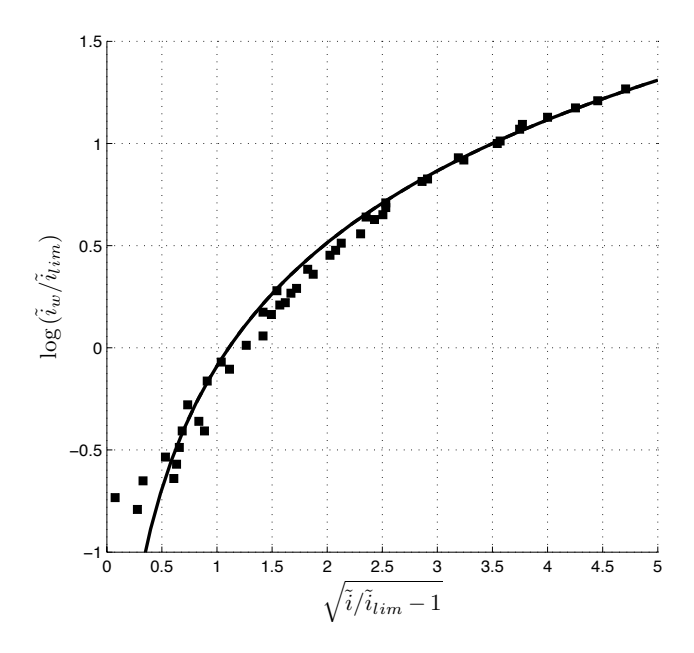


FIGURE 9. $\log \tilde{i}_w/\tilde{i}_{lim}$ as a function of $\sqrt{\tilde{i}/\tilde{i}_{lim}}-1$. \blacksquare - Experimental data reported in the paper by Nikonenko et.al [30]. The solid line is calculated with the model presented in this paper.

curves for different combinations of Υ and α values, that have been applied in our model, falls on top of each other. Thus, the shape of this curve is determined by the coupled transport through the diffusion layers and membrane and not by the reaction mechanism. It actually turns out that the curve obtained from our simulations is exactly that obtained by using the Kharkats (eq. 65) expression for the overlimiting current density. The only mechanisms responsible for the overlimiting current density captured by our model are water dissociation and the exaltation effect. Hence, from the relatively good agreement with the experimental data presented in figure 9, one can conclude, that in these experiments most of the overlimiting current density can be explained by dissociation of water and the exaltation effect. Contribution from a coupled convective mechanism to the overlimiting current density must be rather small.

The model for the enhanced water dissociation presented here can easily be incorporated as a heterogeneous surface reaction in simulations of electromembrane processes. A powerful tool for theoretical investigations of limitations and possibilities of different electromembrane processes is obtained by adding the possibility to predict when, where and at which rate dissociation of water can be expected to take place.

5. Conclusions

A model for the enhanced dissociation of water, encountered in many electromembrane applications, has been presented. By using a heterogeneous boundary condition to capture the dissociation rate a simple and computationally cheap way to include the enhanced water dissociation into simulations of electromembranes processes is obtained. This is very similar to the treatment of electrode reactions taking place at the surfaces of electrodes. The two parameters $\mathbf{k}_b^{'0}$ and α need to be determined via experiments. By performing simulations on a simple 1-D model problem it was shown that the model is able to predict a sufficiently fast water dissociation rate compared to experiments reported in the literature.

Due to the exaltation effect also the flux of the salt ions increased when the current of the dissociation products increased. At very high current densities the fraction of the current carried by chloride through the membrane reached a steady level of about 0.2.

At overlimiting current densities the dissociation of water in the diffusion layers is negligible compared to that in the heterogeneous surface reaction. All the hydroxide ions that carries the main part of the overlimiting current are produced by the surface reaction.

The rate of water dissociation is mass transfer controlled, if the enhanced water dissociation reaction can be assumed to be sufficiently fast. This is very convenient since the parameters Υ and α does not need to be determined as long as Υ is taken to be sufficiently large.

References

- [1] G.C. Ganzi, Y. Egozy, A.J. Giuffrida, and A.D. Jha. Deionization-high purity water by electrodeionization Performance of the ionpure continuous deionization system. *Ultrapure Water*, 4(3):43–48, 1987.
- [2] S. Thate, N. Specogna, and G. Eigenberger. Electrodeionization, a comparison of different EDI concepts used for the production of high-purity water. *Ultrapure Water*, 16(8):42–49, 1999.
- [3] H. Strathmann. Ion-Exchange Membrane Separation Processes. Elsevier, 2004. ISBN 0-444-50236-X.
- [4] C-.O. Danielsson, A. Velin, M. Behm, and A. Dahlkild. Nitrate removal by continuous electropermutation using ion-exchange textile: Part II experimental investigation. *Journal of The Electrochemical Society*, 153(4):D62–D67, 2006.
- [5] L. Jialin, W. Yazhen, Y. Changying, L. Guangdou, and S. Hong. Membrane catalytic deprotonation effects. *Journal of Membrane Science*, 147:247–256, 1998.
- [6] L. Onsager. Deviations from Ohm's law in electrolytes. J. Chem. Phys., 2:599, 1934.
- [7] R. Simons. Strong electric field effects on proton transfer between membrane-bound amines and water. *Nature*, 280:824–826, 1979.
- [8] R. Simons. Electric field effects on proton transfer between ionizable groups and water in ion exchange membranes. *Electrochimica Acta*, 29(2):151–158, 1984.
- [9] R. Simons. Water splitting in ion-exchange membranes. Electrochimica Acta, 30(3):275–282, 1985.
- [10] A.J.B. Kemperman. Bipolar membrane technology, Handbook. Twente University Press, 1st edition, 2000.
- [11] S.F Timashev and E.V. Kirganova. Mechanism of the electrolytic decomposition of water molecules in bipolar ion-exchange membranes. Soviet Electrochem., 17:366–369, 1982.
- [12] S. Mafé, P. Ramres, and A. Alcaraz. Electric field-assisted proton transfer and water dissociation at the junction of a fixed-charge bipolar membrane. *Chemical Pysics Letters*, 294:406–412, 1998.
- [13] H.D. Hurwitz and R. Dibiani. Investigation of electrical properties of bipolar membranes at steady state and with transient methods. *Electrochimica Acta*, 47:759–773, 2001.
- [14] H.D. Hurwitz and R. Dibiani. Experimental and theoretical investigations of steady and transient atates in systems of ion exchange bipolar membranes. *Journal of Membrane Science*, 228:17–43, 2004.
- [15] V.I. Zabolotskii, V.V. Nikonenko, N.M Korzhenko, R.R Seidov, and K.Kh. Urtenov. Mass transfer of salt ions in an electromembrane system with violated electroneutrality in the diffusion layer: The effect of a heterolytic dissociation of water. *Russian Journal* of *Electrochemistry*, 38(8):810–818, 2002.
- [16] A. Elattar, A. Elmidaoui, N. Pismenskaia, C. Gavach, and G. Pourcelly. Comparison of transport properties of monovalent anions through anion-exchange membranes. *Journal* of Membrane Science, 143:249–261, 1998.
- [17] E. Nilsson, J. Berendson, and E. Fontes. Electrochemical treatment of tumours: a simplified mathematical model. *Journal of Electroanalytical Chemistry*, 460:88–99, 1999.

- [18] I. Rubinstein. A diffusional model of "water splitting" in electrodialysis. The Journal of Physical Chemistry, 81(14):1431–1436, 1977.
- [19] V.I. Zabolotsky, V.V. Nikonenko, N.D Pismenskaya, E.V. Laktionov, K.Kh. Urtenov, H. Strathmann, M. Wessling, and G.H. Koops. Coupled transport phenomena in overlimiting current electrodialysis. *Separation and Purification Technology*, 14:255–267, 1998.
- [20] J. S. Newman. Electrochemical Systems. Prentice Hall, 2nd edition, 1991. ISBN: 0-13-248758-6.
- [21] I. Rubinstein and B. Zaltzman. Electro-osmotically induced convection at a permselective membrane. *Physical Review E*, 62(2):2238–2251, 2000.
- [22] M. Taky, G. Pourcelly, F. Lebon, and C. Gavach. Polarization phenomena at the interfaces between an electrolyte solution and an ion exchange membrane part I. ion transfer with a cation exchange membrane. J. Electroanal. Chem., 336:171–194, 1992.
- [23] I. Rubinstein and L.A. Segel. Breakdown of a stationary solution to the nernst-planck equations. *J. Chem. Soc.-Faraday Trans. II*, 75:936–940, 1979.
- [24] Yu. I. Kharkats. The mechanism of supralimiting currents at ion-exchange membrane electrolyte interfaces. Soviet Electrochemistry, 21:917–920, 1985.
- [25] J.J. Krol and H. Strathmann. Concentration polarization with monopolar ion-exchange membranes: Current-voltage curves and water dissociation. *Journal of Membrane Sci*ence, 162:145–154, 1999.
- [26] I. Rubinstein and L. Shtilman. Voltage against current curves of cation exchange membranes. J. Chem. Soc.-Faraday Trans. II, 75:231–246, 1979.
- [27] I. Rubinstein, B. Zaltzman, and O. Kedem. Electric fields in and around ion-exchange membranes. *Journal of Membrane Science*, 125:17–21, 1997.
- [28] V.I. Zabolotskii and V.V Nikonenko. Electrodialysis of dilute electrolyte solutions: Some theoretical and applied aspects. Russian Journal of Electrochemistry, 32(2):223–230, 1996.
- [29] C.-O. Danielsson, A. Dahlkild, A. Velin, and M. Behm. Nitrate removal by continuous electropermutation using ion-exchange textile: Part I modeling. *Journal of The Electro*chemical Society, 153(4):D51–D61, 2006.
- [30] V.V Nikonenko, N.D. Pismenskaya, and E.I. Volodina. Rate of generation of ions H⁺ and OH⁻ at the ion-exchange membrane/dilute solution interface as a function of the current density. Russian Journal of Electrochemistry, 41(11):1351–1357, 2005.
- [31] H. Strathmann, J.J. Krol, H.-J. Rapp, and G. Eigenberger. Limiting current density and water dissociation in bipolar membranes. *Journal of Membrane Science*, 125:123–142, 1997.

Appendix A

The catlytic protonation/deprotonation reaction at anion-exchange membranes proposed by Simons can be written as,

$$B + H_2O \underset{k_{-2}}{\overset{k_2}{\rightleftharpoons}} BH^+ + OH^-$$

$$BH^+ + H_2O \underset{k_{-3}}{\overset{k_3}{\rightleftharpoons}} B + H_3O^+$$
(68)

The following relations between the rate constants is found in the litterature [8, 9, 31]:

$$k_{2} = \frac{k_{-2} \cdot 10^{-pK_{b}}}{c_{H_{2}O}} s^{-1}$$

$$k_{3} = \frac{k_{-3} \cdot 10^{-(14-pK_{b})}}{c_{H_{2}O}} s^{-1}.$$
(69)

If B is a weak base the second reaction step is rate determining [13, 31]. Thus, the first reaction step is assumed to be in equilibrium, which gives that

$$c_B = \frac{c_{BH} + c_4^m}{10^{-pK_b}}. (70)$$

The rate of water decomposition due to the catalytic protonation/deprotonation reaction is given by;

$$R_{s} = k_{-3} 10^{-(14-pK_{b})} c_{BH^{+}} \exp\left[\frac{\alpha F}{RT} \Delta \phi_{r}\right] - k_{-3} \frac{c_{BH^{+}} c_{3} c_{4}^{m}}{10^{-pK_{b}}} \exp\left[-\frac{(1-\alpha)F}{RT} \Delta \phi_{r}\right]$$

$$= K_{w} k_{-3} c_{BH^{+}} 10^{pK_{b}} \exp\left[\frac{\alpha F}{RT} \Delta \phi_{r}\right] \left(1 - \frac{c_{3} c_{4}}{Kw}\right). \tag{71}$$

From this we can identify the reaction rate $k_h^{'0}$,

$$k_b^{'0} = k_{-3}c_{BH^+}10^{pK_b}\lambda. (72)$$

The rate constant k_{-3} is in the literature given in the order of 10^{10} M⁻¹s⁻¹ [9]. Here it is assumed that the ratio k_{-3}/k_b is approximately 0.1. The concentration of the catalytic groups is assumed to be of the order 1 M [14, 31], and the pK_b value is assumed to lie in the range 4 -6 where almost all of the catalytic groups are in BH⁺ form. Using these values together with a λ value of 10 nm, corresponds to Υ values that are between 0.1 and 10.

Paper 4

4

Modeling Continuous Electropermutation with Effects of Water Dissociation Included

By Carl-Ola Danielsson¹, Anders Dahlkild¹, Anna Velin² & Mårten Behm³

To be submitted

The repeating unit consisting of a cell pair of one concentrate and one feed compartment of an electropermutation stack is modeled. Both the feed and the concentrate compartments are filled with an ion-exchange textile material. Enhanced water dissociation taking place at the surface of the depleted membrane surface is included in the model as a surface reaction. Results from simulations of nitrate removal for drinking water production are presented and comparisons with previous experimental results are made. The influence of both conductive and inert textile spacers on the process is investigated via simulations.

1. Introduction

Ion exchange and electrodialysis are two widely used process alternatives for separation of ionic impurities from water. The advantage of ion exchange is that it is capable of treating solutions with very low levels of polutants [1]. However, ion exchange is not a continuous process. Electrodialysis on the other hand is a continuous process but is not suitable for treatment of solutions with very low conductivity. In electrodeionization (EDI) [2, 3] both these processes are combined into a continuous process, which is capable of treating solutions of very low conductivity. EDI is mainly used for production of ultrapure water. The main application for EDI is production of ultrapure water that is used in the power, microelectronics and pharmaceutical industry. In these applications all ions in the water need to be removed. Hence, an ion exchange bed that contains both cation and anion exchange material is used.

Continuous electropermutation [4, 5, 6, 7] is a process, which is similar to EDI in that it combines conventional ion-exchange with an electromembrane process. Instead of removing all ions either the anions or the cations are selectively replaced by other more desirable ions. Thus, the ion exchange bed should consist of either anion or cation exchange material. An application where electropermutation is an interesting process alternative is the removal of nitrate

¹Department of Mechanics, KTH, SE-100 44 Stockholm, Sweden.

²Vattenfall Utveckling AB, SE-162 87 Stockholm, Sweden.

 $^{^3{\}mbox{Department}}$ of Chemical Engineering and Technology, Applied Electrochemistry, KTH, SE-100 44 Stockholm, Sweden.

in drinking water production. Depending on the quality of the raw water one might like to selectively replace the nitrate ions. The principle for nitrate removal using continuous electropermutation is presented in figure 1. The water to be treated is passed through the feed compartment (F.C), which is delimited by two anion permeable membranes. Under the influence of an applied electric field the anions in the system migrates towards the anode. The anions present in the feed water migrate over the membrane into the C.C located on the anode side of the F.C. To ensure that electroneutrality is maintained these anions are replaced by other anions entering from the C.C on the cathode side of the F.C. This way it is possible to replace the anions initially present in the feed by anions from the concentrate solution, whereas the cations are preserved. In the schematic presented in figure 1 the nitrate ions migrate out of the F.C over the right hand side membrane at the same time as chloride ion enters the F.C over the left hand side membrane. The solution in the concentrate compartment in this example is a concentrated sodium chloride solution. Depending on the quality of the feed water the concentrate solution can be tailored, e.g. to adjust the pH by replacing the nitrate ions partially with hydroxide.

In two previous papers [6, 7] the removal of nitrate by continuous electropermutation using ion exchange textile as conducting spacer was studied both experimentally and theoretically. From the experimental investigation it was concluded a conducting spacer is needed, in the feed compartment, for the electropermutation process to be operated at reasonable current densities. Without a conducting spacer the limiting current density was very low and increasing the potential further led to an intense water dissociation, which made the process efficiency very poor. Incorporation of an ion exchange textile as a conducting spacer in the feed compartment greatly increased the efficiency of the process. It was concluded that the electropermuation process is an interesting process alternative for production of drinking water. However, also with the ion exchange textile incorporated as a conducting spacer it was noted that water dissociation was starting to become important at an average current densities of 25 A/m². In the previously presented model of the electropermutation process the effect of water dissociation was not included. The purpose of the present paper is to improve our previously presented model of the electropermutation process [6] by adding the effect of water dissociation. It is known that under certain conditions enhanced water dissociation takes place at the surface of anionpermeable membranes. This enhanced water dissociation is included as a heterogeneous surface reaction by a previously presented model [8]. Thus, an important task of the present work is to test the model for the enhanced water dissociation in a simulation of a real electromembrane process. Finally the presented model will be used to study how the incorporation of the textile influences the dissociation of water.

2. Problem formulation

The repeating unit in an electropermutation stack consists of one concentrate and one feed compartment. A sketch of the domain included in the model is

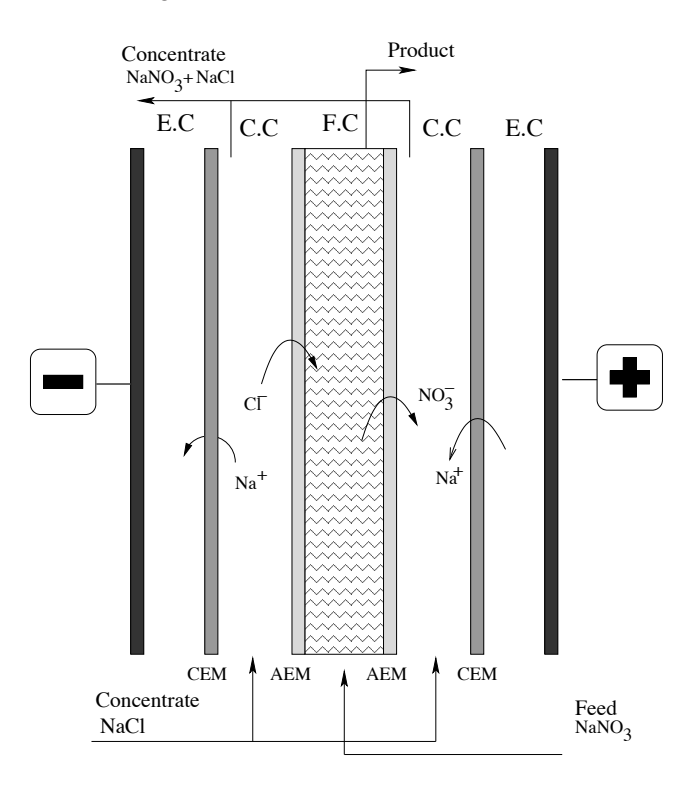


FIGURE 1. A schematic over the behind principles continuous electropermutation for nitrate removal. The water to be treated is passed through the feed compartment (F.C), which is separated from the concentrate compartments by anion permeable membranes on each side. Under the influence of an applied electric field, the nitrate ions in the F.C are replaced by chloride ions from the C.C.

presented in figure 2. In the model the C.C is split into two halves, sub domains I and V, these are located on opposite sides of the central feed compartment, sub domain III. Anion permeable membranes, sub domains II and IV, separate the concentrate and feed compartments. Periodic boundary conditions are applied at the center of the concentrate compartment, i.e. between sub domain I and V, except for the potential.

In a previous paper a steady state model of the F.C, filled with an ion exchange textile as a conducting spacer, together with adjacent ion exchange membranes in an electropermutation cell was presented [6]. In the present paper that model will be extended to include also the effect of water dissociation. Hence, the homogeneous reaction

$$H_2O \underset{k_b}{\overset{k_f}{\rightleftharpoons}} OH^- + H^+ \tag{1}$$

is considered. It is known that enhanced water dissociation can occur at the surface of the anion exchange membrane. The heterogeneous model used to incorporate this enhanced water dissociation was presented in a separate paper [8]. Mass balance equations are formulated for the following species NO_3^- , Cl^- , Na^+ , OH^- and H^+ which will be denoted as species 1-5, respectively. Thus, a whole elementary cell is now included in the model. Furthermore, the boundary layers next to the membranes are resolved instead of using the simplified Nernst layer model.

The feed and concentrate compartments are filled with an ion-conducting textile. Besides providing a good conductivity in the feed compartment this textile material will help to accomplish a good mixing of the solution as well as providing mechanical support to the membranes. The feed compartment is delimited by two anion permeable membranes, which are assumed to be ideally selective. The coordinate intervals of the five sub domains of the model domain,

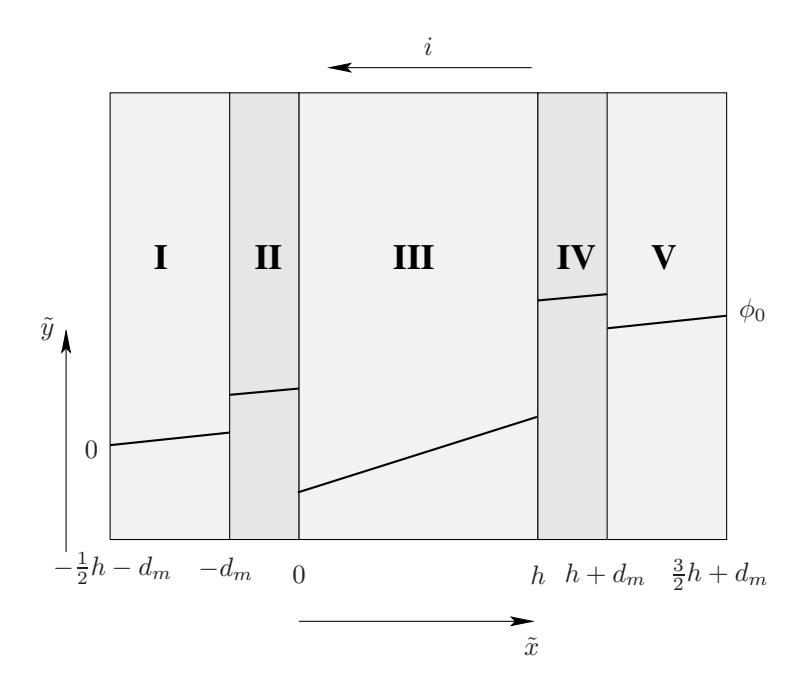


FIGURE 2. A schematic of the domain included in the model. I: Half of the adjacent C.C. II: Anion permeable membrane. III: F.C. IV: Anion permeable membrane. V: Half of the adjacent C.C. The solid line is a schematic of the potential through the cell.

shown in figure 2, are

I) Half of the adjacent concentrate compartment $-\frac{h}{2}-d^m \leq \tilde{x} \leq -d^m$

II) Anion-permeable membrane

$$-d^m \leq \tilde{x} \leq 0$$

III) Feed compartment

 $0 \le \tilde{x} \le h$

IV) Anion-permeable membrane

 $h \leq \tilde{x} \leq h + d^m$

V) Half of the adjacent concentrate compartment $h+d^m \leq \tilde{x} \leq \frac{3}{2}h+d^m$

2.1. Momentum balance

In the previous model [6] the flow through the textile-filled feed compartment was modeled with Darcy's law, which in the case of a uni-directional pressure gradient and a homogeneous textile gave a plug flow through the feed compartment.

$$\tilde{\mathbf{j}} = -\frac{K}{\mu} \frac{\partial P}{\partial y} \mathbf{e}_y \tag{2}$$

where $\tilde{\mathbf{j}}$ is the velocity vector, K is the permeability of the textile, μ the dynamic viscosity and P is the pressure. The effect of velocity boundary layers, satisfying the no-slip condition at the membrane walls, on mass transport next to the membranes was modeled by a stagnant Nernst layer. Due to the rapid reaction kinetics of the introduced homogeneous water dissociation/recombination reaction, the simplified Nernst layer model will not account for the non-equilibrium reaction layer close to the membrane. In order to resolve this reaction layer, also the momentum boundary layers are resolved. This is done by adding the Brinkman extension to Darcy's law [9]. The flow field is obtained by solving the following equation

$$\frac{\partial^2 \tilde{j}_y}{\partial \xi^2} - \frac{(1-\epsilon)}{K} \tilde{j}_y - \frac{(1-\epsilon)}{\mu} \frac{\partial P}{\partial y} = 0 \tag{3}$$

with the boundary conditions

$$\tilde{j}_y(\xi=0) = 0, \quad \frac{\partial \tilde{j}_y}{\partial \xi}(\xi=\infty) = 0,$$
 (4)

where ξ is the coordinate in the wall normal direction. ϵ in the equation above is the volume fraction of the fibers.

The permeability is taken to be a function of the porosity and the fiber diameter [10]. For a fibrous media the following expression can be found in the literature [11, 12]

$$K = \frac{3d_f^2}{20\epsilon} [-\ln(\epsilon) - 0.931]. \tag{5}$$

The pressure gradient is assumed to be constant. Thus, the velocity profile is given by

$$\tilde{j}_y(\xi) = j_0(1 - \exp(-\sqrt{(1 - \epsilon)K^{-1}}\xi)),$$
(6)

where j_0 is the "plug flow" velocity in the bulk of the textile bed. The non-dimensional velocity is obtained by scaling with j_0 ,

$$\mathbf{j} = \frac{\tilde{\mathbf{j}}}{j_0}.\tag{7}$$

2.2. Mass balance equations

2.2.1. Feed and Concentrate compartments

The textile filled feed and concentrate compartments, i.e. sub domains I,III and V, are modeled as a porous medium and volume averaged mass balance equations are formulated. In a previous paper [6] it was shown that the liquid phase and the fiber phase can be considered to be in ion-exchange equilibrium with each other. Thus it is necessary to solve one mass balance equation for each species. The non dimensional mass balance equations in the feed are given by [6],

$$j_{y}\frac{\partial c_{i}}{\partial y} = \left(\theta j_{y} + (1 - \epsilon)^{3/2} \frac{D_{i}}{\mathcal{P}}\right) \frac{\partial^{2} c_{i}}{\partial x^{2}} + z_{i} \chi (1 - \epsilon)^{3/2} D_{i} \frac{\partial}{\partial x} \left(c_{i} \frac{\partial \phi}{\partial x}\right) + \frac{0.15 \epsilon^{3/2} Z}{\mathcal{P}} D_{i} \frac{\partial^{2} \bar{c}_{i}}{\partial x^{2}} + z_{i} 0.15 Z \chi \epsilon^{3/2} D_{i} \frac{\partial}{\partial x} \left(\bar{c}_{i} \frac{\partial \bar{\phi}}{\partial x}\right) \quad \text{for i=1,2}$$

$$(8)$$

$$j_y \frac{\partial c_3}{\partial y} = \left(\theta j_y + (1 - \epsilon)^{3/2} \frac{D_3}{\mathcal{P}}\right) \frac{\partial^2 c_3}{\partial x^2} + z_3 \chi (1 - \epsilon)^{3/2} D_i \frac{\partial}{\partial x} \left(c_3 \frac{\partial \phi}{\partial x}\right). \tag{9}$$

The mass balance equations for two new species OH⁻ and H⁺ will have the same form but with the reaction term added;

$$j_{y}\frac{\partial c_{4}}{\partial y} = \left(\theta j_{y} + (1 - \epsilon)^{3/2} \frac{D_{4}}{\mathcal{P}}\right) \frac{\partial^{2} c_{4}}{\partial x^{2}} + z_{4} \chi (1 - \epsilon)^{3/2} D_{4} \frac{\partial}{\partial x} \left(c_{4} \frac{\partial \phi}{\partial x}\right) + \left(\frac{0.15 \epsilon^{3/2}}{\mathcal{P}} D_{4} \frac{\partial^{2} \bar{c}_{4}}{\partial x^{2}} + z_{4} 0.15 \chi \epsilon^{3/2} D_{4} \frac{\partial}{\partial x} \left(\bar{c}_{4} \frac{\partial \bar{\phi}}{\partial x}\right) + \kappa (1 - c_{4} c_{5}),$$

$$(10)$$

$$j_{y}\frac{\partial c_{5}}{\partial y} = \left(\theta j_{y} + (1 - \epsilon)^{3/2} \frac{D_{5}}{\mathcal{P}}\right) \frac{\partial^{2} c_{5}}{\partial x^{2}} + z_{5} \chi (1 - \epsilon)^{3/2} D_{5} \frac{\partial}{\partial x} \left(c_{5} \frac{\partial \phi}{\partial x}\right) + \kappa (1 - c_{4} c_{5}).$$

$$\tag{11}$$

The non-dimensional mass balance equations in the concentrate compartment have the same form but they are scaled somewhat differently,

$$j_{y}\frac{\partial c_{i}^{cc}}{\partial y_{cc}} = \left(\theta j_{y} + (1 - \epsilon)^{3/2} \frac{D_{i}}{\mathcal{P}}\right) \frac{\partial^{2} c_{i}^{cc}}{\partial x_{cc}^{2}} + z_{i} \chi (1 - \epsilon)^{3/2} D_{i} \frac{\partial}{\partial x_{cc}} \left(c_{i}^{cc} \frac{\partial \phi^{cc}}{\partial x_{cc}}\right) + \frac{0.15 \epsilon^{3/2} Z}{\mathcal{P} C^{cc}} D_{i} \frac{\partial^{2} \bar{c}_{i}^{cc}}{\partial x_{cc}^{2}} + z_{i} 0.15 \frac{Z}{C^{cc}} \chi \epsilon^{3/2} D_{i} \frac{\partial}{\partial x_{cc}} \left(\bar{c}_{i}^{cc} \frac{\partial \bar{\phi}^{cc}}{\partial x_{cc}}\right) \quad \text{for i=1,2}$$

$$(12)$$

$$j_y \frac{\partial c_3^{cc}}{\partial y_{cc}} = \left(\theta j_y + (1 - \epsilon)^{3/2} \frac{D_3}{\mathcal{P}}\right) \frac{\partial^2 c_3^{cc}}{\partial x_{cc}^2} + z_3 \chi (1 - \epsilon)^{3/2} D_3 \frac{\partial}{\partial x_{cc}} \left(c_3^{cc} \frac{\partial \phi^{cc}}{\partial x_{cc}}\right). \tag{13}$$

$$j_{y}\frac{\partial c_{4}^{cc}}{\partial y_{cc}} = \left(\theta j_{y} + (1-\epsilon)^{3/2} \frac{D_{4}}{\mathcal{P}}\right) \frac{\partial^{2} c_{4}^{cc}}{\partial x_{cc}^{2}} + z_{4} \chi (1-\epsilon)^{3/2} D_{4} \frac{\partial}{\partial x_{cc}} \left(c_{4}^{cc} \frac{\partial \phi^{cc}}{\partial x_{cc}}\right) + \frac{0.15\epsilon^{3/2}}{\mathcal{P}} D_{4} \frac{\partial^{2} \bar{c}_{4}^{cc}}{\partial x_{cc}^{2}} + z_{4} 0.15 \chi \epsilon^{3/2} D_{4} \frac{\partial}{\partial x_{cc}} \left(\bar{c}_{4}^{cc} \frac{\partial \bar{\phi}^{cc}}{\partial x_{cc}}\right) + \kappa (1 - c_{4}^{cc} c_{5}^{cc}), \tag{14}$$

$$j_{y} \frac{\partial c_{5}^{cc}}{\partial y_{cc}} = \left(\theta j_{y} + (1 - \epsilon)^{3/2} \frac{D_{5}}{\mathcal{P}}\right) \frac{\partial^{2} c_{5}^{cc}}{\partial x_{cc}^{2}} + z_{5} \chi (1 - \epsilon)^{3/2} D_{5} \frac{\partial}{\partial x_{cc}} \left(c_{5}^{cc} \frac{\partial \phi^{cc}}{\partial x_{cc}}\right) + \kappa (1 - c_{4}^{cc} c_{5}^{cc}).$$

$$(15)$$

The following non-dimensional variables were introduced,

$$x = \frac{\tilde{x}}{h} \quad 0 \le \tilde{x} \le h, \quad y = \frac{\tilde{y}}{L} \quad 0 \le \tilde{y} \le L,$$

$$x_{cc} = \frac{\tilde{x} + d_m + h}{h} \quad -\frac{h}{2} \le \tilde{x} \le -d_m,$$

$$x_{cc} = \frac{\tilde{x} - d_m}{h} \quad h + d_m \le \tilde{x} \le h, \quad y_{cc} = \frac{\tilde{y}}{L} \quad 0 \le \tilde{y} \le L,$$

$$c_i = \frac{\tilde{c}_i}{c_0} \quad \text{for i=1-3}, \quad c_i^{cc} = \frac{\tilde{c}_i}{c_0^{cc}} \quad \text{for i=1-3},$$

$$c_i = \frac{\tilde{c}_i}{\sqrt{K_w}} \quad \text{for i=4-5}, \quad c_i^{cc} = \frac{\tilde{c}_i}{\sqrt{K_w}} \quad \text{for i=4-5}$$

$$\bar{c}_i = \frac{\tilde{c}_i}{w} \quad \text{for i=1-2}, \quad \bar{c}_4 = \frac{\tilde{c}_4}{\sqrt{K_w}}$$

$$\bar{c}_i^{cc} = \frac{\tilde{c}_i}{w} \quad \text{for i=1-2}, \quad \bar{c}_4^{cc} = \frac{\tilde{c}_i}{\sqrt{K_w}}$$

$$\phi = \frac{\tilde{\phi}}{\phi_0}, \quad \bar{\phi} = \frac{\tilde{\phi}}{\phi_0}, \quad \phi^{cc} = \frac{\tilde{\phi}}{\phi_0}, \quad \bar{\phi}^{cc} = \frac{\tilde{\phi}}{\phi_0},$$

where the tildes are over the dimensional variables. The scaling of the \tilde{x} coordinate is chosen so that x goes between 0 and 1 in the F.C. In the C.C x_{cc} goes between 0.5^- and 1 in the half C.C on the left hand side of the F.C and between 0 and 0.5^+ in the half C.C on the right hand side of the feed compartment.

The non-dimensional diffusion coefficients are defined according to;

$$D_i = \frac{\tilde{D}_i}{D_0}, \ \bar{D}_i = \frac{\tilde{D}_i}{D_0}, \tag{17}$$

furthermore, it was assumed that the diffusion coefficients in the fiber phase are related to those in water according to

$$\bar{D}_i = 0.15D_i. \tag{18}$$

The correlation used for the non-dimensional transverse dispersion coefficient is given by [10, 13],

$$D_T = \lambda j_y P e_{df} D_0 \frac{L}{j_0 h^2} = \frac{\lambda j_y d_f L}{h^2} = j_y \theta, \tag{19}$$

where

$$\theta = \frac{\lambda d_f L}{h^2} \tag{20}$$

 Pe_{df} in the above expression is the Peclet number based on the fiber diameter, i.e., $Pe_{df} = \frac{j_0 d_f}{D_0}$. In our previous paper [6] the empirical parameter, λ was chosen as 0.27, this value will also be used in the present paper.

The flow velocity, j_y , is given by,

$$j_y = 1 - \exp(-\Lambda x_x)$$
 $0 \le x_x \le 0.5$
 $j_y = 1 - \exp(-\Lambda (1 - x_x))$ $0.5 \le x_x \le 1$ (21)

where $x_x = x$ in the F.C and $x_x = x_{cc}$ in the C.C and

$$\Lambda = \sqrt{\frac{(1-\epsilon)}{K}}h. \tag{22}$$

 ϵ is the volume fraction of the fiber phase. In the present paper it is assumed that this is constant and use a value $\epsilon=0.15$. The above equations were derived under the assumption that the two phases are in a parallel arrangement with each other. Effective diffusion coefficients, given by a Bruggeman relation, have been used in both phases

$$D_{i,eff} = (1 - \epsilon)^{1+\beta} D_i$$
 and $\bar{D}_{i,eff} = \epsilon^{1+\beta} \bar{D}_i$. (23)

The use of the effective diffusion coefficients compensate to some extent for the assumption of a parallel arrangement of the phases. The non-dimensional parameters introduced in equations 8-15 are defined according to;

$$Pe = \frac{j_0 L}{D_0}, \ \sigma = \frac{h}{L}, \ \mathcal{P} = \sigma^2 Pe, \ \mathcal{V} = \frac{F\phi_0}{RT},$$

$$\kappa = \frac{(1 - \epsilon)L\sqrt{K_w}k_b}{j_0}, \ \chi = \frac{\mathcal{V}}{Pe\sigma^2}, \ Z = \frac{w}{c_0}, \ C^{cc} = \frac{c_0^{cc}}{c_0}.$$
(24)

The ion-exchange fibers are taken to be in equilibrium with the solution, which in the feed compartment gives

$$\bar{c}_2 = \alpha_1^2 \frac{\bar{c}_1 c_2}{c_1}
\bar{c}_4 = \alpha_1^4 Z \frac{\bar{c}_1 c_4}{c_1}.$$
(25)

In the concentrate compartment the concentration in the ion-exchange fibers are given by

$$\bar{c}_2 = \alpha_1^2 \frac{\bar{c}_1 c_2^{cc}}{c_1^{cc}}
\bar{c}_4 = \alpha_1^4 \frac{Z}{C^{cc}} \frac{\bar{c}_1 c_4}{c_1^{cc}}.$$
(26)

Furthermore, the potential gradient in the two phases are related through

$$\frac{\partial \bar{\phi}}{\partial x} = \frac{\partial \phi}{\partial x} + \frac{1}{\mathcal{V}} \frac{\partial}{\partial x} \ln \left[\frac{Z}{c_1 + \alpha_1^2 c_2 + \alpha_1^4 C^w c_4} \right],\tag{27}$$

in the feed compartment and

$$\frac{\partial \bar{\phi}}{\partial x_{cc}} = \frac{\partial \phi}{\partial x_{cc}} + \frac{1}{\mathcal{V}} \frac{\partial}{\partial x_{cc}} \ln \left[\frac{Z}{C^{cc}(c_1 + \alpha_1^2 c_2) + \alpha_1^4 C^w c_4} \right]$$
(28)

in the concentrate compartment.

2.2.2. Membranes

In the membranes only the anionic species (i=1,2,4) are present. Contribution to the flux through the membranes by convection is neglected, thus, the non-dimensional form of the mass balance equations in the membranes are given by,

$$-\frac{\partial^2 c_i^m}{\partial x_m^2} + \mathcal{V} \frac{\partial}{\partial x_m} \left(c_i^m \frac{\partial \phi^m}{\partial x_m} \right) = 0 \quad \text{for i=1,2,4.}$$
 (29)

where the following new dimensionless variables were introduced;

$$x_{m} = \frac{\tilde{x} + d^{m}}{d^{m}} \quad \text{for } -d^{m} \leq \tilde{x} \leq 0 \quad x_{m} = \frac{\tilde{x} - h}{d^{m}} \quad \text{for } h \leq \tilde{x} \leq h + d^{m}$$

$$c_{i}^{m} = \frac{\tilde{c}_{i}^{m}}{c_{0}^{m}} \quad \text{for } i=1,2 \quad c_{4}^{m} = \frac{\tilde{c}_{4}^{m}}{\sqrt{K_{w}}}, \quad \phi^{m} = \frac{\tilde{\phi}^{m}}{\phi_{0}}.$$

$$(30)$$

2.3. Electroneutrality condition

Electroneutrality is assumed in all regions of the model and the non-dimensional form of this constraint is given by;

$$\begin{split} c_1^m + c_2^m + \frac{C^w}{C^m} c_4^m &= 1 \quad \text{in sub-domains II and VI} \\ c_1 + c_2 + C^w c_4 &= c_3 + C^w c_5 \quad \text{in the liquid phase in sub-domain III} \\ \bar{c}_1 + \bar{c}_2 + \frac{C^w}{Z} \bar{c}_4 &= 1 \quad \text{in the fiber phase in sub-domain III} \\ c_1^{cc} + c_2^{cc} + \frac{C^w}{C^{cc}} c_4^{cc} &= c_3^{cc} + \frac{C^w}{C^{cc}} c_5^{cc} \quad \text{in the liquid phase in sub-domains I,V} \\ \bar{c}_1^{cc} + \bar{c}_2^{cc} + \frac{C^w}{Z} \bar{c}_4^{cc} &= 1 \quad \text{in the fiber phase in sub-domains I,V}, \end{split}$$

where

$$C^w = \frac{\sqrt{K_w}}{c_0}$$
 and $C^m = \frac{c_0^m}{c_0}$. (32)

2.4. Boundary conditions

The composition of the feed water gives the boundary conditions at the inlet boundary

$$c_i^{cc}|_{y=0,0 \le x^{cc} \le 1} = c_{i0}^{cc} \quad \text{for } i = 1 - 5$$

 $c_i|_{y=0,0 < x < 1} = c_{i0} \quad \text{for } i = 1 - 5.$ (33)

Periodic boundary conditions are applied for all concentrations at the center of the concentrate compartment,

$$c_i^{cc}|_{x_{cc}=0.5^-} = c_i^{cc}|_{x_{cc}=0.5^+}.$$
 (34)

The potential difference over the cell is prescribed leading to the following boundary conditions;

$$\phi|_{x_{cc}=0.5^{-}}=0 \quad \text{left boundary} \tag{35}$$

$$\phi|_{x_{cc}=0.5^+}=1$$
 right boundary. (36)

2.4.1. Internal boundary conditions

At the internal boundaries all electrochemical potentials as well as all fluxes are continuous except for the fluxes of H⁺ and OH⁻ which are allowed be discontinuous at the membrane interfaces due to the enhanced water dissociation which is modeled as a surface reaction. The model for this reaction was presented in a previous paper [8].

The continuity of electrochemical potential gives rise to the following internal boundary conditions for the potential,

$$\phi = \phi^m + \frac{1}{\mathcal{V}} \ln \left[\frac{C^{cc}(c_1^{cc} + c_2^{cc}) + C^w c_4^{cc}}{C^m} \right]$$
 (37)

at boundary between sub-domains I/II and IV/V, and

$$\phi^{m} = \phi + \frac{1}{\mathcal{V}} \ln \left[\frac{C^{m}}{(c_{1} + c_{2} + C^{w} c_{4})} \right]$$
 (38)

at boundary between sub-domains II/III and III/IV. Internal boundary conditions for the concentrations are also obtained from the continuity of the electrochemical potential according to,

$$c_2^m = \alpha_1^{m2} \frac{c_1^m c_2^{cc}}{c_1^{cc}} \quad \text{and}$$

$$c_4^m = \alpha_1^{m4} \frac{C^m}{C^{cc}} \frac{c_1^m c_4^{cc}}{c_1^{cc}}$$
(39)

at boundary between sub-domains I/II and IV/V, and

$$c_2^m = \alpha_1^{m2} \frac{c_1^m c_2}{c_1} \quad \text{and}$$

$$c_4^m = \alpha_1^{m4} C^m \frac{c_1^m c_4}{c_1}$$
(40)

at boundary between sub-domains II/III and III/IV.

The fluxes in the x-direction in the concentrate compartment, scaled by $\frac{D_0c_0}{h}$ for i=1-5, are given by

$$N_{i,x_{cc}}^{cc} = C^{cc} \left(-\left(\lambda j_y P e_{df} + (1 - \epsilon)^{3/2} D_i \right) \frac{\partial c_i^{cc}}{\partial x_{cc}} - z_i \mathcal{V} (1 - \epsilon)^{3/2} D_i c_i^{cc} \frac{\partial \phi^{cc}}{\partial x_{cc}} \right) \quad \text{for i=1-3}$$

$$(41)$$

and

$$N_{i,x_{cc}}^{cc} = C^w \left(-\left(\lambda j_y P e_{df} + (1-\epsilon)^{3/2} D_i\right) \frac{\partial c_i^{cc}}{\partial x_{cc}} - z_i \mathcal{V} (1-\epsilon)^{3/2} D_i c_i^{cc} \frac{\partial \phi^{cc}}{\partial x_{cc}} \right) \quad \text{for i=4-5},$$

$$(42)$$

in the liquid phase, and

$$\bar{N}_{i,x}^{cc} = -0.15Z\epsilon^{3/2}D_i \left(\frac{\partial \bar{c}_i}{\partial x} - z_i \mathcal{V} \bar{c}_i \frac{\partial \bar{\phi}}{\partial x}\right) \quad \text{for i=1,2}$$
(43)

and

$$\bar{N}_{4,x}^{cc} = -0.15Z\epsilon^{3/2}D_i \left(\frac{\partial \bar{c}_4}{\partial x} - z_4 \mathcal{V}\bar{c}_4 \frac{\partial \bar{\phi}}{\partial x}\right) \tag{44}$$

in the fibrous phase.

Using the same scaling of the fluxes through the membranes gives

$$N_{i,x_m}^m = -C^m \Theta \left(D_i^m \frac{\partial c_i^m}{\partial x_m} - z_i \mathcal{V} D_i^m F c_i^m \frac{\partial \phi^m}{\partial x_m} \right) \quad \text{for i= 1,2,}$$
 (45)

and

$$N_{4,x_m}^m = -C^w \Theta \left(D_4^m \frac{\partial c_4^m}{\partial x_m} - z_4 \mathcal{V} D_4^m F c_4^m \frac{\partial \phi^m}{\partial x_m} \right), \tag{46}$$

where

$$\Theta = \frac{D_0^m h}{D_0 d^m}. (47)$$

Finally the fluxes in the feed compartment, sub-domain III, are given by

$$N_{i,x} = -\left(\lambda j_y P e_{df} + (1 - \epsilon)^{3/2} D_i\right) \frac{\partial c_i}{\partial x} - z_i \mathcal{V} (1 - \epsilon)^{3/2} D_i c_i \frac{\partial \phi}{\partial x} \quad \text{for i=1-3, (48)}$$

$$N_{i,x} = -C^w \left(\lambda j_y P e_{df} + (1 - \epsilon)^{3/2} D_i \right) \frac{\partial c_i}{\partial x} - z_i \mathcal{V} (1 - \epsilon)^{3/2} D_i c_i \frac{\partial \phi}{\partial x} \quad \text{for i=4-5},$$
(49)

in the liquid phase and

$$\bar{N}_{i,x} = -0.15Z\epsilon^{3/2}D_i\left(\frac{\partial\bar{c}_i}{\partial x} - z_i\mathcal{V}\bar{c}_i\frac{\partial\bar{\phi}}{\partial x}\right)$$
 for i=1,2 (50)

and

$$\bar{N}_{4,x} = -0.15Z\epsilon^{3/2}D_i \left(\frac{\partial \bar{c}_4}{\partial x} - z_4 \mathcal{V} \bar{c}_4 \frac{\partial \bar{\phi}}{\partial x}\right)$$
 (51)

in the fiber phase. The fluxes are needed to calculate the current density from Faraday's law and to couple the fluxes at the interfaces between the different sub domains. Note that the flux due to dispersion vanishes at the membrane interfaces and that the contribution to the current density from the dispersion cancels out due to the electroneutrality assumption. This means that λPe_{df} do not need to be specified in order to solve the model equation.

Continuity of the fluxes of specie ${\rm NO_3^-}$ and ${\rm Cl^-}$ over the boundary between sub-domains I and II gives,

$$N_i^{cc}|_{x_{cc}=1} + \bar{N}_i^{cc}|_{x_{cc}=1} = N_i^m|_{x_m=0}$$
 for i=1,2. (52)

The membrane is assumed to be ideally selective which leads to a zero flux condition for sodium at the membrane surface,

$$N_3^{cc}|_{x_{cc}=1} = 0. (53)$$

The fluxes of OH^- and H^+ is not continuous over the membrane boundary due to the enhanced water dissociation which is modeled by a heterogeneous surface reaction. Thus, the flux condition for OH^- and H^+ is given by;

$$N_4^{cc}|_{x_{cc}=1} + \bar{N}_4^{cc}|_{x_{cc}=1} + \mathcal{R}_{cc} = N_4^m|_{x_m=0}$$
(54)

and

$$N_5^{cc}|_{x_{cc}=1} + \mathcal{R}_{cc} = 0,$$
 (55)

where \mathcal{R} is the heterogeneous surface reaction. The model for \mathcal{R} was presented in a previous paper [8],

$$\mathcal{R}_{cc} = C^w \Upsilon \left(\frac{C^m}{C^{cc}(c_1^{cc} + c_2^{cc}) + C^w c_4^{cc}} \right)^{\alpha} (1 - c_4^{cc} c_5^{cc})|_{x_{cc} = 1}.$$
 (56)

The parameter Υ is defined as

$$\Upsilon = \frac{k_b^0 h \sqrt{K_w}}{D_0},\tag{57}$$

where k_b^0 is the reaction rate constant per unit area, at zero potential difference over the reaction layer.

At the boundary between sub domains II and III the concentration next to the membrane will increase and thus the enhanced water dissociation is neglected at this boundary. Continuity of fluxes for the anions gives

$$N_{i,x_m}^m|_{x_m=1} = N_{i,x}|_{x=0} + \bar{N}_{i,x}|_{x=0}$$
 for i=1,2,4. (58)

The ideal selectivity of the membranes gives a zero flux of the cations over the membrane surface, i.e.,

$$0 = N_{i,x}|_{x=0}$$
 for i=3,5. (59)

The continuity of the fluxes of species 1 and 2 at the boundary between III and IV are given by

$$N_i|_{x=1} + \bar{N}_i|_{x=1} = N_i^m|_{x_m=0}$$
 for i=1,2. (60)

The zero flux of sodium at the boundary gives,

$$N_3|_{x=1} = 0. (61)$$

At this boundary the concentration polarization makes the enhanced water dissociation important. Thus, the jump in the OH⁻ flux over the membrane surface is given by,

$$N_4|_{x=1} + \bar{N}_4|_{x=1} + \mathcal{R} = N_4^m|_{x_m=0}.$$
 (62)

The flux of H⁺ at the membrane surface is due to the dissociation of water at the interface,

$$N_5|_{x=1} + \mathcal{R} = 0. (63)$$

The expression for the surface reaction at this interface is given by,

$$\mathcal{R} = \Upsilon \left(\frac{C^m}{(c_1 + c_2) + C^w c_4} \right)^{\alpha} (1 - c_4 c_5)|_{x=1}.$$
 (64)

Finally the flux boundary condition between sub domains IV and V is given by

$$N_i^m|_{x_m=1} = N_i^{cc}|_{x_{cc}=0} + \bar{N}_i^{cc}|_{x_{cc}=0}$$
 for i=1,2,4 (65)

and

$$0 = N_i^{cc}|_{x_{cc}=0}$$
 for i=3,5. (66)

3. Result and Discussion

The model equations were implemented in the commercial finite element package Comsol MultiphysicsTM. The parabolic nature of the equations allowed the equations to be solved using a 1-D transient solver instead of the 2-D steady state. One advantage of this is that the adaptive time stepping ensures that sufficient numerical resolution is obtained in the streamwise direction. Furthermore, a very fine grid could be used because the grid resolves only one space dimension.

3.1. Comparison with experiments

Simulations were performed in order to compare the model predictions with the previously presented experimental results [7]. In figure 3 and 4 the experimental results from two different experimental setups are presented together with results obtained from simulations of these experiments. The stars in figure 3 gives the variation of the nitrate concentration in the product water with the applied current density in experimental case E. In this experiment the F.C was filled with an non conductive net-type spacer. It was found that a significant amount of nitrate was removed by Donnan dialysis, i.e. without the help of an external electric field, whereas applying an electric field did not lead to a great improvement of the nitrate separation. The limiting current density was low

and increasing the current density above this is accomplished by dissociation of water. The pH of the product is given by the stars in figure 4. A sudden drop of the product pH was obtained when the average current density was increased from $5~\rm A/m^2$ to $10~\rm A/m^2$ which indicates that water dissociation has started to occur in the feed compartment when an average current density of $10~\rm A/m^2$ was applied. Increasing the current density even further only gave a small increase in the flux of nitrate out of the feed compartment. Hence, the nitrate level in the product remained more or less constant as the applied current density was increased.

The squares in figure 3 marks the nitrate concentration in the product as a function of the applied average current density as obtained in the experiment with an ion-exchange textile incorporated in the feed compartment. These results were presented as experimental case D in the experimental paper [7]. In this experiment the pressure in the feed compartment was increased in order to press the membranes against the textile in order to establish as good contact between textile and membrane as possible. Without the current applied it was found that the incorporation of the textile into the feed compartment led to an increased nitrate separation due to Donnan dialvsis. This is believed to be due to an improved mixing of the liquid induced by the inherent structure of the network of fibers in the textile. When the current density was applied the nitrate level in the product decreased to levels which were well below the recommended maximum of 25 ppm. The squares in figure 4 gives the pH of the product as a function of the applied average current density for the same experimental case. It was found that increasing the current density did not lead to the same dramatic change of the pH as was found in the case with a non conductive textile. However, the pH of the product started to go down, indicating that water dissociation took place, when a current density of about 25 A/m^2 was applied.

The values of the model parameters used in the simulations are presented in table 1. These values were obtained by considering the experiments, where a solution containing 105 ppm nitrate (1.7mM) was treated. The geometry of the cell and the flow rate used in the experiments were used to calculate the corresponding dimensionless parameter values. This will be the base case, which will be used to interpret the results from the simulations. The values of the unknown parameters in the enhanced water dissociation model are chosen according to the estimates presented together with that model [8]. In the present paper the diffusion coefficients of nitrate, chloride and hydroxide in the membranes are taken to be 2% of their value in water, compared to 1.9% for chloride and 1.5% for nitrate which was used in the simulations presented previously [6, 7]. The estimates made for the quantities related to the ion exchange textile were discussed in the experimental paper [7]. In the experiments the concentrate compartments were filled with a net-type spacer instead of an ion exchange textile. However, the relatively high concentration of the solution in

the C.C makes the influence on the results of the simulations by the presence of the textile in those compartments negligible.

D_1	1.90 [14]	$Z = \frac{w}{c_0}$	410
D_2	2.03 [14]		1000
D_3	1.33 [14]	$C^m = \frac{c_0^m}{c_0}$ $C^{cc} = \frac{c_0^{cc}}{c_0}$	120
D_4	5.26 [14]	α	0.1
D_5	9.31[14]	$\chi = \frac{V}{\sigma^2 Pe}$	0-0.66
D_0	$1 \cdot 10^{-9} \ [m^2 s^{-1}]$	ϵ	0.15
c_{10}	1	$\kappa = \frac{L\sqrt{K_w}k_b}{j_0}$	$3.5 \cdot 10^{-11}$
c_{30}	1	$\Lambda = \sqrt{(1 - \epsilon)K^{-1}}h$	230
c_{40}	0.1	$\theta = \frac{\lambda d_f L}{h^2}$	0.10
c_{50}	10	$\Theta = \frac{\tilde{D}_0^m h}{D_0 d^m}$	0.35
c_{10}^{cc}	0.05	$\Upsilon = rac{k_b^{0.04} \sqrt{K_w}}{D_0}$	0.45
c_{30}^{cc}	1.0	$\mathcal{P} = \sigma^2 P e$	380
c_{40}^{cc}	0.1	α_1^2	0.5
$\begin{array}{c} c_{30}^{cc} \\ c_{40}^{cc} \\ c_{50}^{cc} \end{array}$	10	$\alpha_1^2 \\ \alpha_1^4, \alpha_1^{m2}, \ \alpha_1^{m4}$	1
c_0	$1.7 \ [mol \ m^3] \ [15]$		

TABLE 1. Values of the non dimensional parameters, coefficients and inlet concentration used to obtain the results presented in figure 3 and 4.

During the experiments only the cell voltage, applied over the entire cell, the total current passed through the cell and the concentrations of the product and concentrate could be measured. This restricts the comparisons that can be made between model and experiments. Only the nitrate concentration and pH of the product as a function of the average current density applied can be compared.

The solid line in figure 3 shows the nitrate concentration in the product as calculated with the model for the case where a ion conducting textile was incorporated. A good agreement is obtained with the experimental case D [7]. A comparison between the pH obtained in the experiments and with the simulations is presented in figure 4. According to the simulations the pH of the product should not change significantly when the current density is increased up to $30~\text{A/m}^2$. Conversely, in the experiments a decrease of the product pH, down to 4.3, was found also in the case where the textile was incorporated in the feed compartment. This decrease of the pH indicates that water dissociation was starting to become important also in this case, which was not predicted by the model.

The dashed line in figure 3 shows the result from a simulation with a textile with no functional groups incorporated, i.e., Z=0. For low current densities this

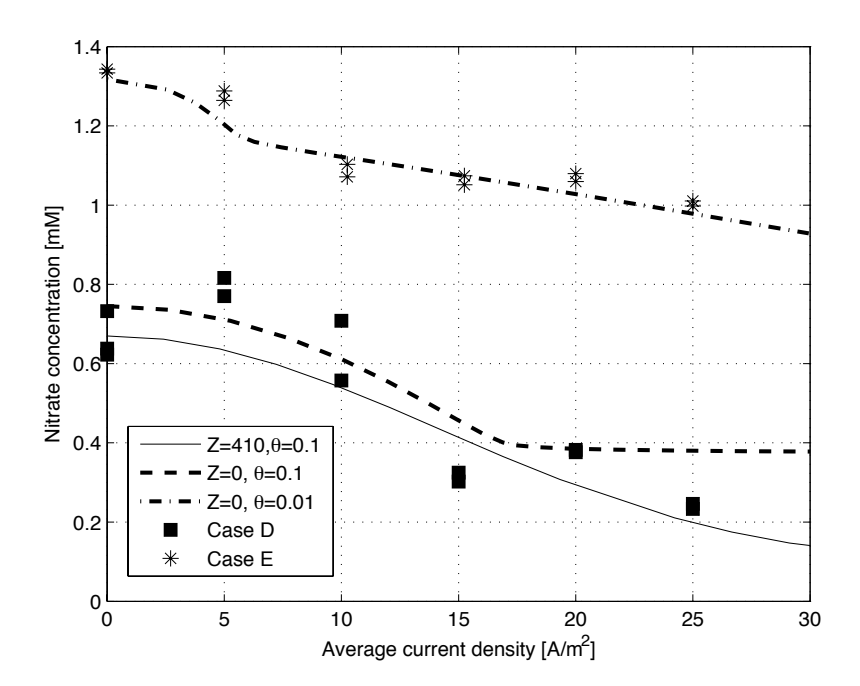


FIGURE 3. Nitrate concentration in the product water as a function of the applied current density. Comparison between simulations with different textiles and the experimental results presented in a previous paper [7].

simulation agrees well with the experimental points obtained with the conductive textile, i.e. case D given by the squares in figure 3. However, compared to the simulations with a conductive textile a higher χ value is required to obtain a specific current density. Thus, the use of a conductive textile reduces the power consumption. At about 17 A/m² the limiting current density is reached and to increase the current density further water dissociation has to take place. This is also reflected in the pH of the product as shown in figure 4. The pH is almost constant up to the point where the limiting current density is reached. Above this point the pH drops rather dramatically down to around three at 30 A/m^2 . Looking at the concentration of nitrate one finds that it is more or less constant after the limiting current density is exceeded. The reason for this is that the additional current is carried by hydroxide ions produced by the dissociation of water.

Using a non conductive textile seems very close to the experimental case E where a non conductive net-type spacer was used in the feed compartment. In the simulations with non-conductive textile, dashed line in figures 3 and 4, far more nitrate was removed by Donnan dialysis, i.e., when the current density

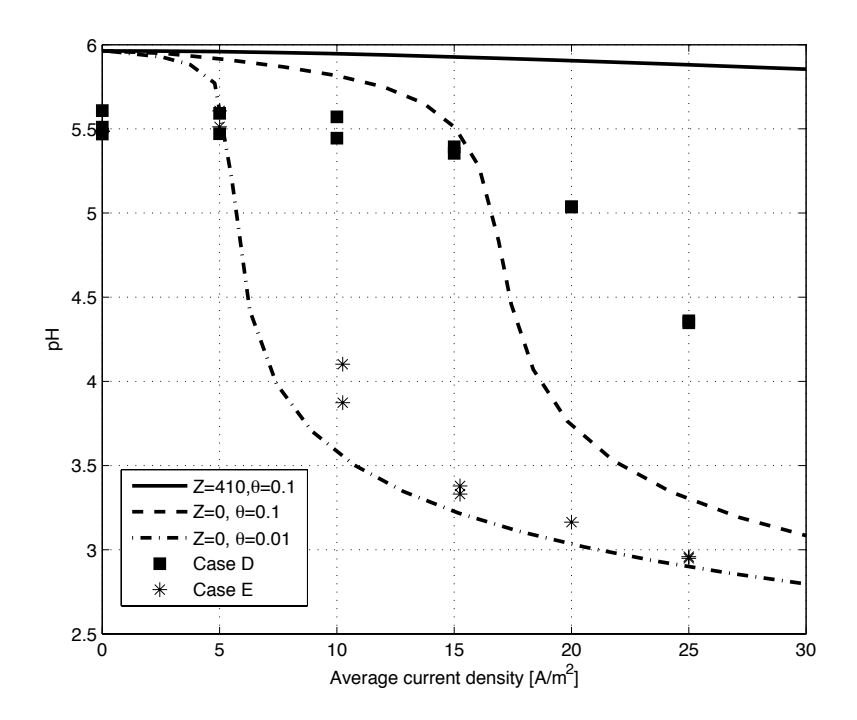


FIGURE 4. pH as a function of the applied current density. Comparison between simulations with different textiles and experimental results presented in a previous paper [8].

was not applied, compared to the experimental case E. As discussed above this can be explained by the good mixing induced by the fiber net-work of the textile. The limiting current density, indicated by the sudden drop in pH of the product, is for the same reason higher when the textile is used as a nonconductive spacer. Hence, also a textile without the ion exchange groups will improve the efficiency of the process due to its mechanical structure, which will improve the mass transport in the feed compartment. The dash-dotted lines in figure 3 and 4 correspond to a simulation where the coefficient of transversal dispersion was lowered by one order of magnitude, i.e. $\theta = 0.01$ as to mimic the effect of a less effective dispersion for the net-type spacer compared to the textile. This gives a much better agreement with the experiments with the non-conductive net-type spacer, case E; both the nitrate concentration and the pH curves are found to agree rather well. Thus, our model is capable of describing the water dissociation phenomenon in an electropermutation process with inert spacers relatively well. To make a better validation of the model new experiments should be made with reference electrodes located in the center of the concentrate compartments. One could then compare the potential drop

over the repeating unit with the response in both current density, pH and nitrate removal.

There are a number of possible explanations for the discrepancy between the prediction of the product pH made by the model and the experiments for the case where a conductive spacer was incorporated. Below some of these will be discussed.

The model assumes a homogeneous textile, i.e., both the porosity and the distribution of the functional groups are assumed to be homogeneous. In the literature several models for heat transfer to/from solid boundaries into porous beds introduce a variable porosity in the near wall region [16, 17]. The variable porosity is then commonly described by an exponential function according to [17],

$$(1 - \epsilon) = (1 - \epsilon)_{\infty} \left(1 + b \exp\left(-\frac{c\xi}{d_f}\right) \right). \tag{67}$$

where b and c are empirical parameters, $(1-\epsilon)_{\infty}$ is the void fraction in the bulk of the bed and ξ is the coordinate in the wall normal direction. Not only does this effect the heat conduction in this region but it also gives a higher permeability close to the wall with a possible flow channeling in that region. In our case where the fiber diameter is very small and the void fraction in the bulk is rather high the effect of flow channeling can be considered negligible. The effective mass transfer to the membrane is, however, affected. The value of the empirical parameter b is usually such that the void fraction at the wall is very close to unity. As a consequence of this the current density would be forced out into the liquid phase in a thin layer next to the membrane. The thickness of this layer is controlled by the other empirical parameter, c. Furthermore, the correlation for the mechanical dispersion used in the bulk is not likely to be valid all the way in to the membrane wall. This problem has been discussed in the literature and several different ways to model this has been proposed. A van Driest type of wall function was proposed by Cheng [16, 17, 18],

$$\lambda = \lambda_{\infty} \left(1 - exp\left(-\frac{m\xi}{d_f} \right) \right), \tag{68}$$

where λ_{∞} is the transversal coefficient of dispersion in the bulk and m is a empirical parameter. Simulations have been carried out with both of these corrections included. However, using parameter values which can be found in the literature, did not improve the pH predictions dramatically. Thus, it is not believed that the correlation used for the mechanical dispersion in the near wall region nor the assumption of a constant porosity should be responsible for the failure to accurately predict the pH drop with a conductive textile incorporated.

Another assumption made in the model is that the textile and the membrane are in perfect contact with each other. Ideally one would like the conducting spacer to be a porous continuation of the membrane with a very high specific area filling the whole feed compartment [19]. The situation in the experiments was that the textile spacer is made of a different material than the

membrane and the fibers in the textile are not attached to the membrane surface. In the experiment the pressure in the C.C was higher than in the F.C to force the membrane to be in contact with the textile. Even if this way of operating the process greatly improved the separation of nitrate and reduced the change of the pH, it does not mean that an ideal contact was established. It is very likely that some part of the membrane was not in direct contact with the membrane. Thus, it should be possible to improve the performance of the process by reducing the contact resistance between membrane and spacer. This contact resistance be captured by the model used for the variable porosity, by tuning the parameters. This is however outside the scope of the present paper.

3.2. Simulations with a non conductive textile

The model will now be used to study the electropermutation process with a non-conducting textile, i.e., Z=0, in more detail. The role of the textile in such a process would be to provide mechanical support to the ion exchange membranes as well as improving the mixing of the liquid phase in the feed compartment. Later the capacity of the textile will gradually be increased in order to study the influence of a conductive spacer. In all these simulations it will be assumed that the textile has a constant porosity and is in ideal contact with the membranes. Furthermore, the mechanical dispersion is assumed to be given by the same correlation used in the bulk all the way out to the membrane. Thus the model is more likely to underestimate the rate of water dissociation rather than over predict it.

The concentration of nitrate averaged over the thickness of the feed compartment as a function of the streamwise coordinate is shown in figure 5. Each line represents simulations with a specific value of the non-dimensional parameter χ , all other parameters are given in table 1 except for Z which is set to zero. The dotted line, $\chi = 0$ represents the nitrate removal by Donnan dialysis. In this case the nitrate level decreases steadily through the cell. Indicating that the whole compartment is active in the separation of nitrate. As the value of χ is increased the rate of nitrate separation initially increases until the limiting current is reached. When the value of χ is increased above this point water dissociation becomes important. The partial current carried by OH⁻ in the membrane then increases rapidly when χ is further increased. For $\chi = 0.92$, which is the highest value presented in figure 5, the nitrate removal is quite fast in the beginning of the cell. Then as water starts to dissociate the rate of nitrate removal decreases. In fact the averaged nitrate concentration passes through a minimum and in the last section of the compartment more nitrate enters over the membrane on the cathode side than what leaves the feed compartment over the membrane on the anode side. As a result the nitrate level in the product actually is higher for $\chi = 0.92$ than for $\chi = 0.61$. Thus the nitrate removal can not be improved by increasing the applied potential further.

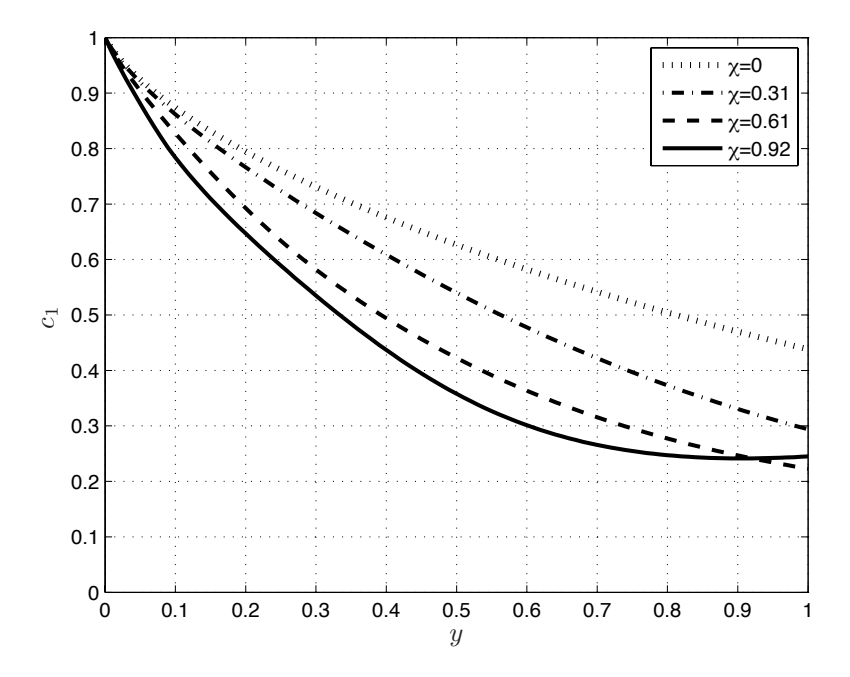


FIGURE 5. Nitrate concentration averaged over the F.C thickness as a function of streamwise coordinate. Theses curves were calculated for an inert textile, Z=0, other model parameters are according to table 1

The membrane is assumed to be ideally selective so the flux of H^+ out of the membrane surface is that which is produced by the heterogeneous water dissociation. In figure 6 the H^+ flux from the membrane surface is presented as a function of the streamwise coordinate for different values of χ . Close to the entrance of the feed compartment the water dissociation is close to equilibrium. As one moves downstream through the feed compartment the concentration boundary layer develops and the driving force for the enhanced water dissociation increases. The streamwise position for the onset of the enhanced water dissociation moves towards the inlet of the F.C with increasing value of χ .

The pH of the liquid averaged over the F.C thickness is presented as a function of the streamwise coordinate in figure 7. Close to the inlet where water dissociation is not significant the pH stays constant. Once the enchanced water dissociation has started the pH drops through the whole F.C. The pH distribution in both the F.C and the C.C for a simulation with $\chi=0.51$ is shown in figure 8. The location of the onset of water dissociation is clearly seen if one looks at the pH distribution in the C.C, at $y\approx0.15$ there is a sharp increase of the pH next to the membrane in the concentrate compartment. The

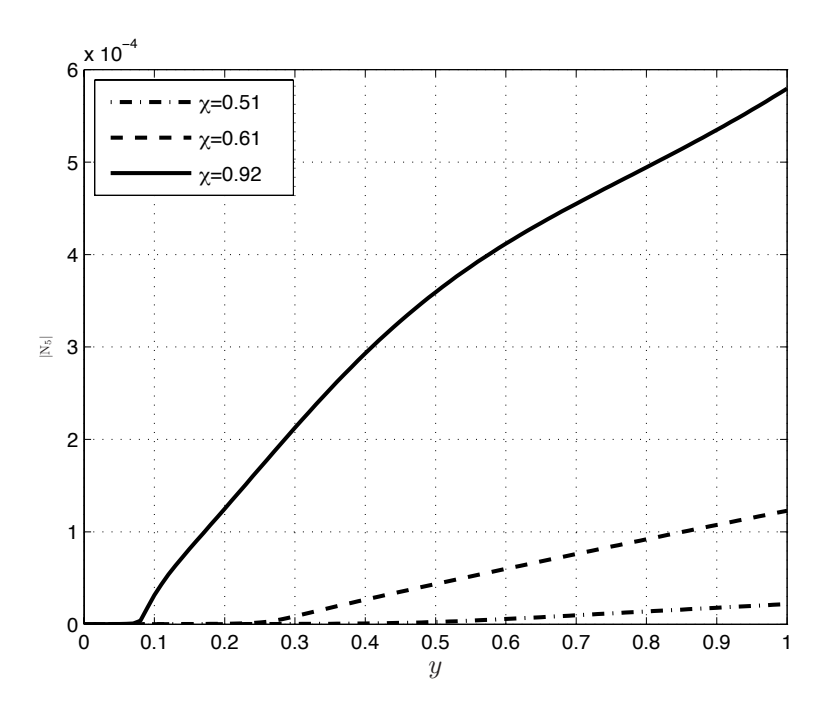


FIGURE 6. The flux of H^+ at x=1. This flux is given by the dissociation of water in the heterogeneous surface reaction.

pH next to the membrane in the C.C then increases steadily through the whole cell and reaches levels well above 11 at the outlet. The high pH next to the membrane in the concentrate compartment may be a serious problem for the reliability of the process. Most metal hydroxides have a low solubility and if the OH⁻ concentration becomes too high precipitation of salts such as iron hydroxides can foul the membrane [20].

The total ionic concentration of the water in the feed compartment increases when water begins to dissociate. This will lead to an increased conductivity of the liquid, which will influence the current distribution. In figure 9 the current density scaled with the current density at the inlet is shown as a function of streamwise coordinate for different values of χ . When the applied potential is very low the current density is almost constant all the way through the cell. Then if the applied potential drop is increased, but not enough for water dissociation to become important, one finds that the current density is highest in the beginning of the feed compartment and then gradually decreases as one moves through the cell. Since nitrate ions in the feed are replaced by slightly more mobile chloride ions this decrease of the current density can not be explained by the change in the composition of the feed water. A more likely explanation would be that concentration polarization taking place close to the

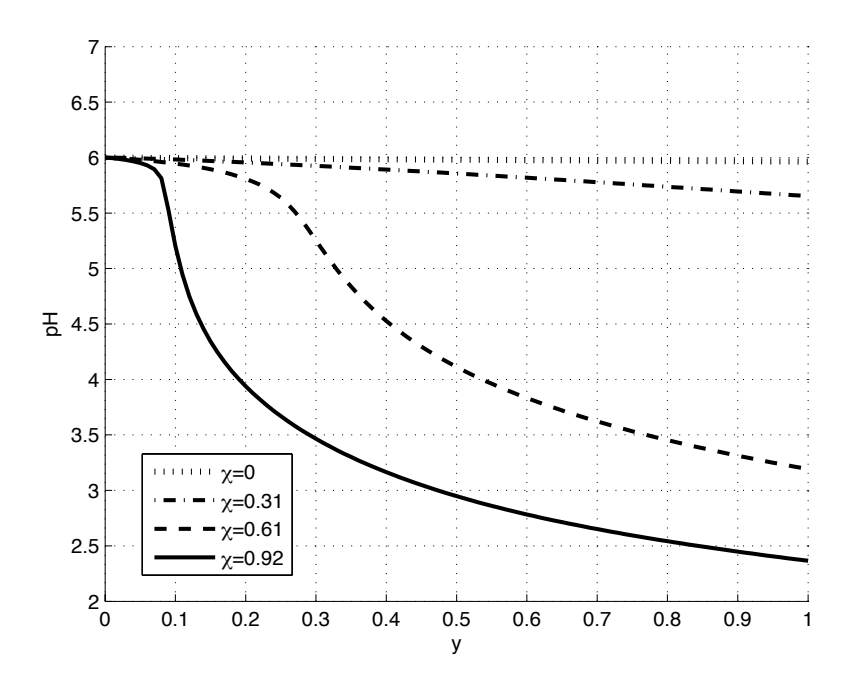


FIGURE 7. pH averaged over the F.C thickness as a function of the stream wise coordinate. Calculated with a non conducting textile, Z=0, and all other parameters as in table 1

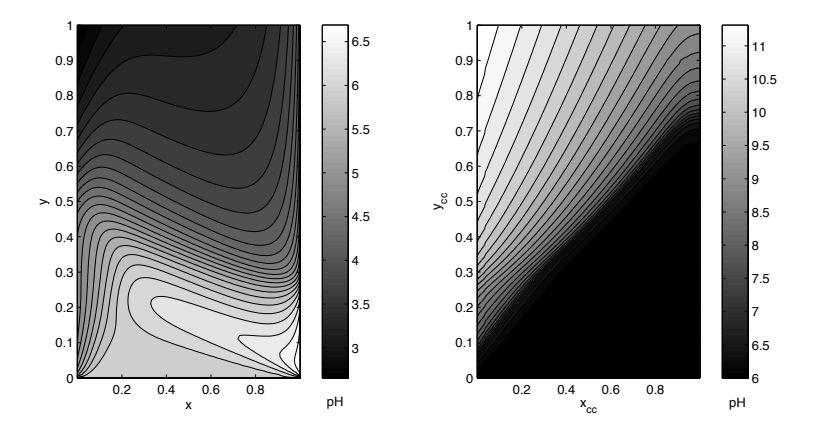


FIGURE 8. pH distribution in the F.C to the left and the C.C to the right calculated for a non conductive textile, Z=0, and χ =0.51. All other parameters as given in table 1.

membranes leads to an increased resistance of the cell. If the potential is further increased water dissociation will eventually start to become important. This will increase the total salinity of the water in the F.C by producing highly mobile H⁺ ions that remains in the F.C. A consequence of this is that the conductivity of the F.C increases, which is seen by the increase in current density as one moves downstream through the cell. Thus at $\chi=0.92$ the highest current density close to the outlet is almost three times higher than at the inlet. At the same time the nitrate removal is very poor in the region close to the outlet.

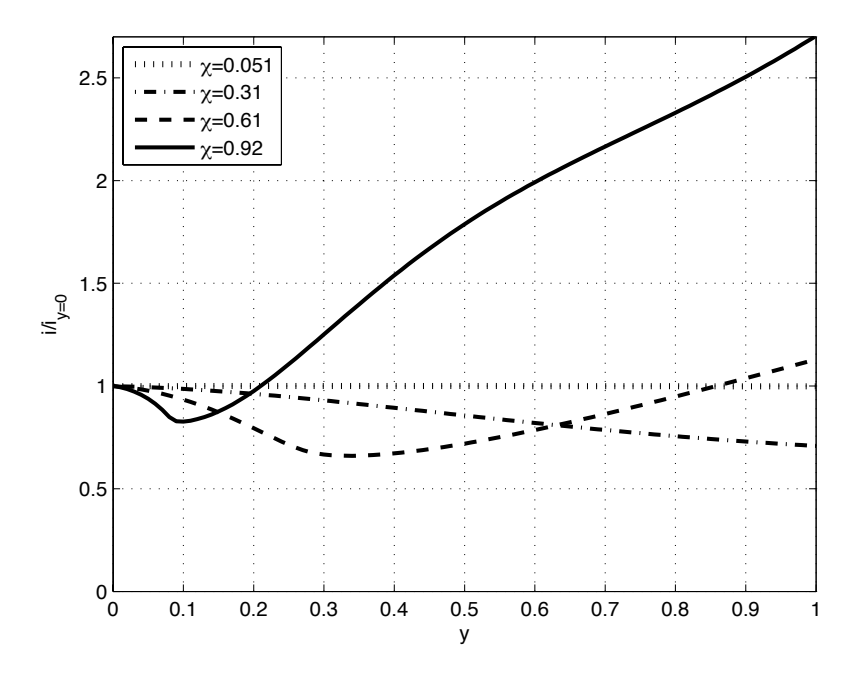


FIGURE 9. The current density distribution, scaled by the current density at the inlet, through the cell as predicted by the model in a simulation for a non conducting textile, i.e. Z=0. All other parameters as given in table 1.

In summary, simulations with a non-conductive textile were performed in order to gain some insight into this simplified process. The maximum nitrate separation possible to accomplish was found to be just under, 75%, with the chose set of parameter values. In the base case studied in this paper where the initial nitrate level is 105 ppm this gives that the lowest nitrate level that could be obtained is that which is the recommended maximum level, i.e. 25 ppm. However, the pH of the product in this case would be about 3 which is very low, and the local pH next to the membrane in the C.C would be as high as

11 close to the outlet. Furthermore, it is likely so that if the flow rate through or the thickness of the feed compartment is increased, in order to increase the productivity per unit membrane area, the nitrate level of maximum 25 ppm in the product cannot be reached. Thus, in order to increase the productivity a conductive spacer has to be used.

3.3. Simulations with a conductive textile

To study the influence of a conductive textile in the F.C simulations were performed with different textile capacities. The parameter values used in the simulations are given in table 1 except for the scaled textile capacity Z which was varied.

In figure 10 the nitrate level in the product is presented as a function of χ for three different values of Z. The dash dotted line represents a simulation with a non-conductive textile, Z=0. As was discussed above the nitrate concentration of the product passes through a minimum as the value of χ is increased. This minimum is located somewhere between $\chi \approx 0.55 - 0.75$ in the simulations presented here. If instead a textile with a very low capacity, Z=10, is used; the nitrate level decreases with increasing χ all the way up to $\chi = 1$. The nitrate concentration in the product at $\chi = 1$ is just above 10% of the feed water concentration. Hence, a feed water with around 100 ppm of nitrate could be treated, and a level under the recommended level of max 25 ppm nitrate [21, 22] could be reached using this textile. The solid line figure 10 represents results from simulations were a textile with a higher capacity, Z=100. It is clear that the nitrate separation is very fast with this textile. At $\chi \approx 0.5$ the limit of the separation possible to achieve is reached. As was concluded in our previous paper [6] an increased textile capacity makes the optimal value of χ decrease in such a way that the product between the optimal χ value and Z is constant.

The current density passed through the cell at a given value of χ is dependent on the capacity of the textile. In figure 11 polarization curves for three different textile capacities, i.e. Z=0, 10 and 100, are presented. The polarization curve obtained with a non conductive textile, represented by the dash-dotted line, have three different regions. First the current density increases linearly with χ up to $\chi \approx 0.3$. Around the limiting current density is the plateau region, $0.3 \lesssim \chi \lesssim 0.5$, where there is very slow increase in the current density as χ is increased. In the third and final region the current density again rises with increasing χ . This super limiting current density is in our simulations a result of the enhanced water dissociation. Due to the dissociation of water the conductivity of the liquid in the F.C increases. As a consequence of this the current density, obtained in our simulations with a non conductive textile, is higher than when a conductive textile, Z=100, is used at $\chi=1$.

The dashed line represents the polarization curve obtained in from a simulation with a textile with poor conductivity, Z=10. In this case the most of the current is passed through the liquid phase. Thus, the initial slope of the polarization curve is very close to the case with a non conductive textile. When

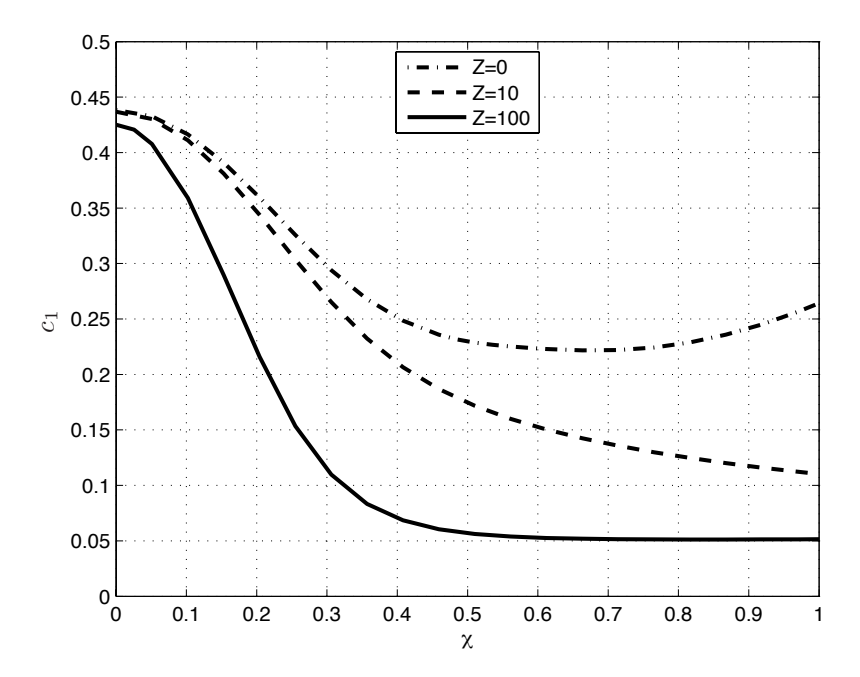


FIGURE 10. Nitrate concentration in the product as a function of the dimensionless parameter χ . Each line corresponds to a different textile capacity.

the concentration close to the membrane approaches zero the conductivity of this phase becomes very low and the current moves into the fiber phase in this region. This reduces the sharp increase of the electric field in the liquid phase next to the membrane. The current density in the liquid phase close to the membrane surface is kept low and hence the dissociation of water is suppressed. Thus, the partial current of $\rm H^+$ and $\rm OH^-$ remains low even for rather high χ values. This explains why the conductive textiles reduce the water dissociation intensity.

The polarization curve for the textile with Z=100 is represented by the solid line in figure 11. In this case the fiber phase has a reasonable conductivity. Both phases carry almost half of the current each in the bulk of the F.C. This makes total conductivity of the F.C higher compared to the case with an inert textile. Hence, the initial slope of the polarization curve is higher. As the concentration in the liquid phase becomes low the current moves into the fiber phase instead and the limiting current behavior is not seen. Compared to the case when the textile had a relatively poor conductivity the resistance close to the membrane in the fiber phase is lower and the slope of the polarization curve is therefore higher.

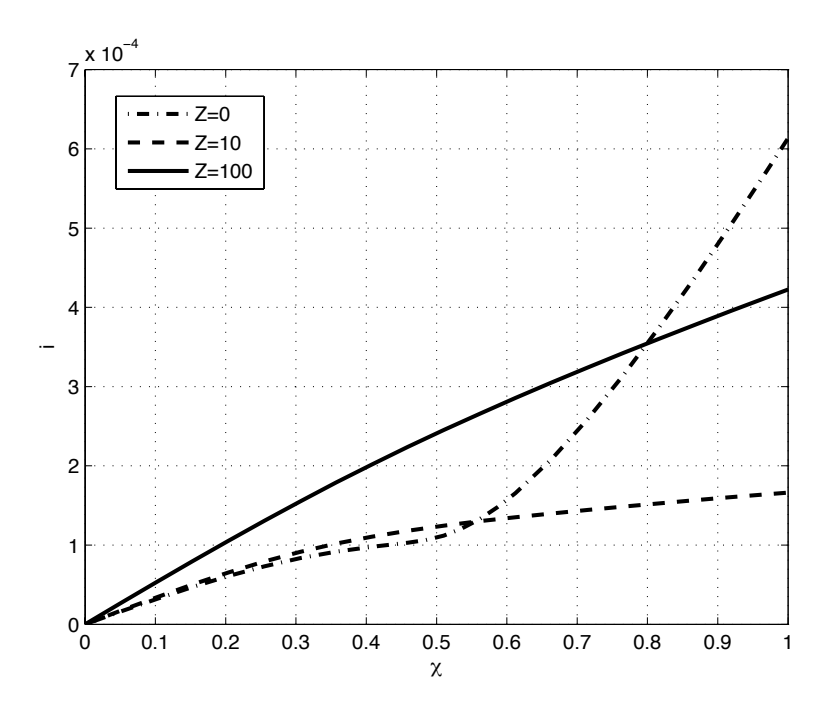


FIGURE 11. Current density as function of χ , i.e. polarization curves, for different Z values. Not that due to the water dissociation the highest current density is obtained for the system without the conducting spacer.

In both cases when a conductive textile was used the enhanced water dissociation was suppressed. Thus, most of the current is carried through the membrane by NO_3^- and Cl^- for all values of the current density. As a consequence of this no minimum for the nitrate separation for $\chi \leq 1$ could be found. In figure 12 the flux of nitrate at the membrane, $\mathrm{x=}1$, in simulations with $\chi = 0.51$ is presented as a function of streamwise position, y. The dash-dotted line is obtained in a simulation with Z=0. In this case the total nitrate flux is passed through the liquid phase. The solid and dashed lines represent the nitrate fluxes in the fiber and liquid phases respectively in a simulation with Z=100. The nitrate flux in the fiber phase is rather high close to the inlet of the cell, where most nitrate is replaced by chloride. This also explains the low nitrate fluxes in the last part of the cell.

As was pointed our earlier, not only the pH of the product should be considered when finding suitable operating conditions for the process. Also the local pH in C.C next to the membrane should be taken into account. In figure 13 the pH, averaged over the thickness of the F.C, as a function of stream wise coordinate in a simulation with Z=100 and $\chi=0.36$ is given by the solid

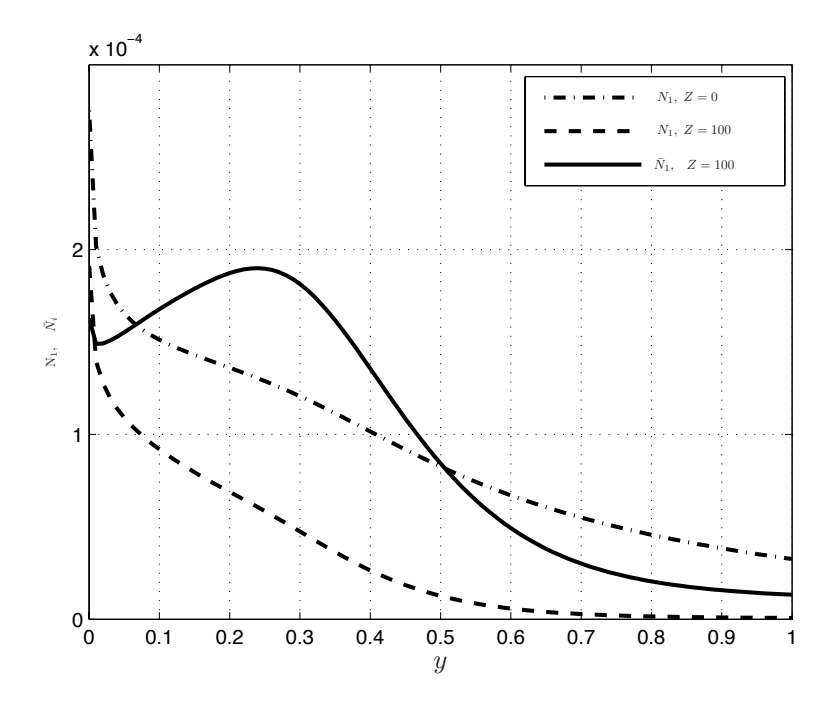


FIGURE 12. Nitrate flux in the different phases at the membrane surface x=1, for two different capacities of the textile and $\chi=0.51$.

line. The dashed line represents the local pH next to the membrane in the C.C, i.e. $x_{cc}=0$. It is found that the pH of the product decreases only slightly from pH 6 down to 5.7, which can be acceptable. The pH next to the membrane in the C.C reaches a value of about 8.5 close to the outlet of the cell. This value is not very high and can be acceptable. If however this pH should increase to higher values there might be problems with fouling of the membrane due to precipitation of hydroxides.

4. Conclusion

The model for the enhanced water dissociation at surfaces of ion exchange materials was successfully implemented in the simulations of nitrate removal by continuous electropermutation. For the case where a net-type spacer was used the model could predict pH variations in the product that were in line with the experimental observations previously reported. Thus, it was concluded that the model of the enhanced water dissociation is a powerful tool that can be used to include the effect of water dissociation in simulations of electromembrane processes. It could for example be used to gain better understanding of the influence of the local pH within an EDI cell.

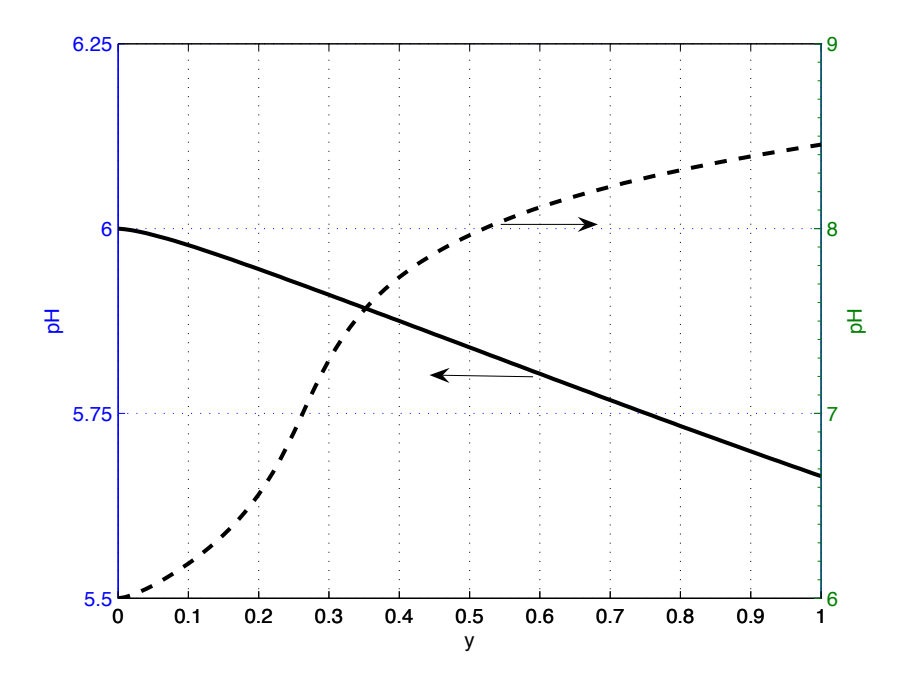


FIGURE 13. The solid line represents the pH (scale on the left y-axis) averaged over the thickness of the feed compartment, obtained in a simulation with Z=100 and $\chi=0.36$. The dashed line is the local pH (scale on the right y axis) next to the membrane in the concentrate compartment.

Simulations with a non conductive textile highlighted the limitations of such a process configuration. The separation of nitrate possible to accomplish is limited by concentration polarization taking place close to the surface of the membrane. Increasing the current density above the limiting current density gives rise to an enhanced water dissociation, which leads to a change of the pH of the product water. Furthermore the pH in the C.C need to be considered since a high pH in the region close to the membrane might lead to fouling problems due to precipitation of hydroxide salts. In the base case considered in this paper the minimum nitrate level that could be reached in the product when a non conductive textile was used was 25 ppm. However, the pH would then be as low as three in the product and as high as 11 close to the membrane in the concentrate compartment. Thus, the productivity has to be lowered if a non conductive textile is used.

To investigate the influence of the capacity of the ion exchange textile simulations were performed with two different capacities of the fiber phase. It was found that using both of these textiles the dissociation of water was reduced considerably. The optimal χ value is reduced when Z is increased in such a way that the product χ Z remains constant. Thus a higher Z value reduces the power consumption of the process by reducing the resistance of the feed compartment. As the concentration of the liquid phase approaches zero close to the membrane, due to the concentration polarization, the current density moves into the fiber phase. Concentration polarization does not take place in the fiber phase due to the fixed counter ions. Thus, the limitation for the nitrate flux is moved from the surface of the ion exchange membrane to the much larger surface of the fiber phase.

Simulations performed with conductive textiles indicated that incorporation of an anion-conductive textile in the feed compartment of the electropermutation equipment reduces the water dissociation tendency. The model did not predict the pH shift that was found in the experiments with ion-exchange textile in the feed compartment. It is believed that an insufficient contact between the textile and the membranes in the experiments can explain this discrepancy. Poor contact increases the power consumption of the process as well as increases the risk of enhanced water dissociation. The dissociation of water is an unwanted phenomenon in the process studied in this paper. First of all it will decrease the current efficiency of the process. Furthermore it will lead to pH changes of the product water, but perhaps even more disturbing is the increase of the pH next to the membrane in the concentrate compartment, which may cause fouling of the membrane as previously discussed.

The first step to take for improving the process would be to solve the contact problems related to the poor contact between the membrane and the textile.

References

- [1] F. Helfferich. Ion Exchange. Dover, 1995. ISBN 0-486-68784-8.
- [2] G.C. Ganzi, Y. Egozy, A.J. Giuffrida, and A.D. Jha. Deionization-high purity water by electrodeionization Performance of the ionpure continuous deionization system. *Ultra*pure Water, 4(3):43–48, 1987.
- [3] G. C. Ganzi, A. D. Jha, F. DiMascio, and J. H. Wood. Electrodeionization therory and practice of continuous electrodeionization. *Ultrapure Water*, 14(6):64–68, 1997.
- [4] S. Ezzahar, A. Cherif, J. Sandeaux, R. Sandeaux, and C. Gavach. Continuous electropermutation with ion-exchange textiles. *Desalination*, 104:227–233, 1996.
- [5] A. Smara, R. Delimi, C. Poinsignon, and J. Sandeaux. Electroextraction of heavy metals from dilute solutions by a process combining ion-exchange resins and membranes. Separation and Purification Technology, 44:271–277, 2005.
- [6] C-.O. Danielsson, A. Dahlkild, A. Velin, and M. Behm. Nitrate removal by continuous electropermutation using ion-exchange textile: Part I modeling. *Journal of The Electro*chemical Society, 153(4):D51–D61, 2006.
- [7] C.-O. Danielsson, A. Velin, M. Behm, and A. Dahlkild. Nitrate removal by continuous electropermutation using ion-exchange textile: Part II experimental investigation. *Journal of The Electrochemical Society*, 153(4):D62–D67, 2006.
- [8] C-.O. Danielsson, A. Dahlkild, M. Behm, and A. Velin. A model for the enhanced water dissociation on monopolar membranes. To be submitted, 2006.
- [9] S. Whitaker. The Method of Volume Averaging. Kluwer Academic Publisher, 1999. ISBN 0-7923-5486-9.
- [10] J. Bear. Dynamics of Fluids in Porous Media. Dover, 1988. ISBN 0-486-65675-6.
- [11] D. S. Clague, B. D. Kandhai, R. Zhang, and P. M. A. Sloot. Hydraulic permeability of (un)bounded fibrous media using lattice boltzmann method. *Physical Review E*, 61(1):616–625, January 2000.
- [12] A. Koponen, D. Kandhai, E. Hellén, A. Hoekstra, M. Kataja, K. Niskanen, P. Sloot, and J. Timonen. Permeablility of three-dimensional random fiber webs. *Physical Review Letters*, 80(4):716–719, 1998.
- [13] R.A. Greenkorn. Flow Phenomena in Porous Media. Dekker, 1983.
- [14] J. S. Newman. Electrochemical Systems. Prentice Hall, 2nd edition, 1991. ISBN: 0-13-248758-6.
- [15] M. Passounaud, J.C. Bollinger, B. Serpaud, and S. Lacour. Water nitrate removal with ion-exchanger grafted textiles. *Environmental Technology*, 21:745–753, 2000.
- [16] M. Kaviany. Principles of Heat Transfer in Porous Media. Springer, 2nd edition, 1999.
- [17] P. Cheng. Fully developed forced convective flow through an annular packed-sphere bed with wall effects. *Int. J. Heat. Mass Transfer*, 29(12):1843–1853, 1986.
- [18] C. T. Hsu and P. Cheng. Thermal dispersion on a porous medium. Int. J. Heat. Mass Transfer, 33(8):1587–1597, 1990.
- [19] I. Rubinstein, Y. Oren, and B. Zaltzman. Multi-phase model of a sparse ion-exchange speer. *Journal of Membrane Science*, 239:3–8, 2004.

- [20] H. Strathmann. Ion-Exchange Membrane Separation Processes. Elsevier, 2004. ISBN 0-444-50236-X.
- [21] Council directive of 3 november 1998. Official J.Europ.Commun., L330, 05/12/1998 P. 0032 0054, 1998.
- [22] WHO. Guidlines for drinking water quality; recomendations i, geneva, 2004. 3rd Edition.